LBNL-41247

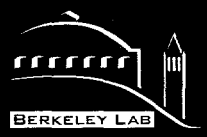

ERNEST ORLANDO LAWRENCE
BERKELEY NATIONAL LABORATORY

The Synthesis, Characterization and Reactivity of High Oxidation State Nickel Fluorides

Lisa C. Chacón

Chemical Sciences Division

December 1997

Ph.D. Thesis

LBNL-41247

The Synthesis, Characterization and Reactivity of High Oxidation State Nickel Fluorides

Lisa Carine Chacón
Ph.D. Thesis

Department of Chemistry
University of California, Berkeley

and

Chemical Sciences Division
Lawrence Berkeley National Laboratory
University of California
Berkeley, CA 94720

December 1997

This work was supported by the Director, Office of Energy Research, Office of Basic Energy Sciences, Materials Sciences Division, of the U.S. Department of Energy under Contract No. DE-AC03-76SF00098.

The Synthesis, Characterization and Reactivity of High Oxidation State Nickel Fluorides

by

Lisa Carine Chacón

B.S. (California State University, Sacramento) 1990

A dissertation submitted in partial satisfaction of the

requirements for the degree of

Doctor of Philosophy

in

Chemistry

in the

GRADUATE DIVISION

of the

UNIVERSITY of CALIFORNIA at BERKELEY

Committee in charge:

Professor Neil Bartlett, Chair
Professor Angelica Stacy
Professor Alex Zettl

Fall 1997

Abstract

The Synthesis, Characterization and Reactivity of

High Oxidation State Nickel Fluorides

by

Lisa Carine Chacón

Doctor of Philosophy in Chemistry

University of California, Berkeley

Professor Neil Bartlett, Chair

The research described in this thesis has mainly addressed the challenge of the synthesis of thermodynamically unstable nickel fluorides, which cannot be made by traditional thermal methods. A low-temperature approach towards the synthesis of such transition metal fluorides exploits the greater thermodynamic stability of high oxidation states in anions and involves the use of anhydrous hydrogen fluoride (aHF) as a solvent. The general method consists of combining an aHF soluble starting material (e.g. K_2NiF_6) with a Lewis fluoroacid (e.g. BF_3), which precipitates a neutral polymeric solid state fluoride:

$$2\,K^+ \quad + \quad NiF_6^{2-} + 2\,BF_3 \quad \longrightarrow NiF_4 \quad + \quad 2\,BF_4^- \quad + 2\,K^+ \qquad (1)$$

NiF_4 is formed in aHF below -60 °C, but loses F_2 on warming to give the rhombohedral form of NiF_3 (*R*-NiF_3). *R*-NiF_3 is itself thermodynamically unstable, and loses F_2 above 0 °C in aHF to give a lower fluoride. However, if separated from the byproduct (KBF_4) and dried below 0 °C, *R*-NiF_3 is stable at room temperature. It is shown from the unit

cell dimensions, a_o=5.1606(1) Å, α=55.594(1)° to be the smallest trifluoride of the first transition series. Variable temperature neutron powder diffraction experiments indicate that *R*-NiF_3 is the mixed valence species, $Ni^{II}Ni^{IV}F_6$ at 2 K, with two distinct close Ni–F interatomic distances: Ni(II)–F = 1.968(3) and Ni(IV)–F = 1.804(3) Å.

At room temperature, reaction (1) yields a different structural phase, with composition K_xNiF_3 ($x \approx 0.18$). This material has a pseudo-hexagonal tungsten bronze structure (*H*$_O$-K_xNiF_3), and is an ionic conductor, probably due to K^+ ions hosted in the lattice channels.

R-NiF_3 is capable of fluorinating a wide range of inorganic and organic substrates. These reactions have probably shed light on the mechanism of the Simons Electrochemical Fluorination (ECF) Process, an important industrial method of fluorinating organic compounds. It has long been speculated that NiF_3 plays a role in the ECF process, which uses nickel electrodes in aHF solvent. K_2NiF_6 also fluorinates organic compounds in aHF, but interestingly, yields different fluorinated products. The reduction of *R*-NiF_3 and K_2NiF_6 during fluorination reactions yields NiF_2. A method has been developed to regenerate NiF_6^{2-} from NiF_2.

The Synthesis, Characterization and Reactivity of High Oxidation State Nickel Fluorides

Table of Contents

List of Figures

List of Tables

Acknowledgments

I would like to thank Professor Neil Bartlett who provided guidance and shared his knowledge while giving me the opportunity to follow my research interests.

I am grateful to several Bartlett group members for their assistance and companionship as we shared space and time in the Bartlett lab: Bill Casteel, Byron Shen, George Lucier, Jörg Münzenberg, Phillippe Botkovitz, and Scott Elder. Another special colleague was Professor Boris Žemva, whose warm personality and ready willingness to teach made for fruitful collaborations. My gratitude also extends to those I have worked at the National Institute of Standards and Technology: Dr. Nicholas Rosov, and Dr. Jeffrey Lynn, who assisted in the collection and interpretation of the neutron powder diffraction data. I also thank Professor Angelica Stacy for her guidance and support .

I want to thank my dear family, friends and Numini for their encouragement and love through the good times and the hard times. Finally, I thank my husband Marc Whalen, to whom I am indebted for the gifts of his friendship, support and patience.

This work was supported by the U. S. Department of Energy under contract No. DE-AC03-76SF00098. I am also grateful to the National Physical Sciences Consortium for a graduate fellowship sponsored by the National Institute of Standards and Technology.

Chapter 1. Introduction and Experimental Methods

1.1. General Introduction

Examination of the highest attainable oxidation states of the transition metals reveals some periodic trends. In general, high oxidation states are more easily accessible for second and third transition series metals than for first transition series metals. The attainable oxidation states across a series increase as the d-orbitals are filled, until the greatest number of possible oxidation states for a given series is found near the middle of the series. The effective nuclear charge of the metal atoms increases to the right, since the poorly shielding d-electrons do not compensate for the increasing positive charge of each successive proton per element. This factor dominates finally, limiting the number of attainable oxidation states, due to the greater difficulty in removing an electron from an increasingly

Mn	**Fe**	**Co**	**Ni**	**Cu**
2	2	2	2	2
3, ***3***	3, ***3***	3, ***3***	3, ***3***	***3***
4, ***4***	4	4, ***4***	4, ***4***	***4***
Tc	**Ru**	**Rh**	**Pd**	**Ag**
			2	2
	3, ***3***	3, ***3***		3, ***3***
4	4, ***4***	4, ***4***	4, ***4***	
5	5. ***5***	5		
6	6	6		
Re	**Os**	**Ir**	**Pt**	**Au**
				2
		3		3, ***3***
4, ***4***	4, ***4***	4, ***4***	4, ***4***	4
5, *5*	5, ***5***	5, ***5***	5	5, ***5***
6, ***6***	6	6	6	
7, ***7***	7			

Figure 1.1. Range of Oxidation States for Late Transition Metal Fluorides (binary, ***anion***)

electronegative atomic core (Figure 1.1.). Thus, the most powerful oxidizers are found in high oxidation states of the late transition metal fluorides.

High oxidation states are readily generated by reaction with F_2, due to the low dissociation energy of the F–F bond (37.8 kcal·mol^{-1}), and the small size and high electronegativity of the fluorine ligand. The univalence of the fluorine ligand leads to high coordination numbers in high oxidation states, and this usually limits the attainable oxidation state in a binary fluoride to six (occasionally seven).

Nickel is near the end of the first transition series. Its effective nuclear charge is therefore high, and prior to recent work in these laboratories, the only known binary fluoride was NiF_2 with d-electron configuration d^8.[1,2] The new fluorides, NiF_4 and NiF_3 are both thermodynamically unstable with respect to loss of F_2, the former at -65 °C. The next neighbor to the right, copper, is found in oxidation states (III) and (IV) in anionic fluoride complexes,[3,4] but the red neutral parent binary fluoride (probably CuF_3) generated from CuF_6^{3-}, liberates F_2 at -78 °C in aHF, and this has prevented its isolation to date.[5]

A second general trend in high oxidation state chemistry is that the most stable high oxidation state available for a transition metal element will be found in an anionic species. For a given metal-ligand family of related species, the relative stability is: anionic > neutral > cationic. This is due to the lower electronegativity of the oxidized metal center in the electron-rich anion. As the negative charge is removed upon transition from an anion to a binary fluoride to a cation, the metal center becomes more

electronegative, causing the species to become an aggressive oxidizer, "hungry" for electrons. Neutral binary fluorides of high oxidation state Ni, Cu and Ag are all thermodynamically unstable, and form lower oxidation state metal fluorides at relatively low temperatures with liberation of fluorine.[1,2,5,6] The cationic species are some of the most powerful oxidizers known.[7]

In the case of silver, it has been shown from work in these laboratories[7] that even cationic silver(II) will oxidize oxygen (to O_2^+) or xenon (to XeF_2 derivatives) whereas the binary fluoride AgF_2 has long been known[8] and is thermodynamically stable. On the other hand, the binary fluoride AgF_3 loses F_2 (in aHF) at room temperature[6] although the long known salts of AgF_4^- are thermodynamically stable.[9]

The nickel system has similarities to that of silver. As with $KAgF_4$, $K_2Ni^{IV}F_6$ has been known for nearly fifty years.[10] The neutral parent of the anionic species NiF_6^{2-}, is NiF_4, the existence of which was demonstrated in these laboratories in 1989,[1] but which has yet to be structurally and magnetically characterized. NiF_4 exhibits thermodynamic instability with respect to the decomposition products, NiF_3 and F_2, above -60 °C when in the presence of anhydrous hydrogen fluoride (aHF). NiF_3 is itself thermodynamically unstable and liberates F_2 above 0 °C in aHF but has kinetic stability at 20 °C when dry. This product is designated *R*-NiF_3, due to its close packed rhombohedral structure (characteristic of other first row transition metal trifluorides), and is described in Chapter 2. There is an additional "trifluoride" obtained from the decomposition of NiF_4 with a pseudo-hexagonal tungsten bronze structure (H_O-K_xNiF_3). H_O-K_xNiF_3 hosts

potassium ions in open channels within the lattice, and has the molecular formula K_xNiF_3 ($x \approx 0.18$). This material will be described in Chapter 3.

Further attempts toward the isolation of NiF_4 are presented in Chapter 4, along with a description of two novel nickel compounds. In Chapter 5, the powerfully oxidizing behavior of NiF_4 in Lewis-acidified aHF (cationic Ni^{IV}) is described.

An important industrial process in the fluorination of organic compounds, the Simons Electrochemical Fluorination (ECF) Process, has long been speculated to involve a higher nickel fluoride. Some beginning work on the organic fluorination chemistry of *R*-NiF_3 and K_2NiF_6, and a comparison with analogous systems in the Simons ECF Process is presented in Chapter 6.

The inorganic endproducts of the organic fluorinations using NiF_3 or K_2NiF_6 are NiF_2 and KHF_2. Chapter 7 presents a novel room temperature method of regenerating NiF_6^{2-} salts from NiF_2 and alkali fluoride. The synthesis of the novel ternary fluoride, Li_2NiF_6 (which has not been previously synthesized because of the failure of conventional high temperature methods), is also presented in this chapter.

Since CuF_6^{2-} salts have been claimed,[4,11] it may be possible to isolate CuF_4. That should be even more potent in oxidation than even NiF_4. For the present, however, NiF_4 probably represents the most potent oxidizer achievable for the first transition series elements and certainly the highest binary fluoride likely to exist for nickel.

1.2 Experimental Methods

1.2.1. Apparatus

All solid reagents and products were handled in the dry argon atmosphere of a Vacuum Atmospheres (Hawthorne, CA) DRILAB drybox.

1.2.1.1. Vacuum Manifold

All reactions were carried out on a vacuum manifold (shown in Figure 1.2.), which was constructed of stainless steel and Monel tubing, and equipped at one end to withstand high pressures (≤ 30 atm) with Autoclave Engineers high pressure valves (▭) and unions (□) (Erie, PA, series 30VM). A fluorine gas supply was connected to a high-pressure (500 psi, 3.8 x 105 torr) fluorine service Helicoid gauge (Watertown, CT) (A). Lower pressures (to 5 atm) were employed at the other end of the manifold, which was constructed of ¼" o.d. stainless steel tubing, ¼" stainless steel Swagelok cross (✙) and "T" (⊤) unions, and equipped with Whitey valves (○) (Oakland Valve and Fitting Co., Oakland, CA). The vacuum line pressure was monitored with a Helicoid gauge (B) (F_2 service, 1500 torr, Watertown, CT), and low pressure measurements were made with the use of a thermocouple gauge head (C) (Varian Vacuum Products, Santa Clara, CA; model 0531) which was read by a millitorr gauge (Varian, model 801, 0-2 torr). There was a Monel cylinder (tower) packed with soda lime (D) which was connected at two points to the manifold, through which F_2, aHF, and other volatile fluorides were passed, in order to destroy them. Volatiles issuing from the soda lime tower were trapped in a liquid nitrogen cooled trap (E) before passing through a rotary vane mechanical pump.

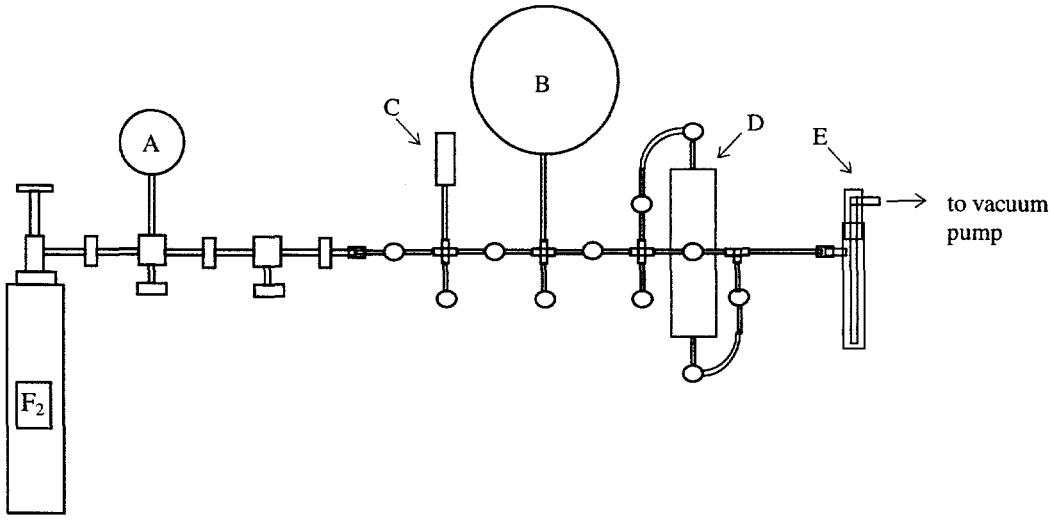

Figure 1.2. A Typical Fluorine-Handling Manifold

1.2.1.2. Fabrication of Reactors

For reactions carried out in aHF solvent, a sub-manifold was constructed of FEP (fluorinated ethylene propylene) tubing (AIN Plastics, Santa Clara, CA), Teflon valves (U. C. B. Chem. Dept. Machine Shop) as described elsewhere,[12,13] and Teflon Swagelok compression unions (Oakland Valve and Fitting Co., Concord, CA). The typical reactor was fabricated from the same materials, using a ⅜" or ½" Teflon T-union, and lengths of the appropriate size of FEP tubing which had been heated and crimped with pliers at one end to form a seal. The tubes were joined at right angles by the T-union, and fitted to a Teflon valve by a section of ⅜" tubing fused to ¼" tubing. Reactors were passivated for at least 2 h under ~ 2 atm F_2 prior to loading with solid reagents.

The tubes of different diameter were fused together using a forming glass funnel

(Glass Shop, U.C. Berkeley) (Figure 1.3) which had an inner diameter greater than the outer diameter of the FEP tubing.

It was important that the necked-down section of the glass funnel be smooth and gradual otherwise removal of the fused FEP was not possible. An aluminum rod was inserted through both sections of FEP tubing.

The glass funnel was heated (at the indicated area only) in a low flame and the larger diameter FEP tubing was forced into the funnel, which narrowed it down. The smaller diameter FEP tubing was then inserted into the narrowed opening of the larger

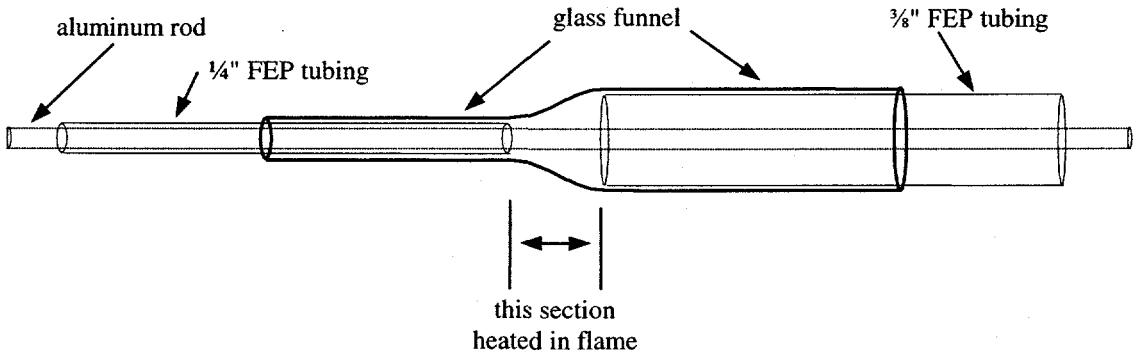

Figure 1.3. Fusing of FEP Tubing of Different Diameters

tubing. The two sections were heated and pressed toward each other repeatedly to eliminate air pockets, until the entire section was melted and fused, indicated by the perfect transparency of the softened plastic. As the fused assembly cooled, the inner forming rod was gently removed and the FEP was gently twisted until it came loose from the glass funnel. The ¼" end was forced over the hosebarb nozzle on the Teflon valve. The valve was connected to the sub-manifold by a section of ¼" FEP bent into an "S"

shape. If a reactor needed a third limb, a Teflon cross union could be used in place of a T-union in joining the tubes.

On occasion, lengths of FEP tubing were bent into unusual shapes, such as a "U" or a "W" by filling the tubing with sodium chloride and plugging both ends with stoppers. The tubing was then heated and bent into the desired shape, cooled with compressed air, and the sodium chloride shaken out and rinsed away with water. Filling the tube with sodium chloride was necessary when bending tubing through angles $\leq 90°$, which would otherwise cause the heated tubing to collapse. With these fabrication techniques, reactors could be optimally designed to fit experimental constraints. For instance, the addition reactor described in Chapter 6 (Figure 6.4.) was designed for the dropwise addition of a room temperature aHF solution to a cooled solution of aHF. The reactor was pressurized with dry N_2 to prevent distillation of the more volatile room temperature aHF.

After a loaded reactor was connected to the Teflon sub-manifold, the stainless steel and Teflon manifolds were passivated under ~2 atm F_2 for at least 2 h and then evacuated before use to prevent any moisture in the air from entering the reactor.

1.2.2. Materials and Preparation

1.2.2.1. Commercially Available Reagents

Gaseous reagents such as SiF_4, BF_3, PF_5, AsF_5, GeF_4 (Ozark Mahoning, Tulsa OK) and F_2 (97%; from Matheson, Newark, CA or Air Products, Allentown, PA) were used as supplied. SbF_5 (Ozark Mahoning) was distilled under dynamic vacuum prior to use. BiF_5 (Ozark Mahoning) was recrystallized from aHF prior to use, or synthesized by

the fluorination of BiF_3 which had been prepared by the addition of F_2 to Bi metal in aHF. Pure BiF_5 was obtained by sublimation of the fluorination product. NiF_2 (Ozark Mahoning) was fluorinated at 250 °C under 15 atm of F_2 before use. Hydrofluoric acid (Matheson) was stored over excess K_2NiF_6 in a reservoir, as the K_2NiF_6 would react with any H_2O present. As long as the red color of NiF_6^{2-} remained in solution, the HF was assured to be anhydrous. Prior to use in reactions, the aHF in the reservoir was frozen to -196 °C and then the reservoir opened to vacuum to remove non-condensable gases such as O_2 or O_3 which result from the oxidation of water present in the HF cylinder as supplied. The frozen aHF was then thawed and warmed with a hot water bath to ~ 30 °C. This freeze-pump-thaw (FPT) process was repeated twice, for a total of three FPT cycles before condensation of aHF into a reactor.

1.2.2.2. Rigorous Purification of K_2NiF_6

K_2NiF_6 (Ozark Mahoning, Tulsa, OK) was washed and recrystallized from aHF prior to use. It has been observed in this lab and noted by others[14,15,16] that upon addition of aHF to K_2NiF_6 a red-brown solid is precipitated. That this occurs with the material as supplied is not a surprise, since the high temperature/pressure synthesis may yield some Ni^{III} as K_3NiF_6, which disproportionates in aHF to form a reactive red-brown solid. However, sometimes a precipitate is observed even with rigorously purified K_2NiF_6. This reduction was not observed on every occasion of adding aHF to K_2NiF_6, nor was it related to the quality of a particular batch of K_2NiF_6. For instance, two separate reactors loaded with rigorously purified K_2NiF_6 from the same batch, gave reduction in one case and not

the slightest hint of reduction in the other. It is therefore quite certain that this is not a characteristic of K_2NiF_6 in aHF solution, but rather an indication of either (1) a small leak in the system, (2) incomplete passivation of the reactor or vacuum manifold, (3) presence of a reducing agent in the system (possibly H_2 produced by reaction of F_2 with the vacuum manifold), or (4) reaction with the container (even the largely inert FEP is thermodynamically capable of reducing the NiF_6^{2-}). In any case, because this insoluble solid would contaminate any insoluble products of reaction, the solution was decanted to the other arm of the reactor and the reaction carried out after separating the solution from the residue.

The rigorous purification of K_2NiF_6 from this red-brown solid and resultant KF (from $K_2NiF_6 \rightarrow 2\ KF + NiF_x + \frac{4-x}{2} F_2$) was effected through the use of a special reactor assembled with a ⅜" Teflon cross union and three 1" o.d. FEP tubes drawn down to ⅜" o.d. (Figure 1.4.). In this process, the K_2NiF_6 was first completely dissolved in aHF (in arm ①) and then the volume of the solution reduced until most of the K_2NiF_6 had recrystallized, save for ~0.5 mL. This solution, containing the highly soluble KF was decanted away from the bulk of the

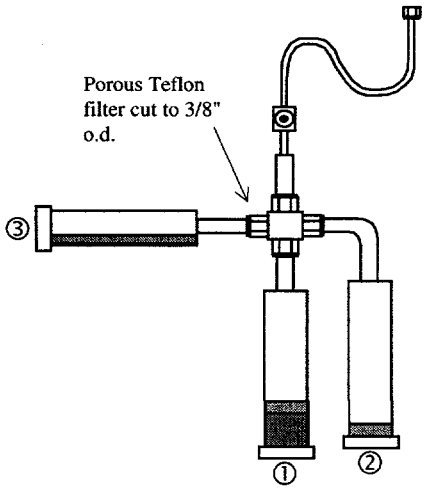

Figure 1.4. K_2NiF_6 Purification

recrystallized K_2NiF_6 into arm ② (sacrificing some K_2NiF_6 in the process). This was repeated three times. The fourth time the K_2NiF_6 was dissolved, it was poured into the third arm of the reactor, the opening of which was fitted with a porous Teflon filter (pore diameter, 5 - 10 μ) to separate the soluble K_2NiF_6 from the insoluble red-brown solid. The aHF was removed and the solids dried under dynamic vacuum for several hours. This yielded dark purple crystalline K_2NiF_6 in ③, a reddish-brown solid in ① (NiF_x, $2 < x < 3$) and an inhomogeneous pink and white solid in ② (K_2NiF_6 and KHF_2).

Purified K_2NiF_6 was used in most reactions. However, the use of purified K_2NiF_6 did not guarantee against the insoluble red-brown solid forming, as stated previously. In cases where this solid was observed to precipitate from the K_2NiF_6 upon dissolution in aHF, the precipitate was allowed to settle and the red solution was decanted to the other arm of the reactor where the reaction was carried out. This resulted in the loss of a small amount of K_2NiF_6, usually forming no more than ~0.005 g of insoluble red-brown solid. Such a solution necessarily contained a small concentration of $KF(HF)_y$.

1.2.2.3. K_3NiF_6

K_3NiF_6 (Ozark Mahoning) was used as supplied. The violet solid reacted with aHF to form a reactive red-brown solid, NiF_x ($2 < x < 3$), and a red solution containing NiF_6^{3-} and NiF_6^{2-}.[17] NiF_x used in organic fluorination chemistry was obtained by this disproportionation, and was subsequently washed free of soluble products by multiple repetitions of decantation and back-distillation of aHF.

1.2.2.4. $Ni(MF_6)_2$ Reagents (M = As, Sb, Bi)

Nickel(II) reagents such as $Ni(AsF_6)_2$, $Ni(SbF_6)_2$, and $Ni(BiF_6)_2$ were prepared by the addition of the respective Lewis acid to NiF_2 in aHF. The $Ni(AsF_6)_2$ was extremely soluble in aHF, $Ni(SbF_6)_2$ less so and $Ni(BiF_6)_2$ least. $Ni(BF_4)_2$ was not preparable by this method, nor by the reaction of Ni with BF_3 and F_2 in aHF. The XRPP of $Ni(AsF_6)_2$, shown in Appendix A, disagrees significantly with that published by Frlec, *et. al.*[18] $Ni(AsF_6)_2$ was found (via XRPD) to undergo a structural and, almost certainly, a compositional transition upon pumping at elevated temperatures or under high vacuum ($\sim 10^{-6}$ torr). The pattern in Appendix A is split into a complicated multi-lined pattern after exposure to high vacuum. Presumably, the $Ni(AsF_6)_2$ loses AsF_5 to form $NiFAsF_6$, which is less soluble in aHF and is expected to be of lower symmetry.

1.2.2.5. Tetramethyl Ammonium Salts of Lewis Fluoroacid Anions

Salts of $(CH_3)_4N^+$ with BF_4^-, PF_6^-, AsF_6^- and SbF_6^- were prepared by the following method. A known quantity of $(CH_3)_4N^+Cl^-$ was loaded into a ⅜" FEP T-reactor and aHF condensed onto it, liberating HCl, which was evacuated from the reactor. Gaseous BF_3, PF_5 or AsF_5 was admitted to the reactor, in each case precipitating a colorless solid. In the case of SbF_5, aHF was added to the liquid SbF_5 to form a solution before decanting onto the $(CH_3)_4N^+$ dissolved in aHF. Solids were evacuated to dryness before use. Solubilities of the $(CH_3)_4N^+$ salts were found to be in accord with:

$$HF_2^- > BF_4^- > PF_6^- \approx AsF_6^- >> SbF_6^-$$

1.2.3. X-ray Powder Diffraction (XRPD)

X-ray Powder diffraction data were collected on Kodak Industrex AA film mounted inside a General Electric Debye-Scherrer camera. An Enraf Nonius FR 590 X-ray generator, fitted with a copper target tube powered at 40 kV and 20 mA provided the Cu K_α X-rays, which were passed through a nickel filter. In most cases the exposure time was 12 hours. The crystalline samples were loaded into 0.5 or 0.3 mm quartz capillaries which had been dried for at least 12 hours at ~700 °C under dynamic vacuum (~5 x 10^{-8} torr). The solids were loaded into the funnel end of the capillary in the DRILAB, and then tapped down to form a column of solid no less than 1 cm in height. A Norelco film-measuring device, with light box, was used to measure the X-ray powder patterns (XRPP). Microsoft Excel for Windows (v. 4.0 through MSOffice 97), U-fit v. 1.2 and Lazy Pulverix were used in the determination and refinement of unit cell dimensions.

1.2.4. SQUID Magnetometry

Magnetic measurements of powder samples were carried out in a Quantum Design (San Diego, CA) SQUID magnetometer (model MPMS). The sample container was fabricated from Kel-F, and was one of two models. The early version was in the form of two cylindrical cups, one of which fit inside the other to provide an internal volume of 6.5 mm in diameter and 6.5 mm in length. The bottom cup was loaded with sample and then capped by the larger cup. A gas-tight seal was achieved by applying a small amount of halocarbon grease around the outside of the bottom cup. The cups were then tied together with nylon line. The later version of the sample container was a cylinder that was

threaded at one end to receive a screwed-in cap. The bottom of the container was solid Kel-F equal to the length of the threaded section, in order to maintain a symmetrical balance of mass about the internal volume of the sample chamber. A seal was made by screwing the lid in tightly with an aluminum screwdriver. Sample containers were suspended by a length of cotton thread in the magnetometer.

1.2.5. Neutron Powder Diffraction

The neutron powder diffraction measurements were made with the high resolution powder diffractometer (BT-1) at the Reactor of the National Institute of Standards and Technology, Gaithersburg, MD, in collaboration with research scientists, Dr. Nicholas Rosov and Dr. Jeffrey Lynn.

Samples for neutron powder diffraction were contained in a cylindrical aluminum sample container, which was 6.95 mm (i.d.), 9.0 mm (o.d.) and 31.8 mm long. The cap for the sample container was threaded and a seal was made with a Teflon o-ring which fit into a groove on the container. The cap was hex-cut so as to facilitate tightening with a wrench. On top of the cap was a threaded connector, such that the sample container could be attached to the end of a pole which was inserted into a cryostat. The crysostat containing the sample was then positioned in the path of the neutron beam. Data were collected at several temperatures to ascertain if nuclear and/or magnetic phase transitions took place at low temperature. Structure solutions were achieved with the General Structure Analysis System (GSAS).[19] The advantage of analyzing these fluorides by neutron powder diffraction is that the absorption cross-sections of Ni and F are

comparable in magnitude, unlike the situation in X-ray powder diffraction, where the atomic form factors are related to the electron density at each atom. Nickel, atomic number 28, diffracts X-rays much more strongly than F, atomic number 9. Thus, except for certain reflections ($h + k + l \neq 2n$), the X-ray diffraction of NiF_3 is largely due to scattering by the nickel. In addition, the absorption correction required in X-ray diffraction is not necessary in neutron diffraction, as there is very little absorption of neutrons.

1.2.6. Infrared Spectroscopy

Infrared spectra were measured on a Nicolet Fourier Transform Spectrophotometer. Volatile materials were expanded into a 10 cm length Monel cell fitted with AgCl windows and a Whitey valve. Usually pressures of 10 - 25 torr were used.

1.2.7. Nuclear Magnetic Resonance (NMR) Spectroscopy

Collection and interpretation of NMR data were carried out in collaboration with Dr. J. Marc Whalen, postdoctoral researcher in the Neil Bartlett Group. The products of organic fluorination reactions were sealed into 4mm (o.d.) FEP tubes, which were then inserted into a standard glass NMR tube for analysis. NMR data were collected on Brüker AM-400 or AM-500 Spectrometers at spectrometer frequencies (MHz): 400.136 (^{1}H), 376.502 (^{19}F), 100.614 (^{13}C) and 36.145 (^{14}N), in aHF solvent at 24 °C. The aHF solvent resonance is a singlet at 8.52 ppm, $\Delta\nu_{1/2}$ = 8 Hz (^{1}H) and at -190.5 ppm, $\Delta\nu_{1/2}$ = 30 Hz (^{19}F). Samples were referenced externally with respect to the neat liquid references:

$CFCl_3$ (^{19}F), $Si(CH_3)_4$ (^{13}C, ^{1}H), and CH_3NO_2 (^{14}N).

Corrected normalized integrations of ^{19}F NMR spectra were used to determine the relative concentrations of the products resulting from the fluorination of organic molecules in Chapter 6. This was done by first assigning the ^{19}F NMR peaks to groups of one or more chemically equivalent nuclei in the fluorinated molecules, by comparison of the chemical shifts with those found in the compilation of Dungan and van Wazer.[20] Since a given NMR resonance may represent a group of chemically equivalent nuclei, the integration of each resonance was corrected by dividing the absolute value of the integration by the number of chemically equivalent nuclei represented by the resonance. This ensured that each integration was proportional to the concentration of the molecule in solution. The relative concentrations of products in a sample were then obtained by normalizing the ratio of corrected integrations to 100.

Since the integration of peaks in solution NMR spectra only measure the relative concentrations of dissolved species, it should be noted that the relative concentrations of fluorocarbons such as CF_4 and CF_3CF_3 may be underestimated due to their partial solubility in aHF.

1.3. References

[1] Žemva, B., Lutar, K., Jesih, A., Casteel, W. J. Jr., and Bartlett N. *J. Chem. Soc. Chem. Commun.* **1989**, 346.
[2] Žemva, B.; Lutar, K.; Chacón, L.; Fele-Beuermann, M.; Allman, J.; Shen, C.; Bartlett, N. *J. Am. Chem. Soc.* **1995**, *117*, 10025.
[3] Klemm, W.; Huss, E. *Z. Anorg. Allg. Chem.* **1949**, *258*, 221.
[4] Harnischmacher, W.; Hoppe, R. *Angew. Chem.* **1973**, *85*, 590.
[5] Bartlett, N.; Lucier, G.; Shen, C.; Casteel, Jr., W. J.; Chacón, L.; Munzenberg, J.; Žemva, B. *J. Fluor. Chem.* **1995**, *71*, 163.
[6] Žemva, B.; Lutar, K.; Jesih, A.; Casteel, W. J. Jr.; Wilkinson, A. P.; Cox, D. E.; Von Dreele, R. B.; Borrmann, H.; Bartlett, N. *J. Am. Chem. Soc.* **1991**, *113*, 4192-4198.
[7] Lucier, G.; Shen, C.; Casteel, Jr., W. J.; Chacón, L.; Bartlett, N. *J. Fluor. Chem.* **9115**, *72*, 157.
[8] Ruff, O.; Giese, M. *Z. Anorg. Allg. Chem.* **1934**, *219*, 143.
[9] Hoppe, R. *Z. Anorg. Allg. Chem.* **1957**, *292*, 28-??
[10] Klemm, W.; Huss, E. *Z. Anorg. Chem.*, **1949**, *258*, 221.
[11] Christe, K. O.; Wilson, W. W.; Wilson, R. D. *Inorg. Chem.* **1980**, *19*, 3254.
[12] Lutar, K.; Jesih A.; Leban, I.; Zemva, B.; Bartlett, N. *Inorg. Chem.* **1989**, *28*, 3467.
[13] Žemva, B.; Hagiwara, R.; Casteel, W. J., Jr.; Lutar, K.; Jesih, A.; Bartlett, N. *J. Am. Chem. Soc.* **1990**, *112*, 4846.
[14] Matwiyoff, N. A.; Asprey, L. B.; Wageman, W. E.; Reisfield, M. J.; Fukushima, E. *Inrg. Chem.* **1969**, *8(4)*, 750.
[15] Stein, L; Neil, J. M.; Alms, G. R. *Inorg. Chem.* **1969**, *8(11)*, 2472.
[16] Court, T. L.; Dove, M. F. A. *J. Chem. Soc. Dalton Trans.* **1973**, 1995.
[17] Stein, L.; Neil, J. M.; Alms, G.R. *Inorg. Chem.* **1969**, *8(11)*, 2472.
[18] Frlec, B.; Gantar, D.; Holloway, J. H. *J. Fuor. Chem.* **1982**, *19*, 485.
[19] Larson, A. C.; Von Dreele, R. B. Los Alamos Laboratory Report No. LA-UR-86-748, 1987.
[20] Dungan, C. H.; van Wazer, J. R. Compilation of Reported F^{19} NMR Chemical Shifts", John Wiley and Sons, New York, 1970.

Chapter 2. Rhombohedral NiF_3 (*R*-NiF_3)

2.1. Introduction

In the early 1970's, Court and Dove[1] claimed to have synthesized nickel trifluoride (NiF_3) by the room temperature reaction in aHF:

$$K_2NiF_6 + 2\ AsF_5 \longrightarrow NiF_3 + 2\ KAsF_6 + \tfrac{1}{2}\ F_2 \qquad (1)$$

They reported that a black precipitate was formed, which decomposed to NiF_2 during attempts to extract the byproduct, $KAsF_6$. With a magnetic moment of 2.41 β obtained from EPR data, they determined that the material must be $Ni^{III}F_3$, with a low-spin d^7 electron configuration. They provided no structural information, as they were unable to isolate the black material. In a later publication, Court and Dove describe the black solid obtained from the reaction of K_2NiF_6 with AsF_5 or BF_3 in aHF.[2] They were still unable to isolate the black solid from the byproducts, $KAsF_6$ or KBF_4, without its undergoing decomposition to a brown fluoride of the composition $NiF_{2.2}$.

Similar chemistry was undertaken by Christe and Wilson,[3] but with the aim of

producing chemically pure fluorine gas through the decomposition of thermodynamically unstable binary fluorides. The following reactions were carried out between dry solids in a stainless steel reactor:

$$A_2MF_6 + 2\,BiF_5 \longrightarrow 2\,ABiF_6 + MF_{4-x} + (x/2)\,F_2 \qquad (2)$$

$$A_2MF_6 + TiF_4 \longrightarrow A_2TiF_6 + MF_{4-x} + (x/2)\,F_2 \qquad (3)$$

where M = Ni, Cu or Mn, and A = K, Cs. Heating the dry solids to 60 - 70 °C liberated chemically pure F_2. While this was significant in producing chemically pure F_2, the possibility of isolating the thermodynamically unstable tetrafluorides was not pursued by these researchers.

A search for a route to authentic AgF_3, stimulated by the claim of Bougon and his coworkers to have prepared that fluoride,[4] led Bartlett and his coworkers to prepare it from AgF_4^- salts using BF_3 or other F^- acceptors.[5] This in turn led to a reinvestigation of the interaction of F^- acceptors with NiF_6^{2-} and similar applications to other systems.[6] This established the existence of AgF_3 and NiF_4 and provided routes to high purity RuF_4 and OsF_4.

In that study, a brown solid precipitated on addition of AsF_5 to a solution of $(XeF_5)_2NiF_6$, and was readily separated from the XeF_5AsF_6 product, which is highly soluble in aHF even at -60 °C:

$$(XeF_5)_2NiF_6 + 2\,AsF_5 \xrightarrow[aHF]{-60\ ^\circ C} NiF_4 + 2\,XeF_5AsF_6 \qquad (4)$$

Addition of two equivalents of KF to the brown solid below -60 °C in aHF

quantitatively converted it to K_2NiF_6:

$$NiF_4 + 2\,KF \longrightarrow K_2NiF_6 \qquad (5)$$

so establishing that the brown solid was the tetrafluoride. The loss of F_2 from the NiF_4 was found to occur above -60 °C and was rapid at temperatures closer to room temperature, the product being a black solid. Rough tensimetric results were in accord with:

$$NiF_4 \longrightarrow \tfrac{1}{2}\,F_2 + NiF_3 \qquad (6)$$

Most of these early studies of NiF_4 and NiF_3 were carried out at the Josef Stefan Institute, in Ljubljana, Slovenia in collaboration with the Bartlett Group at Berkeley.

It was clear from the early studies that NiF_3 could be prepared and separated from highly soluble side products such as XeF_5AsF_6 by working below room temperature. However, at the outset of this work, the conditions for the preparation of high purity NiF_3 from alkali hexafluoronickelate(IV) salts had not been established, nor had structural or magnetic characterization of the NiF_3 been undertaken. The advantage of K_2NiF_6 as a starting material was that it is commercially available, unlike $(XeF_5)_2NiF_6$.

2.2 Experimental

2.2.1 Synthesis of *R*-NiF_3

2.2.1.1. K_2NiF_6 with BF_3

K_2NiF_6 (790 mg; 3.15 mmol) was dissolved in aHF (4-5 mL) in one arm of an FEP T-reactor, which was cooled to 0 °C. A two-fold molar excess of BF_3 (measured out

tensimetrically) was added to the solution over a span of 2 h. A tan precipitate of NiF_4 settled to the bottom of the reactor, below a clear, slightly yellow-tinted solution. The tan color changed to black as F_2 evolved. Decomposition was considered to be complete when F_2 evolution had ceased (~2 h). The byproduct, KBF_4, was extracted by decantation of its solution in aHF at 0 °C followed by back distillation of the aHF and further washing at 0 °C and decantation (7 times). The black residue was dried at 0 °C under dynamic vacuum. This yielded black *R*-NiF_3 (346 mg; 2.00 mmol, 95% yield).

2.2.1.2. K_2NiF_6 with BiF_5

K_2NiF_6 (309 mg; 1.23 mmol) was loaded into one arm of an FEP T-reactor and the solid Lewis fluoroacid, BiF_5 (754 mg; 2.48 mmol) was placed in the other arm. Each reagent was dissolved in aHF (~3 mL each). Both solutions were cooled to 0 °C. The solution of BiF_5 was decanted dropwise into the solution of K_2NiF_6 to precipitate tan NiF_4. When the addition was complete, the supernatant solution was colorless, and the tan color slowly changed to black over 6 h at 0 °C, with evolution of F_2. Cessation of F_2 evolution signaled completion of the reaction. The byproduct $KBiF_6$ was extracted by decantation of its aHF solution at 0 °C (with two back-distillations and washings) and the black residue was dried at 0 °C under dynamic vacuum. This gave *R*-NiF_3 (142 mg; 1.23 mmol, 99% yield).

2.2.1.3. Li_2NiF_6 with BF_3

Li_2NiF_6 has been used in place of K_2NiF_6 (the synthesis of Li_2NiF_6 is described in

Chapter 7). This gave a product of excellent microcrystallinity, due to the lower solubility (relative to K_2NiF_6) of Li_2NiF_6 in aHF (~0.005 g/ mL at 0 °C; K_2NiF_6: ~0.5 g/mL at 0 °C). This lower solubility provided for much slower crystallization of *R*-NiF_3 from the aHF solution.

A mixture of Li_2NiF_6 and $LiHF_2$ (soluble products of the synthesis of Li_2NiF_6; approx. 1.950g $LiHF_2$ and 1.583 g Li_2NiF_6) was placed in one arm of a T-reactor made with 1" (o.d.) FEP tubing, and aHF (~ 40 mL) was condensed onto it. The Li_2NiF_6 was separated from the bulk of the $LiHF_2$ in the same manner as described for the separation of KF from K_2NiF_6 in Section 1.2.3.2. After the separation was effected, the aHF was removed and the solids dried and taken back into the drybox where the arm containing the $LiHF_2$ was replaced with an empty tube. Once again, aHF (~40 mL) was added to the Li_2NiF_6 (approx. 1.35 g; 7.23 mmol), to give a medium-red solution which was cooled to 0 °C, at which temperature the bulk of the Li_2NiF_6 was not soluble. BF_3 (17.8 mmol) was added over a period of 2 days. The reaction between the Li_2NiF_6 and BF_3 was very slow with no perceptible reaction upon addition, but after sitting overnight, a thin film of black solid coated the walls. The reactor was gently agitated to bring more Li_2NiF_6 into solution, and the BF_3 addition and periodic gentle agitation was continued. After the final addition, the black *R*-NiF_3 precipitate was allowed to settle overnight again, before extraction of $LiBF_4$ was begun. The highly soluble $LiBF_4$ (solubility: 304.5 mg/mL at 0 °C) was extracted by three washings, to yield a black solid (0.878 g, ~73% yield) in which small reflective flake-like particles were visible. The XRPP of this sample showed

very sharp lines, characteristic of a highly crystalline powder (Table 2.1).

2.2.2. X-ray Powder Diffraction

The black material gave a rhombohedral XRPP that was characteristic of the trifluorides of the first transition series (Table 2.1.). Data obtained from the sample of *R*-NiF_3 prepared by the reaction of Li_2NiF_6 with BF_3 provided the most precise unit cell

Table 2.1. X-Ray Powder Diffraction Data (Cu K_α radiation, Ni filter) for Rhombohedral NiF_3 (Unit cell: $a_o = 5.168(2)$Å; $\alpha = 55.46(3)°$; $V = 87.3(2)$Å^3, $Z = 2$).

	$1/d^2_{hkl} \times 10^4$				
I/I_o	**obs**	**calc**	***h***	***k***	***l***
vs	810	810	1	1	0
m	1515	1512	2	1	1
vw	1728	1729	1	0	$\bar{1}$
s	2257	2256	2	0	1 *
vvw	2538	2540	2	0	0
w	3243	3242	2	2	0
s	3843	3835	3	2	1
w	4265	4269	2	1	$\bar{1}$
w	4314	4320	3	3	2
vw	4987	4971	3	1	0
w	5178	5188	2	$\bar{1}$	$\bar{1}$
vvw	6036	6049	4	2	2
vw	6455	6425	4	3	3
		6467	4	3	2 *
vvw	6914	6917	2	0	2
vvw	7412	7444	3	1	$\bar{1}$ *
vw	7767	7728	3	0	$\bar{1}$
		7778	4	3	1
vvw	8411	8430	3	2	$\bar{1}$
		8422	4	4	4
vvw	9031	9023	4	2	0
vvw	9463	9457	2	2	2
vvw	9891	9884	5	3	2

*F-only reflections; these also obey $h + k + l = 3(2n + 1)$.
The hexagonal cell has $a_o = 4.809(4)$Å, $c_o = 13.076(2)$Å, $V = 261.9(5)$ Å^3, $Z = 6$, $V/Z = 43.65(8)$ Å^3, $c/a = 2.72$.

parameters. Although the reflections for which $h + k + l \neq 2n$ are due to F atom scattering alone, these are insufficient in number and not sufficiently precise in their relative intensities to provide for the placement of the fluorine atoms (the two nickel atoms, by symmetry are at 0,0,0 and ½,½,½). Nor was it possible, with the X-ray data, to decide which of the two possible space groups, R3c (no. 167) or R3 (no. 165), was appropriate. The first series transition metal trifluorides, TiF_3, VF_3, CrF_3, FeF_3 and CoF_3 were refined in R3c (MnF_3 is an exception due to a Jahn-Teller distortion of the high spin d^4 electron configuration[7]).[8] However, the palladium relative, PdF_3, was demonstrated to have the mixed valence formulation, $Pd^{II}Pd^{IV}F_6$, for which R3 was found to be appropriate.[9] To determine the structure, a neutron diffraction study was undertaken.

2.2.3. Neutron Powder Diffraction

Neutron powder diffraction data were collected at 2 and 295 K, in addition to several temperatures in the 30-60 K range. The 295 K data are shown in Figure 2.1.

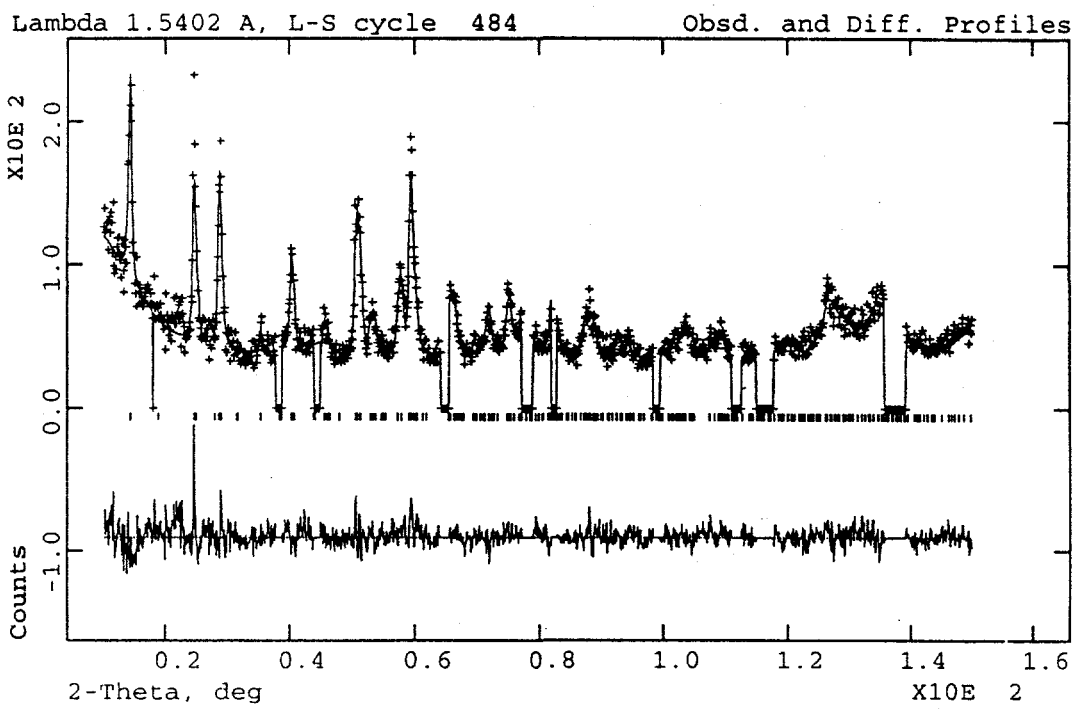

Figure 2.1. Fitted Neutron Powder Diffraction Pattern for *R*-NiF_3. Data collected on BT-1 at 295 K. The observed values are shown as (+) and the calculated values from the best fit are shown as a curve. A difference (I_{obs} - I_{calc}) curve and the reflection positions are also shown.

The nickel atoms were placed in positions 1*a* (0,0,0) and 1*b* (½, ½,½), and the fluorine atoms in 6*f* (*x*, *y*, *z*) of space group R3. The final refined values of structural parameters for the 2 and 295 K refinements are given in Table 2.2.

Table 2.2. Distances and Angles for *R*-NiF_3 at 2 and 295 K, Refined in R3.

		2 K	295 K
a_o (Å)		5.1472(1)	5.1606(1)
α (°)		55.490(1)	55.594(1)
V (Å^3)		86.331(2)	87.246(2)
	x	-0.1191(6)	-0.1173(6)
F	*y*	0.5967(7)	0.6038(7)
	z	0.2641(8)	0.2698(10)
	Ni(1)	0.99(11)	1.64(11)
U_{iso} x10^2	Ni(2)	0.79(11)	1.58(4)
	F	0.89(4)	1.19(11)
Ni(1)–F (Å)		1.958(4)	1.928(4)
Ni(2)–F (Å)		1.814(4)	1.850(4)
Ni(1)–F–Ni(2) (°)		137.58(8)	138.13(9)
χ^2		1.218	1.282
R_P		0.0699	0.0622
wR_P		0.0845	0.0740

At 2 K, two distinct Ni–F bonds indicate that *R*-NiF_3 is a mixed valence material with composition, $Ni^{II}Ni^{IV}F_6$. There are two Ni^{II} distances in NiF_2 (rutile structure): 2.00(2) and 2.01(1) Å,[10] which is comparable to the long Ni–F bond of *R*-NiF_3, Ni(1)–F 1.958(4) Å. The short Ni–F bond is 1.814(4) Å, which is compatible with that reported for K_2NiF_6 at room temperature, 1.776(8) Å.[11] Ni(IV) in K_2NiF_6 has a low spin d^6 configuration, and as such has the smallest possible octahedron of any first transition series metal. The difference in length between the two Ni–F bonds, Ni(1)–F and Ni(2)–F, is 0.144 Å. At 295 K, the difference in length of the two Ni–F bonds has decreased to 0.078 Å. An ORTEP of the room temperature structure is shown in Figure 2.2.

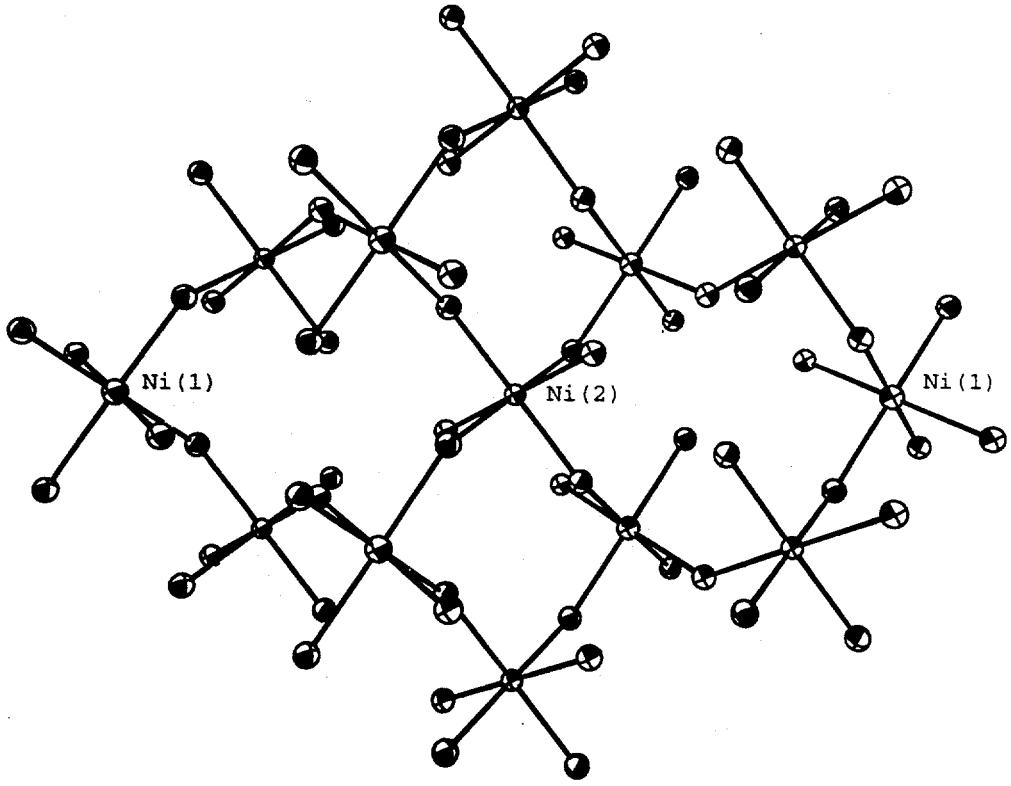

Figure 2.2. View of the Bimolecular Unit Cell of *R*-NiF_3

Initially, extra peaks were observed in the neutron powder diffraction pattern when the temperature was in the 30-60 K range. These peaks disappeared outside of this temperature region and reappeared upon warming or cooling into the region. In order to monitor the temperature more carefully, helium was admitted into the sample, previously filled with argon (argon condenses below 50 K, causing poor heat transfer between the sample and the refrigerant). After helium was admitted to the container, the appearance and disappearance of the peaks in the 30-60 K region was not observed. Later, a second pattern appeared, indicating that the sample had partially decomposed (the moisture content of the helium filled drybox at NIST must have been high). Further experiments

should be undertaken to investigate the peaks observed in the 30-60 K region prior to the accidental decomposition, as they did not correspond to known argon diffraction lines, and may have been evidence of a magnetic superlattice.

2.2.4. Magnetic Susceptibility

The magnetic susceptibility of *R*-NiF_3 between 280 and 6 K is shown in Figure 2.3. There is an onset of field dependence of the susceptibility, beginning around 250 K. This field dependence persists until ~25 K, and then collapses on further cooling. The essentially field-independent magnetic moment at room temperature is 2.1 β.

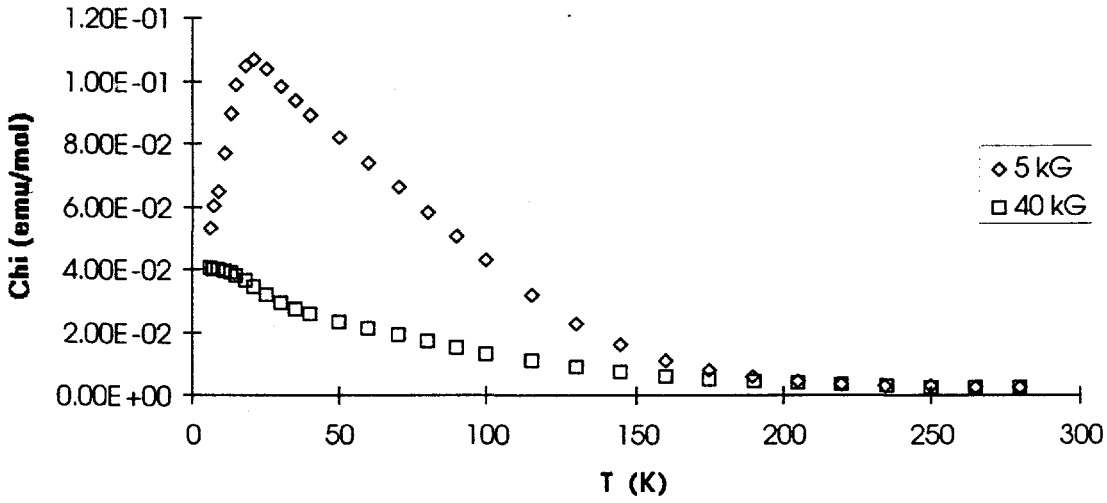

Figure 2.3. Magnetic Susceptibility of *R*-NiF_3 (280 to 6 K; 5 and 40 kG)

2.2.5. Thermal Stability

The thermal stability of *R*-NiF_3 was assessed by determining the decomposition temperature of the dry solid. The sample was heated above room temperature slowly, while the release of F_2 from the solid was detected by the formation of I_2 from KI. The KI

was packed into a column made from ¼" FEP tubing, containing a section of NaF (~1") long, to react with any HF which may still be present in the solid) followed by KI (~12"), and held in place by a small plug of quartz wool at each end. This column was evacuated to 10^{-7} torr before use. The column was installed between the vacuum line and the sample container, a small Pyrex glass bulb. The bulb was heated in an oil bath, with the column opened slightly to dynamic vacuum. A yellowing of the column occurred near 39 °C, which intensified and coincided with the black solid becoming brown. Rapid formation of I_2 at 52-53 °C signaled major decomposition of the *R*-NiF_3 at that temperature. No further major I_2 release occurred until 83 °C. The remaining solid was dark red-brown and was characterized by low crystallinity (XRPP shown in Table 2.3). A similar pattern is obtained for the material remaining after the reaction of solid R-NiF_3 with a molar excess of Xe gas, as will be described in section 2.2.7.

A second measure of thermal stability was the decomposition in aHF at ~ 20 °C. When *R*-NiF_3 was prepared from the reaction of K_2NiF_6 with BF_3, the decomposition of *R*-NiF_3 in aHF at ~ 20 °C was usually complete within 24 h, but in the instance of the *R*-NiF_3 precipitated by a stoichiometric quantity of BiF_5, the decomposition was much slower as follows: aHF (1.5 mL) agitated with *R*-NiF_3 (83.2 mg; 0.72 mmol) showed little evidence of change for 2 days, but after 9 days, the entire sample was pale tan in color. Highly crystalline NiF_2, identified by XRPD (71.5 mg; 0.74 mmol) was recovered.

Table 2.3. X-Ray Powder Diffraction Data (Cu K_α, Ni filter) for NiF_x ($2 < x < 3$), heavy background and broad lines indicate small particle size in each sample.

Thermal Decomposition Product						***R*-NiF_3 (dry) + Xe Product**		
	$1/d^2_{hkl}$ x 10^4						**$1/d^2_{hkl}$ x 10^4**	
I/Io	**obs**	**calc[§]**	***h***	***k***	***l***	**I/Io**	**obs**	**calc[‡]**
s	780	772	1	0	1	---	---	744
w	1465	1468	1	0	2	---	---	1412
m	1634	1620	1	1	0	w	1581	1566
vs	2162	2160	2	0	0	m	2088	2088
vw	2395	2392	2	0	1	---	---	2310
vw	3187	3088	2	0	2	---	---	2978
vs	3712	3712	0	0	4	s	3588	3712
m	4968	4860 5092	3 3	0 0	0 1	vw	4814	4698 4920

[§] hexagonal cell with: $a_o = 4.97(2)$Å, $c_o = 6.57(2)$Å, V = 140.4 Å^3; volume fits ~9 F atoms, with 4 Ni.
[‡] hexagonal cell with: $a_0 = 5.05(2)$Å, $c_o = 6.71(2)$Å,V = 148.3 Å^3; volume fits ~10 F atoms with 4 Ni.

2.2.6. Elemental Analysis

Elemental analyses were performed at the Josef Stefan Institute in Ljubljana, Slovenia. The preparation of pure samples of *R*-NiF_3 for elemental analysis was difficult due to the removal of poorly soluble K^+ salts, which were byproducts of the reactions of K_2NiF_6 with Lewis fluoroacids. The decomposition of *R*-NiF_3 at room temperature in aHF necessitated washing at 0 °C, but this greatly diminished the solubilities of the K^+ salts, requiring repeated washings. Removal of salts was aided by bringing the entire reaction product (*R*-NiF_3 and KX) to dryness before washing with aHF (this probably crystallized K^+ and X^- adsorbed on the *R*-NiF_3). The complete removal of the salts was often associated with some NiF_2 production (XRPD), which was to be avoided, so K^+ salt removal was rarely complete. For a sample of *R*-NiF_3 prepared by the reaction of K_2NiF_6

and BF_3 with an XRPP showing only the lines of the rhombohedral phase, the following was found (two separate analyses for F and Ni): F, 49.7, 49.9; Ni, 48.6, 48.6; K, 0.4; B 1.6%. NiF_3 with a 0.04 KBF_4 impurity requires: F 49.7; Ni, 48.6; K, 1.3; B, 0.4%. NiF_3 requires: F, 49.3; Ni 50.7%. The K, Ni and F analyses were accurate to ± 0.05%, but the B (± 0.25%) analysis was not as reliable. The low K and high B content could signify some $NiFBF_4$ impurity in the case of this analyzed sample but the presence of such an impurity was not indicated by XRPD.

2.2.7. Chemical Reactivity

The oxidizing power of *R*-NiF_3 was tested by reaction with the following inorganic substrates: Xe, XeF_2, KF and LiCl. *R*-NiF_3 is an excellent fluorinator of organic compounds as well, as will be discussed in Chapter 7.

Xe. Dry *R*-NiF_3 does not interact with gaseous Xe at 20 °C, but if *R*-NiF_3 is first exposed to aHF vapor (100 torr), it then reacts with a multimolar excess of Xe (~1 atm), to form XeF_2 (identified by IR[12] and XRPP[13]) and a light red-brown solid. The XRPP of the light red-brown nickel fluoride was broad-lined, and similar to that of the product of thermal decomposition of *R*-NiF_3 at 83 °C, as shown in Table 2.3.

R-NiF_3 in an aHF suspension reacts with gaseous Xe at ~20 °C to form XeF_4 (identified by XRPP[11]) and a tan solid. The trifluoride was suspended in aHF (~2.5 mL) in one arm of an FEP T-reactor, and agitated in the presence of a known quantity of Xe for ~8 h. The colorless soluble products were obtained by decanting the aHF solution to

the other arm, and the aHF removed under vacuum at -50 °C. *R*-NiF_3 (108 mg; 0.93 mmol) with Xe (0.2 mmol) gave XeF_4 (41 mg; 0.2 mmol) and NiF_x (95 mg; 0.8 NiF_2 + 0.13 NiF_3 would give 92.4 mg).

XeF_2. A solution of XeF_2 in aHF at ~20 °C was quickly added to an equivalent quantity of *R*-NiF_3 under aHF at ~20 °C, with agitation, which produced a tan solid in less than 6 h. Decantation of the colorless supernatant aHF solution followed by washing left a tan solid (NiF_2, XRPD) and evaporation of aHF from the combined decantate and washings at ~-40 °C yielded a nearly colorless sublimate identified as XeF_4 (XRPD[11]).

KF. With KF (0.0559 g; 0.962 mmol), *R*-NiF_3 (0.1094 g; 0.946 mmol) formed K_2NiF_6 and NiF_2 when combined in aHF (~2 mL) and agitated for a period of one day at ~ 20 °C:

$$2\ R\text{-}NiF_3 \quad + \quad 2\ KF \quad \longrightarrow \quad K_2NiF_6 \quad + \quad NiF_2 \qquad (7)$$

The products were separated by decantation of the aHF solution with several washings and the products dried and weighed. The gravimetry was in accord with the observation (XRPD) that the soluble product was made up of K_2NiF_6 and KH_2F_3 (0.1040g), and the insoluble product was NiF_2 (0.0587 g).

LiCl. With LiCl, *R*-NiF_3 reacted as a dry solid when an equimolar mixture of *R*-NiF_3 and LiCl were ground together in an agate mortar in the drybox. The reaction was vigorous and incandescent, the yellow green product being a mixture of NiF_2 and LiF (XRPD). The reaction was much more controlled when an aHF solution of LiCl was

added to a suspension of *R*-NiF_3 in aHF, each solution held at 0 °C. Chlorine gas was evolved as the *R*-NiF_3 was simultaneously converted to yellow-green NiF_2 (XRPD).

2.3. Results and Discussion

The first goal of this dissertation research was to isolate and characterize the thermodynamically unstable black solid, NiF_3. The strategy which was successful in the isolation of AgF_3 (low temperature extraction of byproducts and removal of aHF), was employed here as well.[14] The reaction between K_2NiF_6 and BF_3 in aHF was studied at various temperatures between -65 °C and 0 °C (the room temperature reaction forms the structural variant *Ho*-K_xNiF_3, and will be described in Chapter 3). At temperatures below -60 °C (the onset of decomposition of NiF_4 in aHF), the reaction yielded the dark-brown material proven to be NiF_4 by Žemva, *et. al.*:[4]

$$K_2NiF_6 + 2\ BF_3 \xrightarrow[\text{aHF}]{<-\ 60\ ^\circ C} NiF_4 + 2\ KBF_4 \qquad (8)$$

When the reaction mixture was allowed to warm above -60 °C, fluorine evolution was observed, concurrently with a slow change in color of the solid from brown to black:

$$NiF_4 + 2\ KBF_4 \xrightarrow[\text{aHF}]{0\ ^\circ C} R\text{-}NiF_3 + \tfrac{1}{2}\ F_2 + 2\ KBF_4 \qquad (9)$$

The decomposition of NiF_4 was conveniently accomplished at 0 °C in an ice bath. It was observed that when a stoichiometric quantity of BiF_5 was the Lewis acid in reaction (8), (BiF_5, as a solid reagent was amenable to precise measurement), the decomposition of NiF_4 was much slower, the color change from brown to black requiring 6 hours rather than ~2 hours in the case of BF_3. The use of BF_3, a much weaker Lewis acid, requires that

an excess of acid be added to the reaction. This excess acid leads to the formation of a yellow (or brown if very concentrated) solution containing a cationic nickel species, possibly $Ni^{IV}F_3^+$, which may hasten the decomposition of NiF_4 to NiF_3. Chapter 5 discusses the oxidizing properties of cationic Ni^{IV}.

Reaction (8) with BF_3 was also carried out at 0 °C, yielding a dark brown precipitate which evolved F_2 and became black over about 2 hours. The KBF_4 was extracted by repeated decantation of its aHF solution, followed by back-distillation of the aHF. The solid residues were dried under vacuum at 0 °C, to give microcrystalline black *R*-NiF_3, which has the characteristic rhombohedral MF_3 XRPP, represented in Table 2.1. *R*-NiF_3 was also prepared by the reactions of other Lewis fluoroacids (AsF_5, BiF_5, PF_5, and SbF_5) with K_2NiF_6 at 0 °C in aHF. GeF_4 with K_2NiF_6, however, gave $NiGeF_6$ rather than *R*-NiF_3. The novel material $NiGeF_6$ is described in Chapter 4.

The rhombohedral structure of *R*-NiF_3 is characteristic of first series transition metal trifluorides, in which the metal atom resides in octahedral holes, in a nearly hexagonally close-packed F-atom array.[15] The FUV's of the first transition series trifluorides are shown in Figure 2.4., along with the simple crystal field d-orbital configuration. When the formula unit volume (FUV) of *R*-NiF_3 is compared to those of the other first series trifluorides, it is clearly the smallest in the series. The FUV of *R*-NiF_3 (43.7 Å) is comparable to that of AlF_3 (FUV = 43.6 $Å^3$), the smallest of all trifluorides, indicating that the effective nuclear charge of nickel must be high.

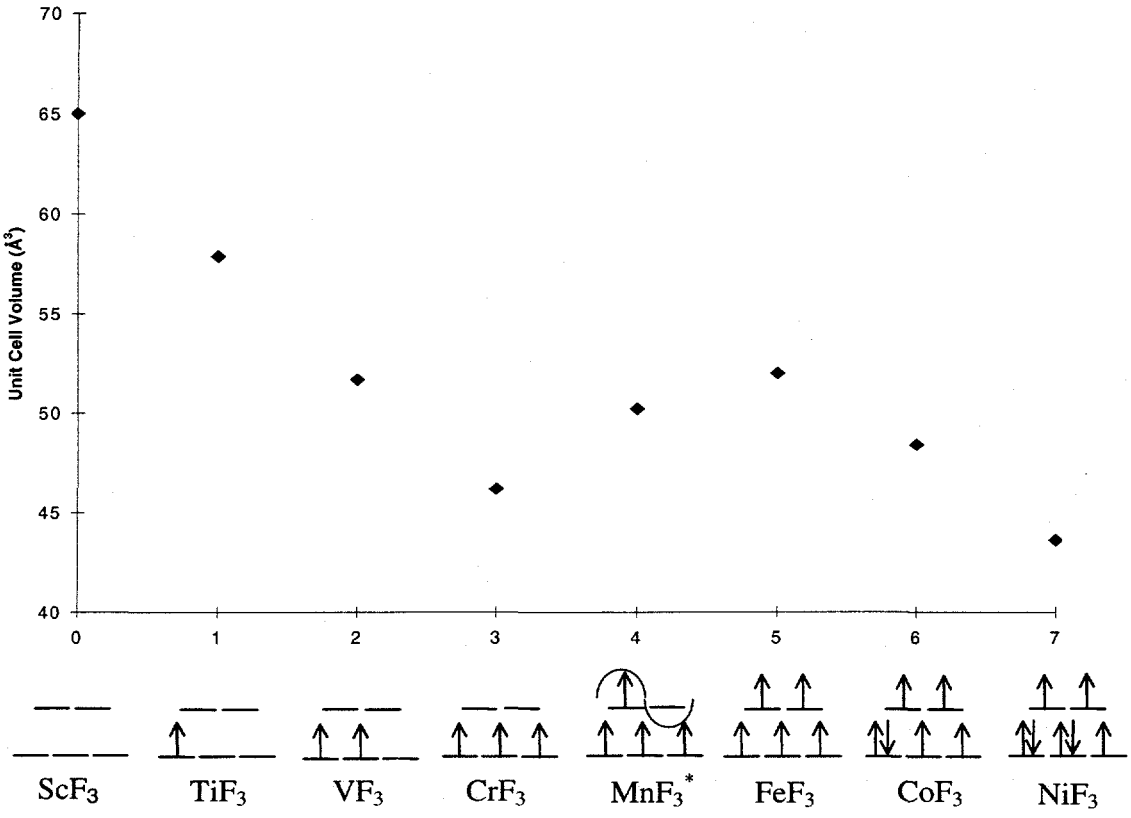

Figure 2.4. Formula Unit Volume (Å^3) for Rhombohedral First-Transition Series Trifluorides (plotted as a function of atomic number). References: *R*-ScF_3,[16] *R*-TiF_3,[17] *R*-VF_3,[18] *R*-CrF_3,[19] MnF_3(monoclinic),[7] *R*-FeF_3 and *R*-CoF_3.[2] *Indicates that the degeneracy of these levels is relieved by a Jahn-Teller distortion.

From ScF_3 to CrF_3 the decrease of FUV is almost linear, as the atomic number, *z*, of M increases. The decrease of FUV must represent the change in effective nuclear charge at M^{III}, since the t_{2g} electrons (which have π^* character) are poorly shielding of the atomic core. With MnF_3 and FeF_3, the FUV increases incrementally, which must be due to the population of the antibonding-σ e_g^* orbitals. The FUV decreases from FeF_3 to CoF_3, and is due to the e_g^* population being the same in both, with the additional electron of the

Co^{III} d^6 configuration being placed in a t_{2g} orbital. Because X-ray powder diffraction data showed no evidence for a Jahn-Teller distortion, it was highly unlikely that the electron configuration would be $t_{2g}^{6}\ e_g^{*1}$. Thus, the rhombohedral cell of *R*-NiF_3 and the value of its FUV are consistent with two possibilities: (1) a Ni^{III} species *d* electron configuration $t_{2g}^{5}e_g^{*2}$, or (2) a mixed-valence formulation, $Ni^{II}Ni^{IV}F_6$, the black appearance of the solid being consistent with the latter. The possible electron configurations for Ni^{IV} were t_{2g}^{6} or $t_{2g}^{4}\ e_g^{*2}$, with Ni^{II} ($t_{2g}^{6}\ e_g^{*2}$), this would lead to ferromagnetic or antiferromagnetic superexchange, respectively. In the first case, all of the Ni-F distances would be equivalent and the space group would be R3c. In the second case (space group R3), there would be two nonequivalent Ni-F bonds (unless the Ni^{IV} had a high spin configuration, which is unlikely). If the Ni^{IV} did have a high spin configuration, the expected difference in length of the two Ni–F bond distances would be subtle, since it is the occupation of the e_g^* orbitals which has the greatest impact on size. In order to determine the electronic configuration of Ni in NiF_3 ($Ni^{III}F_3$ or $Ni^{II}Ni^{IV}F_6$), neutron powder diffraction experiments were undertaken. Scattering of neutrons by fluorine relative to nickel is much more favorable than X-rays, and greatly improve the likelihood of precise F atom parameter determination and unambiguous assignment of the space group.

Neutron powder diffraction data were initially collected for two samples of *R*-NiF_3 prepared by reaction of K_2NiF_6, but the crystallinity was not sufficient to distinguish unambiguously between space groups R3c and R3. Finally, the discovery of the previously unknown Li_2NiF_6 provided for the synthesis of highly microcrystalline

R-NiF_3, which gave excellent quality neutron powder diffraction data. Data were collected at 2, 30-60 and 295 K. Structural refinement of the 2 K data showed two distinct Ni–F bonds, Ni(1)–F = 1.958(4) and Ni(2)–F = 1.814(4) Å, thus indicating the formulation $Ni^{II}Ni^{IV}F_6$ at that temperature. At 295 K, the difference in length of the two Ni–F bond distances, Ni(1)–F = 1.928(4) and Ni(2)–F = 1.850(4) Å, has narrowed from 0.144 to 0.078 Å (the shorter bond having lengthened and the longer bond having shortened). This indicates that at room temperature the nickel centers are moving towards equivalence, probably as a consequence of charge transfer, with each Ni^{II} and Ni^{IV} approaching a low spin d^7 configuration. Occupancy of one e_g* orbital should increase the Ni–F distance for the F ligands on the axes associated with that orbital. The empty e_g* orbital on the other hand, should be associated with the short Ni–F distances. Each Ni^{III} $t_{2g}^6\ e_g^{*1}$ species would then be in a D_{4h} environment. These findings (which for the room temperature data are still in the process of refinement) probably represent an extensive population of such Ni^{III} species mixed with Ni^{II} and Ni^{IV}, the latter pair being $t_{2g}^6\ e_g^{*2}$ and t_{2g}^6 respectively, and each asserting O_h site symmetry, thus frustrating the Ni^{III} tendency to distort.

The field dependence in the susceptibility which sets in upon cooling below 220 K indicates superexchange between the Ni centers. This behavior is probably a result of the $Ni^{II}\ t_{2g}^6\ e_g^{*2}$ and $Ni^{IV}\ t_{2g}^6$ configurations being the dominant ones as evidenced by the bond distances at 2 K, the magnetic coupling between these being very weak.[20] At higher temperatures, the population of $Ni^{III}\ t_{2g}^6\ e_g^{*1}$ has probably increased to a level at

which antiferromagnetic (Ni^{II} to Ni^{III}) and ferromagnetic coupling (Ni^{III} to Ni^{III}) become important, giving rise to the field dependence. Above 250 K, the coupling just alluded to is overwhelmed by kT.

Mössbauer spectroscopy has shown that at 6 K, the nickel centers are nonequivalent,[21] which is in harmony with the neutron structural analysis.

R-NiF_3 is thermodynamically unstable, liberating F_2 above 38 °C as a dry solid, and above 0 °C in aHF. Our coworkers in Ljubljana demonstrated that *R*-NiF_3 was even capable of oxidizing Xe to Xe^{VI}. Introduction of Xe to a multimolar excess of *R*-NiF_3 suspended by agitation in aHF at ~20 °C produced a red solution which deepened in color as Xe was introduced (but the Xe added was always much less than required for 2 Xe + 14 $NiF_3 \rightarrow [XeF_5]_2NiF_6$ + 13 NiF_2). Removal of aHF yielded red crystals of $(XeF_5)_2NiF_6$ (by XRPD).[22] When slightly larger xenon quantities were used than required for $(XeF_5)_2NiF_6$ formation, the evaporation of the red solution also gave high purity XeF_4 (XeF_2 and XeF_6 absent).

2.4. Conclusions

R-NiF_3 has been prepared by the reaction of K_2NiF_6 with a Lewis fluoroacid (BF_3, AsF_5, BiF_5, or SbF_5), or Li_2NiF_6 with BF_3 in aHF. It is a black microcrystalline solid, with a rhombohedral structure, characteristic of other first transition series trifluorides. *R*-NiF_3 is thermodynamically unstable, and begins to liberate F_2 at 39 °C. It is a powerful oxidizer, capable of oxidizing Xe to Xe^{VI}.

Neutron powder diffraction data have shown that *R*-NiF_3 has the mixed valence configuration, $Ni^{II}Ni^{IV}F_6$ (with Ni^{IV} low spin d^6), at 2 K. At 295 K, the different nickel centers are nearly the same size, indicating that one of the following has occurred: (1) a crossover from low spin to high spin Ni^{IV}, or (2) charge transfer to form some Ni^{III}. However, small changes in the unit cell parameters with temperature are evidence that scenario (1) is unlikely.

2.5 References

[1] Court, T. L.; Dove, M. F. A. *J. Chem. Soc. Chem. Commun* **1971**, 726.
[2] Court, T. L.; Dove, M. F. A. *J. Chem. Soc. Dalton Trans.* **1973**, 1995.
[3] Christe, K. O.; Wilson, R. D. *Inorg. Chem.* **1987**, 2554.
[4] Bougon, R.; Lance, M. *C. R. Seances Acad. Sci., Ser. 2* **1983**, *297*, 117.
[5] Žemva, B.; Lutar, K.; Jesih, A.; Casteel, Jr., W. J. Wilkinson, A. P.; Cox, D. E.; Von Dreele, R. B.; Borrmann, H.; Bartlett, N. *J. Am. Chem. Soc.* **1991**, *113*, 4192.
[6] Žemva, B.; Lutar, K.; Jesih, A.; Casteel, W. J., Jr.; Bartlett N. *J. Chem. Soc. Chem. Commun.* **1989**, 346.
[7] Hepworth, M. A.; Jack, K. H. *Acta Cryst.* **1957**, *10*, 345.
[8] Hepworth, M. A.; Jack, K. H.; Peacock, R. D.; Westland, G. J. *Acta Cryst.*, **1957**, *10*, 63.
[9] Bartlett, N.; Rao, P. R. *Proc. Chem. Soc.* **1964**, 393.
[10] Stout, J. W.; Reed, S. A. *J. Am. Chem. Soc.* **1954**, *76*, 5279.
[11] Taylor, J. C.; Wilson, P. W. *J. Inorg. Nucl. Chem.* **1974**, *36*, 1561.
[12] Yeranos, W. A. *Mol. Phys.* **1967**, *12*, 529.
[13] Siegel, S.; Gebert, E. *J. Am. Chem. Soc.* **1963**, *85*, 240.
[14] Žemva, B.; Lutar, K.; Jesih, A.; Casteel, W. J. Jr.; Wilkinson, A. P.; Cox, D. E.; Von Dreele, R. B.; Borrmann, H.; Bartlett, N *J. Am. Chem. Soc.* **1991**, *113*, 4192.
[15] Hepworth, M. A., Jack, K. H., Peacock, R. D., Westland, G. J. *Acta Cryst.* **1957**, *10*, 63.
[16] Lösch, R., Hebecker, C., Ranft, Z. Z. *Anorg. Chem.* **1982**, *491*, 199
[17] Erlich, P., Pietzka, G. Z. *Anorg. Chem.* **1954**, *275*, 121.
[18] Gutmann, V., Jack, K. H., *Acta Cryst.* **1951**, *4*, 244.
[19] Jack, K. H., Maitland, R. *Proc. Chem. Soc.* **1957**, 232.
[20] Tressaud, A.; Dance, J. M. in Inorganic Solid Fluorides; Hagenmuller, P.; Ed.; Academic Press: New York, 1985; pp. 371-394.
[21] Jansen, N.; Walcher, D.; Gütlich, P.; Häussinger, D.; Hannebauer, B.; Kniep R.; Lutar, K.; Schmidt, P. D.; Sellman, D.; Žemva, B. *Il Nuovo Cimento,* **1996**, *18D*, 231.
[22] Jesih, A.; Lutar, K.; Leban, I.; Žemva, B. *Inorg. Chem.*, **1989**, *28*, 2911.

Chapter 3. Hexagonal Tungsten Bronze-Type NiF_3 (H_O-K_xNiF_3, $x \approx 0.18$)

3.1. Introduction

In the process of determining an appropriate temperature range for the synthesis of pure *R*-NiF_3, some reactions between K_2NiF_6 and BF_3 were carried out at room temperature:

$$K_2NiF_6 + 2\,BF_3 \longrightarrow R\text{-}NiF_3 + NiF_2 + \text{novel phase} \qquad (1)$$

In these reactions, a mixture of products was determined by XRPD to contain *R*-NiF_3, NiF_2, and a novel phase, but these were not separated due to the insolubility of each in aHF. Later, the same phase (identified by a characteristic intense line at low angle in the XRPP), was produced along with *R*-NiF_3 by the reaction of Ni^{2+} with NiF_6^{2-} salts:

$$K_2NiF_6 + Ni(AsF_6)_2 \longrightarrow R\text{-}NiF_3 + \text{novel phase} \qquad (2)$$

Finally, a pure sample of this phase was obtained free of *R*-NiF_3 by the room temperature reaction of K_2NiF_6 with BF_3 (slow addition) in aHF. The XRPP of this brownish-black

material indicated a hexagonal tungsten bronze (HTB) type structure.[1]

Analogous HTB type "trifluorides" exist for VF_3, CrF_3, and FeF_3, as well. There are two structurally related forms for FeF_3: H_O-$(H_2O)_{0.22}FeF_3$ (orthorhombic), and H-FeF_3, which is hexagonal.[1,2] H-$(NH_4^+)_{0.25}VF_3$ and H-$(NH_4^+)_{0.25}CrF_3$ have hexagonal structures but undergo an orthorhombic distortion of the HTB structure when NH_4^+ is removed, forming H_O-VF_3 and H_O-CrF_3.[3] A range of compositions for A_xVF_3 (A = K, Rb, Tl, Cs),[4,5] A_xCrF_3 (A = K, Rb, Cs),[4,5,6] and A_xFeF_3 (A = K, Rb, Cs)[7] for $x = 0.2$ - 0.3 are known. The HTB-type structures for these can be hexagonal or orthorhombic, depending on the value of x and the size of A^+. Three types of ordering have been observed in these systems: (1) ordering of A^+ sites corresponding to half ($x = 0.167$), two-thirds ($x = 0.22$) and three-quarters ($x = 0.25$) filling,[8] (2) electronic ordering of M^{2+}–M^{3+},[5] and (3) cooperative Jahn-Teller ordering of the Jahn-Teller ions, V^{3+} and Cr^{2+}.[4]

3.2. Experimental

3.2.1. Synthesis of H_O-K_xNiF_3

The preparation of H_O-K_xNiF_3 involved the same reagents used in the synthesis of R-NiF_3 (K_2NiF_6 with a Lewis acid in aHF), but the reactions were carried out at ~20 °C, with slow addition of the acid. Dry solid H_O-K_xNiF_3 has a slight reddish-brown cast, which differentiates it visually from the black R-NiF_3.

---

[1] Nomenclature conventions for HTB-type structures are defined in Appendix B.

3.2.1.1. K_2NiF_6 with BF_3

K_2NiF_6 (0.5554 g; 2.21 mmol) was dissolved in aHF (4-5 mL) in one arm of a T-reactor at room temperature. BF_3 (1600 torr; 5.59 mmol) was slowly admitted into the reactor over a period of several hours with agitation. A visible reaction was observed at the solution-gas interface as the BF_3 was added, precipitating a brownish-black solid which slowly evolved F_2 over ~2 hours. Extracting the soluble KBF_4 by repeated decantation and back-distillation of aHF gave 0.1584 g of brownish-black solid, characterized by the XRPP in Table 3.1 as H_O-K_xNiF_3.

3.2.1.2. K_2NiF_6 with BiF_5

K_2NiF_6 (0.251 g; 1.40 mmol) and BiF_5 (0.860 g; 2.83 mmol) were loaded into opposite arms of a T-reactor. Each reagent was dissolved in aHF (~3 mL per arm), and the BiF_5 solution was added to the K_2NiF_6 solution dropwise with agitation at room temperature. A reaction occurred as the two solutions mixed, precipitating a tan solid which darkened to brownish-black in color while slowly evolving F_2 over ~3 hours. The soluble KBF_4 was extracted by repeated decantation and back-distillation of aHF to give 0.160 g H_O-K_xNiF_3.

3.2.1.3. K_2NiF_6 with $Ni(MF_6)_2$

Mixtures of H_O-K_xNiF_3 and R-NiF_3 were also prepared by the interaction of K_2NiF_6 with $Ni(MF_6)_2$ (M = As, Sb, Bi) in aHF. In a typical reaction, $Ni(AsF_6)_2$ (0.2360 g; 0.54 mmol) was loaded into one arm of a T-reactor and an equimolar quantity of purified K_2NiF_6 (0.1356 g; 0.54 mmol) in the other. The room temperature yellow

solution of $Ni(MF_6)_2$ in aHF was poured slowly into a stirred room temperature solution of the K_2NiF_6, producing a brownish-black precipitate. When the solutions had been completely mixed, the supernatant solution was colorless. The NiF_3 product was washed free of the byproduct ($KAsF_6$; 0.2375 g) with aHF at 0 °C to minimize NiF_2 production. The XRPP of the nickel product (0.1259 g) indicated a mixture of *R*-NiF_3 *H*$_O$-K_xNiF_3.

This reaction always produced mixtures of *R*-NiF_3 and *H*$_O$-K_xNiF_3, however, when the reaction was carried out at 0 °C, the predominant phase was *R*-NiF_3 and when at ~20 °C, the major product was *H*$_O$-K_xNiF_3.

3.2.2. XRPD

H$_O$-K_xNiF_3 has a structure related to that first described[9] by Magnéli for the tungsten bronzes, M_xWO_3 (M = K, Rb, Cs). Magnéli's bronzes and *H*-FeF_3 are hexagonal. The X-ray powder diffraction data was initially indexed on the basis of a hexagonal cell but because of the known existence of *H*$_O$-$(H_2O)_{0.22}FeF_3$, *H*$_O$-CrF_3 and *H*$_O$-VF_3, it was allowed that the symmetry was pseudo-hexagonal only.[10] The neutron diffraction data proved that the symmetry was orthorhombic, the probable space group being *Cmcm*, with *b/a* close to $\sqrt{3}$. The original hexagonal indexing and the more recently obtained orthorhombic indexing are both given in Table 3.1.

Table 3.1. X-ray Powder Diffraction Data (Cu K_α radiation, Ni filter) H_o-K_xNiF_3 Hexagonal unit cell: a_o = 7.074(6) Å; c_o = 7.193(6)Å; V = 311.7(8) Å^3, Z = 6, V/Z = 51.95(13) Å^3).

		$1/d^2_{hkl}$ x 10^4 Hexagonal				$1/d^2_{hkl}$ x 10^4 Orthorhombic			
I/I_o	**obs**	**calc**	***h***	***k***	***l***	**calc**	***h***	***k***	***l***
s	264	266	1	0	0	266	1	1	0
s	772	773	0	0	2	773	0	0	2
w	806	799	1	1	0	799	2	0	0
vs(br)	1052	1040	1	0	2	1040	1	1	2
		1066	2	0	0	1066	2	2	0
m	1566	1573	1	1	2	1573	2	0	2
m	1840	1839	2	0	2	1839	2	2	2
m(br)	2019	2006	1	0	3	2006	1	1	3
		2058	2	1	1	2058	3	1	1
w	2390	2398	3	0	0	2398	3	3	0
ms	3096	3093	0	0	4	3093	0	0	4
ms	3179	3171	3	0	2	3171	3	3	2
		3197	2	2	0	3197	4	0	0
w	3362	3359	1	0	4	3359	1	1	4
vvw	3468	3464	3	1	0	3464	4	2	0
m(-sh)	3943	3892	1	1	4	3892	2	0	4
		3971	2	2	2	3971	4	0	2
ms(+sh)	4151	4158	2	0	4	4158	2	2	4
		4237	3	1	2	4237	4	2	2
---	---	4263	4	0	0	4263	4	4	0
w(br)	5000	5036	4	0	2	5036	4	4	2
vw(br)	5469	5491	3	0	4	5491	3	3	4
vw(br)	5773	5789	4	1	1	5789	5	3	1
w(br)	6264	6290	2	2	4	6290	4	0	4
vvw	6695	6697	2	1	5	6697	3	1	5

For I/I_o, vs > s > ms > m > w > vw > vvw ; br = broad line; ± sh = a shoulder on the high (+) or low (-) angle side.

3.2.3. Neutron Powder Diffraction

Neutron powder diffraction data were collected on two samples of H_O-K_xNiF_3. The first sample was not of sufficient crystallinity to allow for unambiguous determination of the space group. The second sample was of slightly better crystallinity, and data were collected at 2, 150 and 295 K, to determine if any magnetic ordering was present in the sample. There was no evidence of any change in the scattering of the sample at these temperatures. The data were refined in *Cmcm* with Ni in 4*b* at (0, ½, 0) and 8*d* at (¼, ¼, 0) and F and K to give the atomic coordinates shown in Table 3.2.

Table 3.2. Refined atomic coordinates for H_O-K_xNiF_3 in *Cmcm* at 2 and 295 K

Position	Atom	*x, y, z*	2 K	295 K
8*f*	F(1)	*x*	0	0
		y	0.2089(20)	0.2165(17)
		z	0.567(4)	0.5500(34)
		U_{iso} (x 10^2)		2.66(24)
16*h*	F(2)	*x*	0.1925(19)	0.1921(17)
		y	0.3946(10)	0.3945(10)
		z	0.0509(17)	0.0531(17)
		U_{iso} (x 10^2)		1.98(50)
4*c*	F(3)	*x*	0	0
		y	0.5488(30)	0.5330(16)
		z	0.25	0.25
		U_{iso} (x 10^2)		0.78(32)
8*g*	F(4)	*x*	0.202(4)	0.1822(24)
		y	0.2197(24)	0.2108(13)
		z	0.25	0.25
		U_{iso} (x 10^2)		1.82(34)
4*c*	K	*x*	0	0
		y	0.020(4)	0.0240(32)
		z	0.25	0.25
		frac	0.53(5)	0.51(6)
		χ^2	0.9773	1.289
		R_P	0.0763	0.0883
		wR_P	0.0947	0.1105

The refined unit cell parameters and structural features are shown in Table 3.3. Potassium was found to be present in the lattice in site 4c (0, *y*, ¼) with *y* = 0.0246. Refinement of

the fractional occupation of the potassium site indicated the composition $K_{0.18}NiF_3$, although chemical reduction of a portion of this sample indicated a lower K^+ content, ($x \approx 0.14$).

Table 3.3. Distances and Angles for H_O-K_xNiF_3 in *Cmcm* at 2 and 295 K.

	2 K	295 K
a_o (Å)	7.126(2)	7.1437(15)
b_o (Å)	12.195(3)	12.2258(26)
c_o (Å)	7.158(1)	7.1892(12)
V (Å^3)	622.1(2)	
Ni(1)–F(2) (Å)	1.915(14)	1.911(14)
Ni(1)–F(3) (Å)	1.886(12)	1.842(4)
Ni(2)–F(1) (Å)	1.912(8)	1.871(7)
Ni(2)–F(2) (Å)	1.847(12)	1.865(13)
Ni(2)–F(4) (Å)	1.859(6)	1.918(5)
Ni(1)–F(3)–Ni(1) (°)	143.2(2)	154.6(12)
Ni(1)–F(2)–Ni(2) (°)	139.7(8)	139.2(7)
Ni(2)–F(1)–Ni(2) (°)	137.5(13)	145.3(13)
Ni(2)–F(4)–Ni(2) (°)	148.7(14)	139.1(8)

The fitted diffraction pattern for the data is shown in Figure 3.1. The observed values are shown as (+) and the calculated values from the best fit are shown as a curve. A difference (I_{obs} - I_{calc}) curve and the reflection positions are also shown. The peaks due to the aluminum sample can were fitted on the cubic cell ($Fm\bar{3}m$; a = 4.052 Å), and then the intensity due to aluminum extracted from the regions of overlap with the H_O-K_xNiF_3 pattern with a le Bail extraction (a GSAS utility). An ORTEP diagram of the unit cell is shown in Figure 3.2.

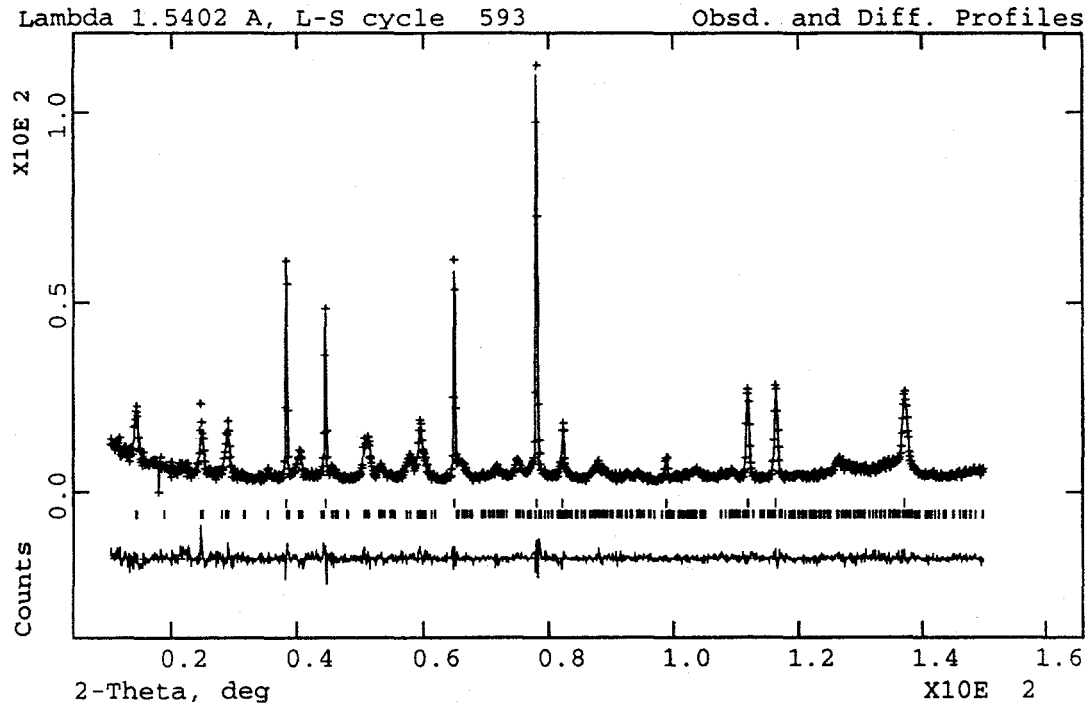

Figure 3.1. Fitted Neutron Powder Diffraction Pattern for H_O-K_xNiF_3. Data collected on BT-1 at 295 K.

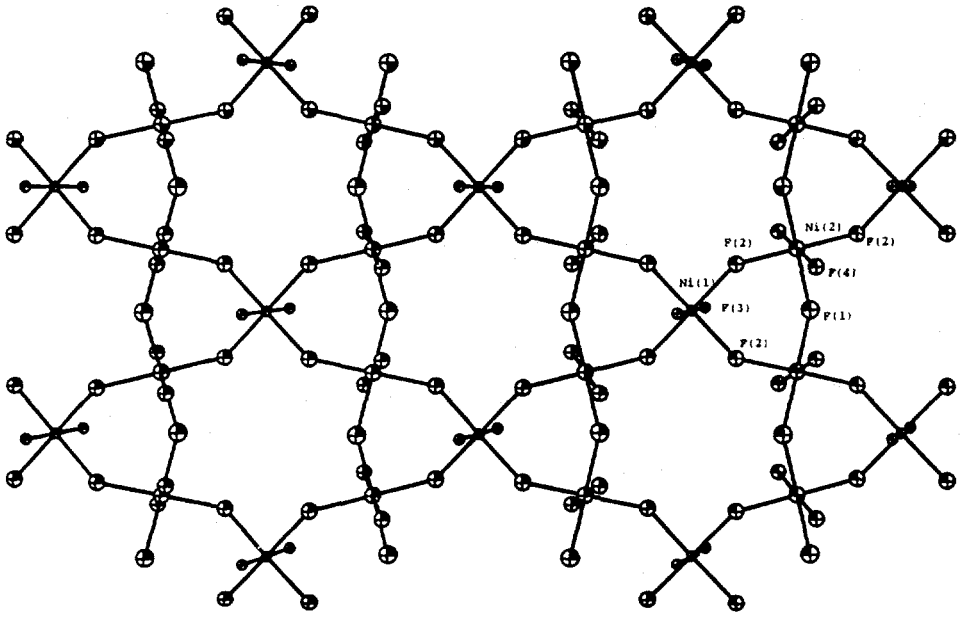

Figure 3.2. One layer of the orthorhombic structure of H_O-K_xNiF_3

3.2.4. Magnetic Susceptibility

The magnetic behavior of H_O-K_xNiF_3 is shown in Figure 3.3.

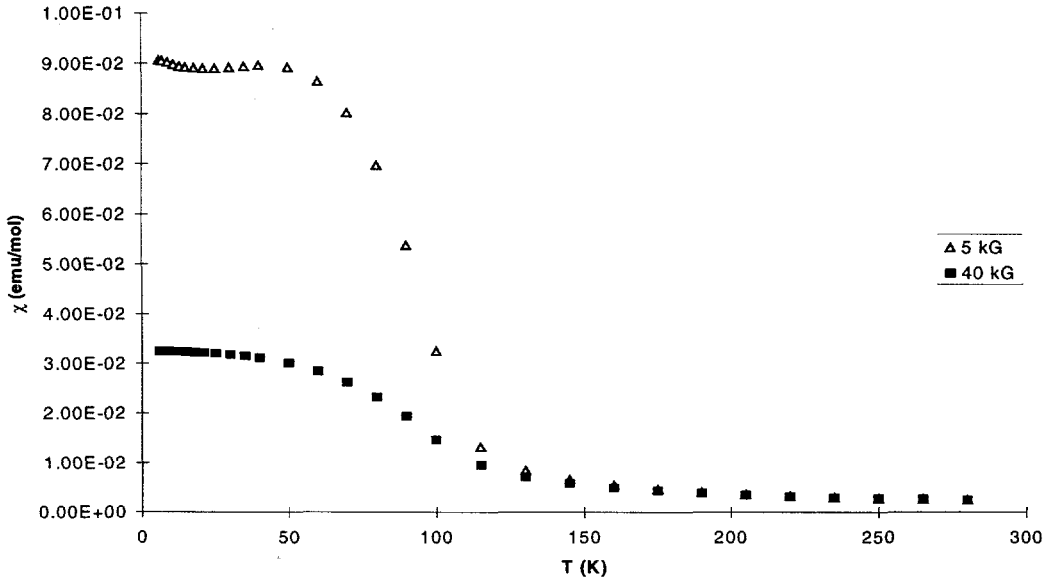

Figure 3.3. Magnetic Susceptibility of H_O-K_xNiF_3 (280 to 6 K; 5 and 40 kG)

As the temperature is lowered, there is an onset of field dependence near 150 K. The field-independent room temperature magnetic moment is 2.36 β.

3.2.5. Thermal Stability

The thermal stability of H_O-K_xNiF_3 was assessed by the same standards applied to R-NiF_3, as described in section 2.2.5. The first measure of thermal stability was the thermal decomposition of dry solid H_O-K_xNiF_3. Again a FEP column packed with KI was used to indicate the release of F_2 from the sample as the latter was slowly heated above room temperature. No F_2 liberation was observed until ~72 °C, and that was slight. At

~103 °C, F_2 was liberated readily, and at 135 °C another surge of F_2 was observed. The XRPP of the solid product from the 135 °C decomposition indicated poorly crystalline NiF_2.

The second measure of thermal stability was the decomposition of H_O-K_xNiF_3 in aHF at room temperature. A sample of H_O-K_xNiF_3 (0.0687 g; 0.59 mmol in NiF_3) was loaded into a T-reactor, and aHF (3 mL) was added to the solid. After 8 days, the dark brown-black color of the solid had become a lighter red-brown, and after 15 days the sample was pale tan. The supernatant aHF solution was decanted to the other arm of the reactor, and the aHF removed, to give a slightly yellow tinted solid. The XRPP of the insoluble tan solid showed it to be NiF_2 (0.0573 g; 0.59 mmol). XRPD showed the soluble yellow-tinted solid to consist mainly of $KBiF_6$ (0.0145 g), indicating that the extraction of the byproduct during the synthesis of the H_O-K_xNiF_3 was incomplete. The faint yellow color of the solid was most likely due to a small amount of suspended NiF_2 being carried over during the decantation, as KHF_2 is colorless.

3.2.6. Elemental Analysis

Elemental analysis was performed on two samples of H_O-K_xNiF_3 by coworkers at the Josef Stefan Institute in Ljubljana, Slovenia. They found that the interpretation of their data was always somewhat ambiguous due to contamination by occluded K^+ salts (KBF_4, $KAsF_6$, etc.) formed during the reaction of K_2NiF_6 with Lewis acid (BF_3, AsF_5, etc.). Further complicating the interpretation was the unreliability of the B analyses (accurate to ±0.25%). This made reliable determination of x in K_xNiF_3 difficult. Found

(two separate analyses for F and Ni): F, 47.1, 47.0; Ni, 48.3, 48.3; K 4.07; B, 0.62%. *HO*-K_xNiF_3 (contaminated with 0.0074 mmol KBF_4 impurity) having a composition $K_{0.12}NiF_3 \cdot 0.0074KBF_4$, requires: F, 47.4; Ni, 48.4; K, 4.09; B, 0.07%. A second sample was analyzed and found to have no excess potassium beyond that required to be present for the B content.

The *HO*-K_xNiF_3 which was used in the successful neutron powder diffraction experiments was reduced by H_2, yielding KHF_2 which was converted to KBF_4 by addition of BF_3. The gravimetry of this reaction is the basis for another value of x found for the K^+ content. *HO*-K_xNiF_3 (0.1423 g) was placed in one arm of a T-reactor, and aHF (6 mL) was condensed onto it. The reactor was pressurized to 2 atm with H_2, with no visible reaction. After several hours, however, the solid began to lighten in color. The mixture was left for 12 hours and the soluble and insoluble products were separated by decantation and back-distillation of aHF. BF_3 was added to the solution to amplify the mass of the liberated K^+, precipitating KBF_4, then the aHF was removed. Colorless KBF_4 (0.0224 g; 0.178 mmol) and tan NiF_2 (0.1235 g; 1.278 mmol) were recovered. The composition of the sample used in the neutron diffraction studies was therefore, $K_{0.14}NiF_3$

3.2.7. Chemical Reactivity

The chemical reactivity of *HO*-K_xNiF_3 was compared with that of *R*-NiF_3 by carrying out reactions similar to those described in section 2.2.7. for *R*-NiF_3 with: Xe, XeF_2, KF and LiCl.

Xe. Dry solid *HO*-K_xNiF_3 did not react with gaseous xenon, but when suspended

in aHF (~ 2.5 mL), did react to form a tan solid. Colorless soluble products were obtained by decanting the aHF solution to the other arm, aHF being removed under vacuum at –50 °C. H_O-K_xNiF_3 (0.180 g) gave colorless soluble products (XeF_2 + KH_2F_3 + KBF_4; 0.0932 g), and a tan solid, NiF_x (0.148 g). Assuming the composition from the analysis for H_O-K_xNiF_3 (i.e. $K_{0.12}NiF_3$·0.0074 KBF_4), there are 1.484 mmol of H_O-K_xNiF_3. There must be 1.484 mmol of NiF_x in the product, which must therefore have a composition $NiF_{2.16}$. Neglecting loss of F_2 by decomposition of the H_O-K_xNiF_3 in the aHF, the yield of XeF_2 is expected to be 0.534 mmol = 0.0904 mg. Expected KH_2F_3 = 0.0175 g and KBF_4 = 0.0009 g. Total (expected) {XeF_2 + KH_2F_3 + KBF_4} = 0.1088 g. Total (actual) {XeF_2 + KH_2F_3 + KBF_4} = 0.0932 g.

XeF_2. H_O-K_xNiF_3 was combined with XeF_2 in two separate reactions with differing stoichiometries; 2:1 and 4:1 (H-NiF_3:XeF_2). A solution of XeF_2 (0.067 g; 0.040 mmol) in aHF (2.5 mL) at ~ 20 °C was added quickly to a suspension of H_O-K_xNiF_3 (0.092 g; 0.80 mmol) with vigorous stirring. This resulted in the brown-black color of the H_O-K_xNiF_3 changing to red-brown in ~50 minutes. The red-brown solid was separated from the soluble products by repeated decantation and back-distillation of aHF. Removal of aHF at –47 °C yielded a nearly colorless solid identified[11] by XRPP as XeF_4 (0.066 g; 0.32 mmol). The XRPP of the reddish-brown residue indicated NiF_2 (0.082 g; 0.85 mmol) although the color and gravimetry indicated a higher F content. A second reaction between XeF_2 (0.048 g; 0.28 mmol) and H_O-K_xNiF_3 (0.130 g; 1.12 mmol) was carried out in aHF (2.5 mL) at ~ 20 °C. The reagents were loaded into opposite arms of the reactor,

aHF was condensed onto the XeF_2, and the resulting solution poured onto the H-NiF_3. After 1 h, the black solid had become reddish-brown, and soluble products were isolated by decantation and back-distillation of aHF. Removal of aHF below –39 °C gave an almost colorless residue (XRPP indicated XeF_4, 0.046 g; 0.22 mmol). The XRPP of the reddish-brown residue (0.121 mg) showed H_O-K_xNiF_3 and NiF_2. Required for 0.56 mmol NiF_2, 0.054 g; and (0.56 mmol) H-NiF_3, 0.0679 g; total 0.1221 g.

KF. H_O-K_xNiF_3 (0.1519 g; 1.252 mmol based on $K_{0.12}NiF_3$•0.0074KBF_4) was combined with an approximately equimolar quantity of KF (0.0869 g; 1.498 mmol), mixed with aHF (~2 mL), and agitated for five days at ~20 °C. A red tint appeared in the solution almost immediately after pouring the KF solution onto the H-NiF_3. After one day the solution was slightly darker red, but the solid was still brown-black. After five days, the solid was a lighter brown. The red solution was isolated by repeated decantation and back-distillation of aHF. The XRPP of the soluble material showed K_2NiF_6 with KHF_2 (0.1647 g) and that of the insoluble material showed NiF_2 (0.1100 g). It was observed that the H_O-K_xNiF_3 produced the K_2NiF_6 much more slowly than the R-NiF_3 did, with the intensity of the solution color growing steadily over five days.

LiCl H_O-K_xNiF_3 (0.1127 g; 0.974 mmol) was loaded into one arm of a T-reactor and LiCl (0.0462 g; 1.09 mmol) was loaded into another, and aHF (~2 mL) was added to it. The LiCl solution was poured onto the H_O-K_xNiF_3 and the mixture was stirred at ~20 °C. Chlorine gas was rapidly evolved as the brown-black color of the solid changed to yellow-green over a few minutes. The aHF solution was decanted away from the

yellow-green solid and the aHF removed. The yellow-green NiF_2 (0.1009 g; 1.04 mmol) was identified by its XRPP, and the colorless solid isolated from the solution was determined to be a mixture of LiF and $LiHF_2$ (0.0483 g; required for 1.09 mmol $LiHF_2$ = 0.0501 g).

3.2.8. Conductivity of H_O-K_xNiF_3

Powder samples of H_O-K_xNiF_3 proved to be conductive when measured by a simple technique performed in the drybox. The H_O-K_xNiF_3 was packed into a small section of passivated ¼" FEP tubing, drawn down to form a tight fit around a 1/16" gold wire. Another gold wire was used to pack the powder against the first wire, and alligator clamps were attached to the two wires. A resistivity was read from an ohm meter and the conductivity was obtained from the relations: $R = \frac{\rho \bullet L}{A}$ and $\sigma = \frac{1}{\rho}$. For a length of packed powder (L = 0.15 cm) and the cross-sectional area of the cylinder of packed powder (A = 0.0201 cm^2), a resistivity, R = 7 MΩ, was obtained. This gave a conductivity, $\sigma = 1.07 \times 10^{-6}$ $(\Omega \bullet cm)^{-1}$. More solid was added to the packed sample to observe that the conductivity was proportional to the length of the sample. For L = 0.5 cm, R = 19 MΩ, and $\sigma = 1.31 \times 10^{-6}$ $(\Omega \bullet cm)^{-1}$.

A second sample of H_O-K_xNiF_3 (L = 0.195 cm) was measured and found to have $\sigma = 2.5 \times 10^{-6}$ $(\Omega \bullet cm)^{-1}$. Although this measurement technique was crude, it clearly demonstrated the conductivity of H_O-K_xNiF_3, and probably represents a minimum value. Furthermore, the magnitude of the conductivity is appropriate for that of an ionic

conductor. Samples of *R*-NiF_3 measured in like manner exhibited no conductivity, and thus it was assumed that the conductivity associated with *H*$_O$-K_xNiF_3 must be due to the mobility of the K^+ ions in the lattice of the HTB structure.

3.2.9. Attempts to Exchange Lithium for Potassium Ions in *H*$_O$-K_xNiF_3

Several attempts were made to replace the K^+ hosted in the *H*$_O$-K_xNiF_3 channels with Li^+, which would be expected to increase the magnitude of the conductivity. These first attempts were directed simply towards trying to "wash" the *H*$_O$-K_xNiF_3 in an aHF solution containing a Li^+ salt, in hopes that some exchange of ions would occur. The Li^+ salts chosen were: $LiOsF_6$, LiF and Li_2GeF_6.

$LiOsF_6$. $LiOsF_6$ was used because OsF_6^- is relatively stable with respect to oxidation, but apparently the *H*$_O$-K_xNiF_3 was a powerful enough oxidizer to oxidize it to OsF_6. An $LiOsF_6$ (0.1065 g; 0.342 mmol) solution in aHF (1.5 mL) was decanted onto *H*$_O$-K_xNiF_3 in aHF (1.5 mL). There was a slight evolution of gas with addition of $LiOsF_6$ solution. After ~5 minutes, the side arm was cooled to -196 °C, and a large amount of bright yellow solid sublimed in that arm, indicating the presence of OsF_6. As the solution warmed to room temperature, the material evaporated to a colorless gas. The color of the *H*$_O$-K_xNiF_3 changed from black to reddish brown under a red solution. The solid was washed several times to separate from soluble products, and the aHF and volatiles were removed. The XRPP's of the soluble red material showed LiF and Li_2NiF_6 (0.0147 g), and that of the insoluble reddish brown material showed NiF_2 (0.0647 g). The reddish brown material was not conductive when measured as described in section 3.2.8.

LiF. Reaction with LiF produced NiF_6^{2-} and NiF_2, which had been observed in the reaction of KF with *R*-NiF_3. LiF (0.0113 g; 0.050 mmol) was loaded into one arm of a T-reactor, H_O-K_xNiF_3 (0.0887 g; 0.767 mmol) was loaded into the other, and aHF (~2.5 mL) was condensed into both arms. The LiF solution was poured onto the H_O-K_xNiF_3 and after about 15 minutes at room temperature, the solution was pink, and gas evolution was observed, although the solid still appeared dark brown. The reaction mixture was cooled to -196 °C and the reactor opened to an evacuated gauge to check for non-condensable F_2, which was present. The pink solution was decanted away from the dark brown solid and the aHF removed. The extraction of soluble products was incomplete, however, and the inhomogeneous dark brown/pink solid gave powder patterns of H_O-K_xNiF_3, NiF_2 and Li_2NiF_6. The soluble products were shown to be a mixture of K_2NiF_6 and Li_2NiF_6 (XRPP).

Li_2GeF_6. Li_2GeF_6 was used because the GeF_6^{2-} ion is stable to oxidation and the greater solubility of K_2GeF_6 might be likely to drive the substitution of Li^+ for K^+ in the lattice. Li_2GeF_6 (0.049 g; 0.244 mmol) was placed in one arm of a T-reactor, H_O-K_xNiF_3 (0.1521 g; 1.31 mmol) was placed in the other, and aHF (~1.5 mL) was condensed onto each reagent. The Li_2GeF_6 solution was added to the H_O-K_xNiF_3 and the mixture stirred for 24 hours at 0 °C (to minimize decomposition of H_O-K_xNiF_3) with no visible reaction. The solubility of Li_2GeF_6 at room temperature is < 19 mg/mL, thus the solubility at 0 °C must have been very low, so the reaction mixture was warmed to room temperature. After 1 hour there was a slight reddish tint to the solution and a layer of tan solid at the solid-

solution interface, indicating decomposition of the H_O-K_xNiF_3. The XRPP's of H_O-K_xNiF_3 and soluble products showed H_o-K_xNiF_3 and Li_2GeF_6/K_2GeF_6 respectively. The conductivity of this sample was not measured due to the evidence of decomposition.

After the discovery of Li_2NiF_6 (as described in Chapter 7), the synthesis of H_O-Li_xNiF_3 was attempted. Two reactions of Li_2NiF_6 with BF_3 in aHF at room temperature were carried out, but each time the products were a mixture of the R-NiF_3 and H_O-Li_xNiF_3 forms. It is possible that elevating the temperature slightly above room temperature during the reaction would preclude the formation of the less stable R-NiF_3, but this has not been attempted.

3.3. Results and Discussion

An idealized representation of the structure of H_O-K_xNiF_3 is shown in Figure 3.4. The unit cell involves two layers, since the value for c_o is 7.189(1) Å. These two layers are related by a mirror plane perpendicular to c, in which the F atoms that link the octahedra along c, are placed. The octahedra are tilted, but the Ni atoms remain coplanar in each sheet, nearest-neighbor Ni atoms being $a_o/2$ (i.e. 3.572 Å) apart. The analytical data, and the KH_2F_3 recovered on reduction of H_O-K_xNiF_3 with H_2, indicated that the K^+ content, x in H_O-K_xNiF_3, ≈ 0.14; is only about one third of that allowed by the structure, which could theoretically accommodate a composition $K_{0.33}NiF_3$. As the H_O-K_xNiF_3 is formed in the aHF solution it must take HF into the hexagonal cavities as well as K^+, since on removal of aHF from the precipitated H_O-K_xNiF_3, the particles of that solid rapidly outgas and are propelled throughout the evacuated container. The cavities are

large enough in diameter (~2.6 Å) to accommodate either K^+ or HF.

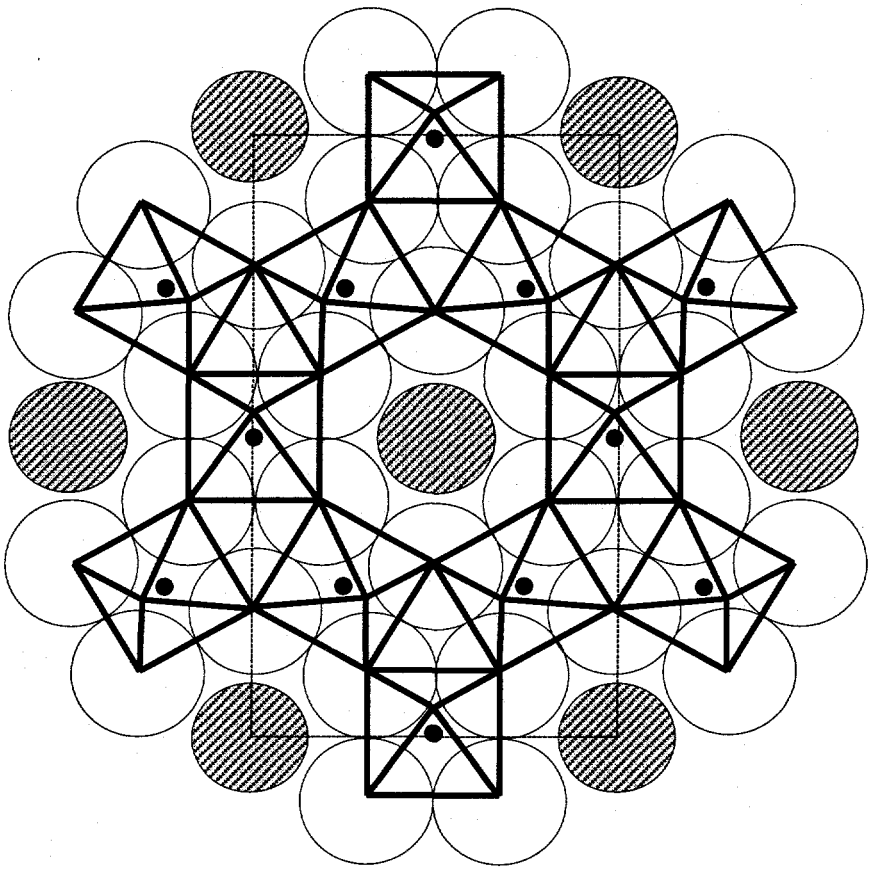

Figure 3.4. Representation of a single idealized sheet of the H_O-MF_3 structure. Open circles represent the F ligands close to the plane containing the M atoms (small black circles). MF_6 octahedra are tilted, which lowers the symmetry from hexagonal to orthorhombic. Shaded circles indicate K^+ sites at $c_o/4$ above or below the plane of the M atoms.

It is probable that in each of the psuedo-hexagonal channels running parallel to *c* that the K^+ are occupying approximately one-third of the available sites in the center of the channels in the mirror planes perpendicular to *c*. An ordered distribution to maximize their separation would be expected, and it is possible that this occupancy is correlated

with that in other channels in the structure, as observed for vanadium and chromium relatives, although the structural solution of H_O-K_xNiF_3 has not yet taken this possibility into account. If there is cation ordering present in H_O-K_xNiF_3, then there might also be a corresponding Ni^{II} (required for charge balance) ordering.

The structure solution presented in this chapter is modeled after that described for H_O-$(H_2O)_{0.33}FeF_3$,[1] and H_O-CrF_3 and H_O-VF_3.[3] In these structures, there is commonly some distortion of the octahedra observed. In the case of H_O-K_xNiF_3, however, this distortion of the octahedra is more severe than in the other structures. Attempts have been made to model the structure based on an ordered arrangement of Ni^{II} and Ni^{III} using long- and short-bonded octahedra respectively, but this did not result in higher quality refinements. The refinement was attempted in a lower space group, which was also unsatisfactory. Adjusting the tilt angle of the octahedra did relieve some of the distortion, which seems to be unavoidable. In addition to this problem, there are some weak lines which do not belong to the calculated pattern. Attempts to fit these with potential impurity phases have failed. It is possible that these lines may be due to cationic ordering, but this has not yet been investigated. It is known that the structures found in the A_xVF_3 and A_xCrF_3 systems can be quite complicated, with several different domains of ordering present in one bulk sample. In one case, superlattice reflections attributed to three types of cation ordering were observed, corresponding to half, two-thirds and three-quarters filling of available cation sites within one bulk sample.[8] In this case a clear unit cell or composition could not be defined. In addition, hexagonal phases are sometimes present

(10-20 %) in the predominantly orthorhombic samples.[4,5,6]

The change in structure from *R*-NiF_3 to H_O-K_xNiF_3 results in a FUV increase of

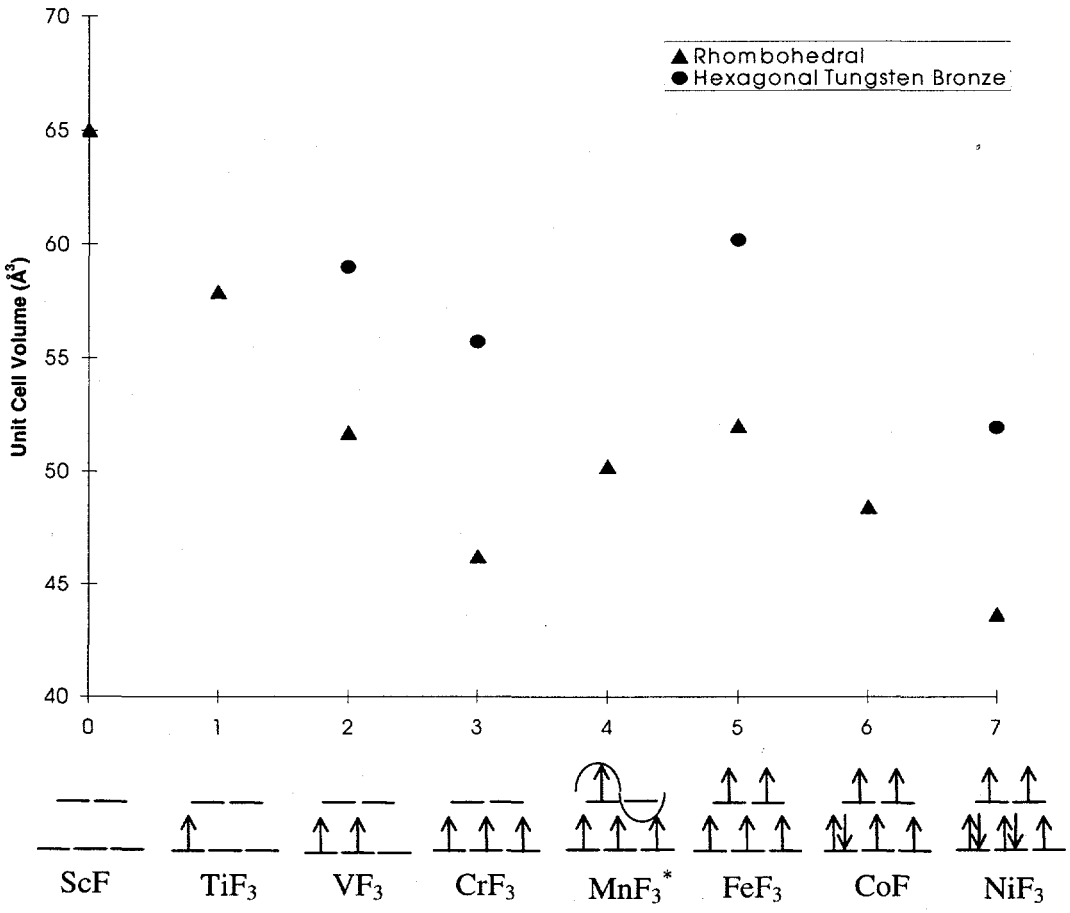

Figure 3.5. Formula Unit Volumes of First Transition Series *R*- and *H*-MF_3.
References: *H*-VF_3 and *H*-CrF_3,[3] *H*-FeF_3.[1] *Indicates that the degeneracy of these levels is relieved by a Jahn-Teller distortion.

8.3 $Å^3$. This volume increase is associated with the open channels of H_O-K_xNiF_3 which have an effective inner diameter close to 2.6 Å. This poorly packed arrangement probably arises from the advantageous lattice energy associated with incorporation of xK^+ in the

channels, which compensate for Ni^{II} in the "Ni^{III}" matrix. The energetics must further benefit from dielectric screening of the K^+ by HF molecules also incorporated into the channels. As shown in Figure 3.5., this FUV increase, of HTB-types over *R*- forms is typical of that reported for other first transition series trifluorides, and the trend in HTB-type MF_3 FUV across the period, is the same as for *R*-MF_3. Although the Ni species in *R*- and H_O-K_xNiF_3 are each octahedrally coordinated by F ligands and each F ligand bridges two Ni species, the structures differ greatly. In the close-packed *R*-NiF_3, the octahedra are linked through bridging F ligands, in 8 membered Ni_4F_4 rings (alternating Ni and F) as seen in Figure 2.1. As shown in Figure 3.4., NiF_6 octahedra in H_O-K_xNiF_3 are linked by corner sharing in the *ab* plane, in 3-fold sets. All Ni species in the *ab* plane are therefore in six-membered Ni_3F_3 rings with alternating Ni and F. It is this closer grouping of the octahedra in H_O-K_xNiF_3 that provides for the open channels that run parallel to *c*.

The structural requirement of the six-membered rings of three-fold sets of octahedra should give rise to a frustrated antiferromagnetism, similar to that found in *H*-FeF_3, as described by Leblanc, *et. al.*,[2] if the dominant species is Ni^{III}, $t_{2g}^5 e_g^{*2}$. In *H*-FeF_3 ($t_{2g}^3 e_g^{*2}$, or even $t_{2g}^6 e_g^{*1}$ perhaps) the only effective antiferromagnetic coupling (T_N = 110 K) occurs parallel to *c*, and is much weaker than the antiferromagnetic coupling (T_N = 365 K) in *R*-FeF_3. The decrease of the temperature for onset of field dependence compared with the *R*-NiF_3 is probably a consequence of magnetic frustration in the Ni_3F_3 rings leaving the only magnetic coupling possibility between the sheets, along the pseudo-hexagonal *c* axis.[2,12]

The magnetic susceptibility data given in Figure 3.3. show marked field dependence below ~150 K. This may be a consequence of an antiferromagnetic coupling of Ni^{III} species along the *c* axis, these coupled spins being canted as observed for Fe^{III} in H_O-$(H_2O)_{0.22}FeF_3$.[1] It is not certain that the Ni^{III} configuration would be $t_{2g}^6\ e_g^{*1}$ rather than $t_{2g}^5\ e_g^{*2}$, but the former would give rise to a Jahn-Teller distortion compatible with the site symmetries offered by the *Cmcm* space group.

The possibility of different compositions of *x* in K_xNiF_3 should not be overlooked, since in this synthetic method, there is no direct control over the amount of K^+ that is incorporated into the structure. The starting material K_2NiF_6, through its solvation in aHF provides two equivalents of K^+ for each equivalent of NiF_6^{2-}. In the reaction to form NiF_3 at room temperature, a solid is deposited as the Lewis acid reacts with NiF_6^{2-}. There is probably formation of NiF_4 as a transient product, which immediately gives up F_2 and falls to Ni^{III} and some Ni^{II}. In the presence of the K^+-rich solution, the NiF_3 surface incorporates what K^+ is required to compensate for the Ni^{II} content. Ni^{III} in *R*-NiF_3 is known to be thermodynamically unstable, giving Ni^{II} and F_2 in aHF at room temperature. Thus any stability it does possess is likely kinetic in nature. Therefore, it is possible that by controlling the temperature during the deposition of the H_O-K_xNiF_3 higher or lower Ni^{II} formation and subsequent K^+ incorporation might be achieved. There may be other factors which could influence K^+ content as well, such as: concentration of K_2NiF_6 in aHF, and rate of addition of the Lewis acid, which would affect the rate of deposition of the solid.

Aside from small peaks in the neutron diffraction pattern that remain unaccounted for as mentioned earlier, another indication that there may be more than one composition of K_xNiF_3 is an observation of anomalous magnetic behavior for one batch of *H*$_O$-K_xNiF_3. An extra "step" was observed in the susceptibility. At first this result was discounted as spurious, and not investigated further, but perhaps it should now be investigated more closely, in an attempt to explain the behavior.

It has been described for certain compositions in the Rb_xCrF_3 system that the magnetic coupling occurs in steps.[5] Each Cr^{2+} ion first couples with one its nearest neighboring Cr^{3+} ions, forming a ferromagnetic dimer, followed at lower temperatures by three-dimensional long-range antiferromagnetic ordering. This was attributed as an effect of M^{2+} and M^{3+} ions occupying specific lattice sites in the structure.

The refinement of neutron powder diffraction data indicated a potassium content of $K_{0.18}NiF_3$, while reduction of a small portion of this sample with H_2 gave a potassium content of $K_{0.14}NiF_3$. The true K^+ content is most likely somewhere in between, as the gravimetric result may be slightly low due to droplets of solution adhering to the walls of the reactor during decantation of the K^+-containing solution.

The reactivity of *H*$_O$-K_xNiF_3 also indicates that the oxidation state of nickel is lower in *H*$_O$-K_xNiF_3 than in *R*-NiF_3. *H*$_O$-K_xNiF_3 reacts more slowly with inorganic substrates than *R*-NiF_3 in all cases, it also reacts less vigorously with organic substrates (Chapter 6). It also has a slower decomposition rate in aHF at room temperature and a higher thermal decomposition temperature, all of which indicate a more stable oxidation

state for nickel in H_O-K_xNiF_3 than in R-NiF_3.

Unsuccessful attempts to substitute Li^+ for K^+ in the lattice suggest that a different approach is needed. The room temperature reaction of Li_2NiF_6 and BF_3 yields a brownish-black solid that gives an XRPP containing patterns of R-NiF_3 and H_O-Li_xNiF_3 (with no change in unit cell dimensions when compared with H_O-K_xNiF_3). This is promising, as it appears possible to synthesize the hexagonal form with Li^+ ions hosted in the channels. However, since it is coprecipitated with R-NiF_3, separation is impossible (both are insoluble in aHF). Perhaps the reaction with Li_2NiF_6 would yield pure H_O-Li_xNiF_3 without R-NiF_3 contamination if carried out at a slightly higher temperature (~30 °C), which would likely discourage formation of the less stable R-NiF_3. A sample of H_O-Li_xNiF_3 would be expected to have a higher conductivity than H_O-K_xNiF_3.

3.4. Conclusion

H$_O$-K_xNiF_3 has been synthesized by the reaction of K_2NiF_6 and BF_3 at room temperature in aHF, and also by the metathetical reaction between $Ni(AsF_6)_2$ and K_2NiF_6. It is a brown-black solid and has been structurally identified as a relative of the hexagonal tungsten bronze class. Neutron powder diffraction data indicate that the unit cell is orthorhombic and that the appropriate space group may be *Cmcm*. The channels in this structure host potassium ions which is confirmed by analytical, gravimetric, neutron powder diffraction and by the weak conductivity of compressed powders of *H*$_O$-K_xNiF_3. Attempts to replace K^+ in *H*$_O$-K_xNiF_3 with Li^+ have been unsuccessful, but an impure *H*$_O$-Li_xNiF_3 has been prepared from the reaction of Li_2NiF_6 with BF_3.

The content of K^+ in the channels has been difficult to quantify, but is certainly less than the allowed structural limit of $K_{0.33}NiF_3$. Regardless of the exact quantity of K^+ (and corresponding Ni^{II}), the bulk oxidation state of nickel in *H*$_O$-K_xNiF_3 is most likely Ni^{III}, as derived from the magnetic behavior and oxidizing power.

H$_O$-K_xNiF_3 is more stable than *R*-NiF_3 as evidenced by higher thermal decomposition temperature, slower decomposition in aHF and in general, slower reactions with inorganic substrates when compared with *R*-NiF_3.

The variations in the conductivity and magnetism of some samples of *H*$_O$-K_xNiF_3 may indicate that there is a range of compositions with unique properties, as is the case for vanadium and chromium analogues. The careful control of synthetic conditions might allow for correlations to be made between composition and properties.

3.5. References

[1] Leblanc, M.; Ferey, G.; Chevallier, P.; Calage, Y.; De Pape, R. *J. Solid State Chem.* **1983**, *47*, 53.
[2] Leblanc, M.; De Pape, R.; Ferey, G.; Pannetier, J. *Solid State Commun.* **1986**, *58*, 171.
[3] De Pape, R.; LeBail, A.; Lubin, F.; Ferey, G. *Rev. Chim. Minér.* **1987**, *24*, 545.
[4] Boo, W. O. J.; Williamson, R. F.; Baker, K. N. *Mol. Cryst. Liq. Cryst.* **1984**, *107*, 195.
[5] Hong, Y. S.; Baker, K. N.; Willimason, R. F.; Boo, W. O. J. *Inorg. Chem.* **1984**, *23*, 2787.
[6] Dumora, D.; Ravez, J.; Hagenmuller, P. *J. Solid State Chem.* **1972**, *5*, 35.
[7] Tressaud, A.; De Pape, R.; Portier, J.; Hagenmuller, P. *Bull. Soc. Chim. Fr.* **1970**, *10*, 3411.
[8] Hong, Y. S.; Williamson, R. F.; Boo, W. O. J. *Inorg. Chem.* **1981**, *20*, 403
[9] Magnéli, A. *Acta Chem. Scan.* **1953**, *7*, 315.
[10] Žemva, B.; Lutar, K.; Chacón, L.; Fele-Beuermann, M.; Allman, J.; Shen, C.; Bartlett, N. *J. Am. Chem. Soc.* **1995**, *117*, 10025.
[11] Siegel, S.; Gebert, E. *J. Am. Chem. Soc.* **1963**, *85*, 240.
[12] Ferey, G.; De Pape, R.; Leblanc, M.; Pannetier, J. *Rev. Chim. Minér.* **1986**, *23*, 474.

Chapter 4. Further Investigation of NiF_4

4.1. Introduction

Although the existence of NiF_4 has been established (see Chapter 2), its low kinetic stability has, so far imposed great difficulties in carrying through structural and magnetic studies. In aHF, NiF_4 decomposes rapidly to *R*-NiF_3 at 0 °C. When NiF_4 is precipitated below -65 °C and the aHF removed, the dry mixture of the tan solid and the byproduct KBF_4 liberates F_2 upon warming above -55 °C to form a dark brown solid identified as the pyrochlore form of nickel trifluoride (P_R-NiF_3). P_R-NiF_3 gave an XRPP which showed it to have a rhombohedral variant of the pyrochlore structure. Like H_O-K_xNiF_3, P_R-NiF_3 also hosts a low concentration of potassium ions in lattice channels, and is formulated as K_yNiF_3 ($y << 1$).[1]

In this chapter, further synthetic schemes, designed to provide for separation of NiF_4 from accompanying products, are described along with evidence for a novel Ni^{IV} containing material.

As mentioned in Chapter 2, the reaction of K_2NiF_6 with the Lewis acids PF_5, BF_3, AsF_5, SbF_5 and BiF_5 in aHF all produce NiF_4 below -65 °C, *R*-NiF_3 at 0 °C, and H_O-K_xNiF_3 at room temperature. In each case, the potassium salt byproducts (KPF_6, KBF_4, $KAsF_6$, $KSbF_6$ and $KBiF_6$) are poorly to moderately soluble in aHF even at room temperature. Their removal at 0 °C requires repeated washings which do not guarantee complete separation, as there appears to be a significant adsorption of solute on the solid product. Compared to the other potassium salt byproducts, the solubility of K_2GeF_6 is high, probably as a consequence of the high solvation energy of GeF_6^{2-}.

The interaction of K_2NiF_6 and GeF_4 was carried out at low temperatures to determine if it would be possible to stabilize NiF_4 in aHF below -60 °C. It was believed that the high solubility of K_2GeF_6 would facilitate purification at low temperatures. It was hoped that complete separation from K^+ salts at low temperature might prevent the ready decomposition of NiF_4 to P_R-NiF_3 as the latter is not formed when K^+ salts are not present (e.g. when $(XeF_5)_2NiF_6$ is the NiF_4 precursor).

4.2. Experimental

4.2.1. Reaction of K_2NiF_6 with GeF_4 at 0°C (molar ratio 1: 1.26)

K_2NiF_6 (3.1085 g; 12.4 mmol) was placed into one arm of a ½" FEP T-reactor, and aHF (~13 mL) was condensed onto it, and the solution cooled to 0 °C. The metal line was filled with a known pressure of GeF_4 (12.4 mmol) and the valve to the reactor opened. The gaseous GeF_4 did not immediately react at the surface of the solution-gas

interface, as is observed with other gaseous Lewis acids (PF_5, BF_3 and AsF_5). This was surmised to be due to low solubility of GeF_4 in aHF. In order to aid the solubility of GeF_4, the reactor tube was periodically cooled with liquid nitrogen, to condense the GeF_4 on to the walls of the tube, and then K_2NiF_6 solution was splashed on the walls. This produced a reaction, precipitating a dark brown solid and forming a deeply tinted brown solution, indicative of a cationic nickel species (see Chapter 5). This process was repeated once again, and between the two aliquots, 12.4 mmol of GeF_4 was added. After six hours, the solution seemed to be red in color again (indicating NiF_6^{2-} in solution), so more GeF_4 (3.2 mmol) was added. The reaction mixture was kept at 0 °C overnight. The following morning there was a colorless solution above a chestnut brown solid. The color indicated that it was not *R*-NiF_3, which is black. The residue (Sample A) was washed three times at 0 °C (at this point some gas evolution was observed, and the solid appeared slightly darker) and the aHF was removed. Unfortunately, during the removal of the aHF, some aHF containing K_2GeF_6 bumped back into the arm containing the nickel product. It was quickly decanted back, taking some of the insoluble chestnut brown product with it, so the gravimetry is not quantitative. Yield of chestnut brown solid, 1.433 g; yield of K_2GeF_6/chestnut brown mixture, 4.5228 g.

4.2.1.1. X-ray Powder Diffraction

The photo of the soluble product (mixed with some of the insoluble material) had the pattern of hexagonal K_2GeF_6. At first glance, the XRPP of the insoluble chestnut-brown solid appeared identical to that of *R*-NiF_3, but closer examination revealed that this

material had a larger unit cell. The reflections were indexed with the same rhombohedral indexing used for *R*-NiF_3 powder data (Table 2.1).

Table 4.1. Chestnut-Brown Product of {K_2NiF_6 + 1.26 GeF_4} in aHF at 0 °C. (CuKα radiation, Ni filter) Unit cell: a = 5.235(1) Å and α = 56.09(2)°, V = 92.28(11) $Å^3$

	$1/d^2_{hkl}$ x 10^4				
I/I_o	**observed**	**calculated**	***h***	***k***	***l***
w	517	517	1	1	1
w	607	608	1	0	0
vs	779	780	1	1	0
ms	1470	1470	2	1	1
w	1647	1651	1	1	0
ms	2168	2168	2	0	1
vw	2437	2431	2	0	0
ms	3118	3120	2	2	0
s	3718	3720	3	2	1
w	4074	4081	2	1	1
vw	4225	4228	3	3	2
w	4769	4771	3	1	0
w	4960	4952	2	1	1
vw	5881	5879	4	2	2
vw	6301	6298	4	3	3

4.2.1.2. Magnetic Susceptibility

The magnetic behavior of this solid is illustrated in Figure 4.1. The Curie-Weiss plot demonstrates that the material is a paramagnet, with a Weiss constant near zero (F.W. = 149.129 g/mol based on gravimetry).

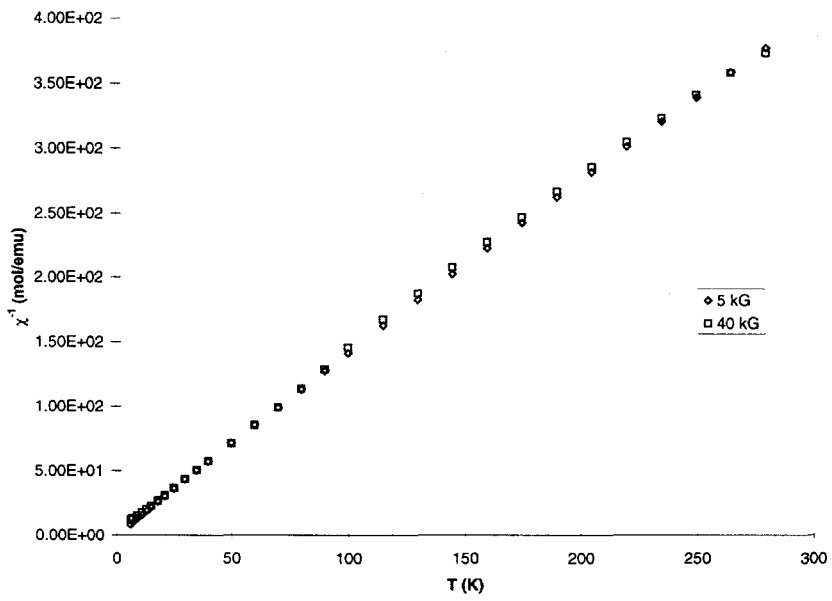

Figure 4.1. Magnetic Behavior of Sample A

4.2.2. Reaction of K_2NiF_6 with GeF_4 at 0 °C (molar ratio 1 : 3.3)

This reaction was a second attempt to prepare *R*-NiF_3 at 0 °C. This time the GeF_4 was allowed to diffuse into the solution slowly. This reaction was carried out in a 1" FEP tube, drawn down at one end to fit into a ½" T-union. The tube containing the K_2NiF_6 solution was held at a nearly horizontal angle, to maximize the area of the gas-solution interface. This experiment was intended to avoid the highly acidic solution produced in the previous reaction by condensing GeF_4 into the solution, which could have accelerated the loss of elemental F_2.

K_2NiF_6 (0.5577 g; 2.22 mmol) was placed in the bent arm of the reactor and aHF (~9.5 mL) was condensed onto it. The K_2NiF_6 completely dissolved in the aHF without

leaving an insoluble residue. The GeF_4 (7.3 mmol) was added to the reactor slowly and without mixing at 0 °C. Three hours later, the solution was deep yellow-brown, indicative of a cationic nickel species. This was kept at 0 °C overnight, and the next morning, a rosy- tan solid lay below a colorless solution. The reactor was checked for non-condensable gas (~2.3 mmol measured tensimetrically), which was evacuated from the reactor. The solid was washed twice at 0 °C and the aHF removed. The rosy-tan solid (Sample B) and the colorless soluble byproduct were recovered and the observed and expected masses are in rough agreement with $NiGeF_6$ and K_2GeF_6 as the products, as shown in Table 4.2.

Table 4.2. Gravimetry of $\{K_2NiF_6 + 3.3\ GeF_4\}$ Reaction at 0 °C

Products	Observed Mass (g)	Expected Mass (g)
$NiGeF_6$	0.5054	0.5452
K_2GeF_6	0.5291	0.5886

4.2.2.1. X-ray Powder Diffraction

The rosy-tan solid (B) showed a pattern similar to that observed for Sample A, but Sample B was more crystalline. The photo was measured and the following indexing and unit cell were derived (Table 4.3.). The photograph of the soluble byproduct showed the hexagonal form of K_2GeF_6. The unit cell parameters obtained for Sample B are slightly larger than those obtained for Sample A.

Table 4.3. X-ray Powder Diffraction Data for the Rose-Tan Colored Product of the reaction of $\{K_2NiF_6 + 3.3\ GeF_4\}$ in aHF at 0 °C. (CuKα radiation, Ni filter)
Unit cell: a = 5.241(1) Å, α = 56.25(2)°, V = 92.94(12) Å^3

	$1/d^2_{hkl} \times 10^4$				
I/I_o	**observed**	**calculated**	***h***	***k***	***l***
w	516	517	1	1	1
w	602	604	1	0	0
vs	774	776	1	1	0
m	1466	1466	2	1	1
w	1636	1639	1	1	0
m	2157	2156	2	0	1
w	2415	2414	2	0	0
m	3107	3104	2	2	0
s	3713	3708	3	2	1
w	4057	4052	2	1	1
vw	4233	4226	3	3	2
w	4743	4742	3	1	0
w	4911	4914	2	1	1
vvvw	5266	5260	3	2	0
vw	5863	5864	4	2	2
vw	6299	6296	4	3	3
vvvw	6428	6551	4	3	2
vvvw	6979	6986	4	1	1
vvvw	8637	8624	4	0	2
vvvw	8968	8969	2	2	2
vvvw	9921	9918	4	3	0

4.2.2.2. Magnetic Susceptibility

The susceptibility of Sample B was paramagnetic, the Curie-Weiss plot in Figure 4.2. shows linearity with an intercept near zero. The form of the magnetism is essentially that of Sample A, and the magnitude of the susceptibility only slightly less (F.W. = 245.270 g for $NiGeF_6$)

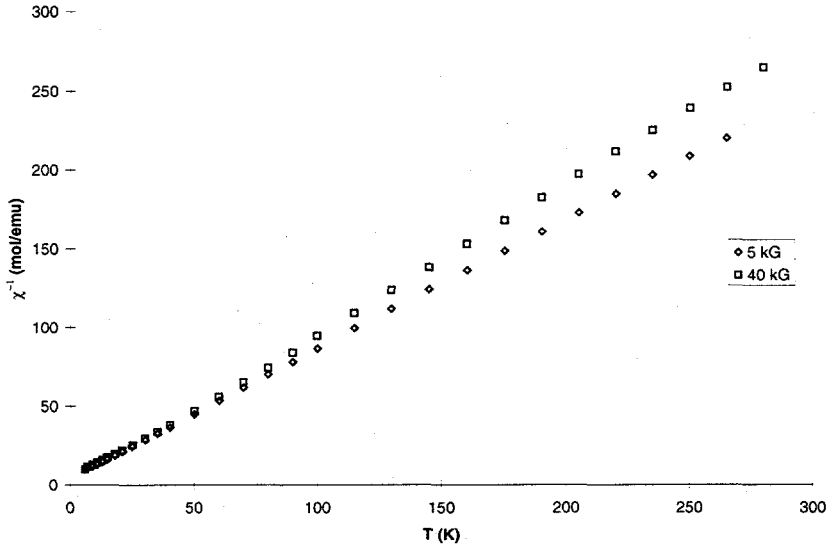

Figure 4.2. Magnetic Behavior of Sample B

4.2.3. Reaction of K_2NiF_6 with GeF_4 at -65 °C (molar ratio 1 : 4.8)

This reaction was carried out below -65 °C in an attempt to isolate NiF_4. It is possible that NiF_4 would be stable, if washed free of the byproduct (K_2GeF_6) and thoroughly dried at low temperatures. K_2NiF_6 (0.4340 g; 1.73 mmol) was placed in one arm of a ½" T-reactor and aHF (~9 mL) was condensed onto it. Although purified K_2NiF_6 was used, a small amount of the insoluble red-brown solid occasionally derived from K_2NiF_6 in aHF (see Section 1.2.3.2.) was observed (~0.005 g), so the red solution was decanted to the opposite arm and the reaction carried out there (therefore, approx. 1.68 mmol of K_2NiF_6). The solution was cooled to -78 °C, and GeF_4 (8.17 mmol, measured tensimetrically) was added slowly. After three hours there was a small amount of tan

solid at the bottom of the reactor, below a deep golden-brown solution. The reactants were kept at -78 °C overnight, and by morning, had not changed in appearance. There was still a brown solution and the same quantity of solid. The reactor was frozen to -196 °C to check for non-condensable gas, of which there was none. The reactor was warmed to -65 °C and opened to vacuum to remove some GeF_4. As this took place, more tan solid was precipitated and the color of the solution lightened. The solution was exposed to vacuum periodically to remove some of the excess GeF_4. The soluble nickel species (in this case probably Ni^{IV}) was very persistent and did not release GeF_4 until the aHF and GeF_4 were removed and the solid was nearly dry. (It was necessary to remove excess GeF_4, otherwise soluble Ni^{IV} would have been transferred to the waste arm with each decantation.) To separate K_2GeF_6 from the tan product, aHF (3-4 mL) was condensed on to the tan solid, the solution decanted and the aHF back-distilled seven times at -65 °C. The aHF was removed and the solid dried under dynamic vacuum. The tan solid was warmed under dynamic vacuum to room temperature over a period of four days. The gravimetry of the recovered products is shown in Table 4.4.

Table 4.4. Products of Reaction of K_2NiF_6 with GeF_4 at -65 °C in aHF

Products	Observed Mass (g)	Expected Mass for (product) (g)
Tan solid	0.3250	0.2330 (NiF_4) 0.3286 ($Ni^{II}Ni^{IV}Ge^{IV}F_{10}$) 0.3335 ($KNiF_5$) 0.3336 (1:1 mixture of NiF_4 and $NiGeF_6$) 0.4343 ($NiGeF_6$)
K_2GeF_6	0.4162	0.4448 (all K^+ as K_2GeF_6) 0.2290 (only half of K^+ as K_2GeF_6, the rest present in $KNiF_5$)

4.2.3.1. X-Ray Powder Diffraction

The tan solid gave a novel diffraction pattern, unlike those obtained for Samples A and B. It was not similar to patterns known for several classes of tetrafluoride, or $KPdF_5$, and contained 29 observed lines. The data are shown in Table 4.5., and have not been indexed. No indexing relationships were found that might indicate a trigonal, orthorhombic or tetragonal system.

Table 4.5. X-Ray Powder Diffraction Data for the Tan-Colored Product of the Reaction of $\{K_2NiF_6 + 4.7\ GeF_4\}$ in aHF at -65 °C. ($CuK\alpha$ radiation, Ni filter)

I/I_o	$1/d^2_{hkl} \times 10^4$	I/I_o	$1/d^2_{hkl} \times 10^4$
w	224	vw	1839
m	325	vvw	1984
w	459	vvw	2122
vw	526	vvw	2177
vw	584	w	2514
s	896	w	2692
vvw	988	vvw	2756
vw	1081	vvw	2883
vw	1137	vvw	3062
vw	1197	vvw	3153
vw	1305	vw	3277
w	1618	vw	3603
vw	1710	vw	4135
vw	1803	vw	4436

4.2.3.2. Magnetic Susceptibility

Surprisingly, the form of the magnetic susceptibility was identical to that of Samples A and B, differing only in magnitude from those. The behavior is that of a simple paramagnet. The data are shown in Figure 4.3.

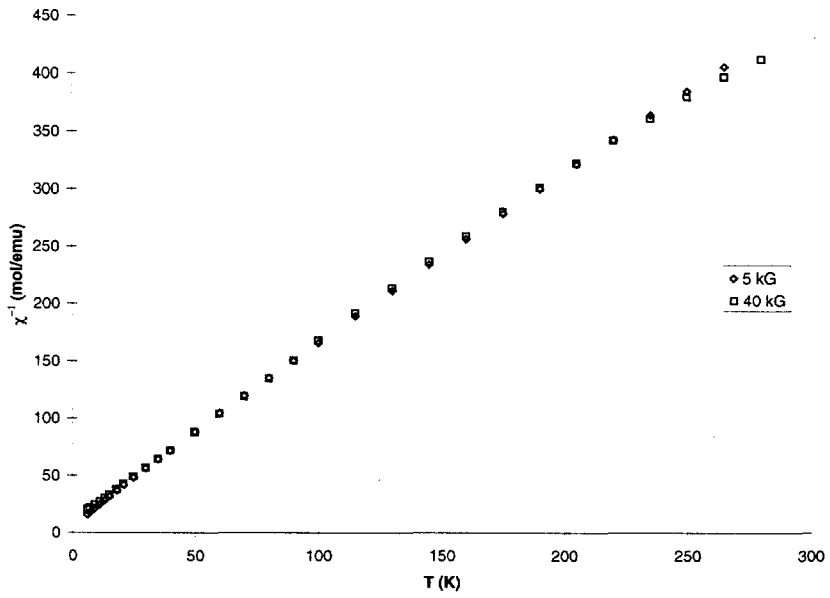

Figure 4.3. Magnetic Behavior of Sample C

4.3. Results and Discussion

The reactions of K_2NiF_6 with GeF_4 surprisingly led to novel products: $NiGeF_6$ and a tan solid with a novel XRPP. The unit cells of *R*-NiF_3, Sample A and Sample B are shown in Table 4.6.

Table 4.6. Comparison of Unit Cell volumes of *R*-NiF_3, Solid Solution of $NiGeF_6$ in *R*-NiF_3 (Sample A), and $NiGeF_6$ (Sample B)

	a (Å)	α (°)	V (Å^3)
R-NiF_3 ($Ni^{II}Ni^{IV}F_6$)	5.1603(2)	55.594(2)	87.228(4)
Sample A	5.235(1)	56.09(2)	92.28(11)
Sample B ($NiGeF_6$)	5.241(1)	56.25(2)	92.94(12)

Sample A, which had a chestnut-brown color clearly incorporated germanium into the product, but the color indicates that Ni^{IV} is present as well. Based on the unit cell in Table 4.6., it appears that this chestnut-brown material is a solid solution of $NiGeF_6$ and $Ni^{II}Ni^{IV}F_6$. The difference in unit cell volume between Sample A and Sample B is 0.6 Å^3, whereas the difference between Sample A and *R*-NiF_3 is 5.7 Å^3. This indicates that Sample A is probably a solid solution, composed largely of $NiGeF_6$ with a small amount of $Ni^{II}Ni^{IV}F_6$ present. This is a larger $NiGeF_6$ yield than that anticipated on the basis of the estimated quantity of GeF_4 added. In this reaction, 12.4 mmol of K_2NiF_6 and 15.6 mmol of GeF_4 (measured tensimetrically) were used. An equimolar quantity of K_2NiF_6 and GeF_4 probably would have reacted according to:

$$K_2NiF_6 + GeF_4 \longrightarrow R\text{-}NiF_3 + K_2GeF_6 + \tfrac{1}{2}F_2 \qquad (1)$$

however, excess GeF_4 present apparently reacted with the NiF_3 to give $NiGeF_6$:

$$NiF_3 + GeF_4 \longrightarrow NiGeF_6 + \tfrac{1}{2} F_2 \qquad (2)$$

In this case, if all of the K_2NiF_6 reacted with 12.4 mmol of GeF_4, then *R*-NiF_3 (12.4 mmol) would have been produced. The excess 3.2 mmol of GeF_4 would then react with the 3.2 mmol of *R*-NiF_3 to give 3.2 mmol $NiGeF_6$. If this were so, the mass balance expected would be 5.1324 g, whereas 5.9558 g was observed. It must be concluded that the tensimetry on which the GeF_4 consumption was based grossly underestimated the GeF_4 usage. Indeed the unit cell dimensions derived from the XRPD clearly indicate a higher GeF_4 uptake, in accord with the observed mass of the $NiGeF_6/Ni^{II}Ni^{IV}F_6$ product. A more accurate measure of the ratio of $NiGeF_6$ to $Ni^{II}Ni^{IV}F_6$ might be obtained by comparing the volumes of GeF_6^{2-} vs. NiF_6^{2-} anions in isostructural A_2MF_6 salts. The volume increase of the solid solution over the $Ni^{II}Ni^{IV}F_6$ unit cell could be related to the volume difference of the two anions and the composition formulated assuming that Ni^{III} is largely Ni^{II} and Ni^{IV} as in *R*-NiF_3 itself, *i.e.* $Ni^{II}_{x+y}Ge^{IV}_{x}Ni^{IV}_{y}F_6$.

The magnetism of this solid solution indicates that the superexchange connectivity of Ni^{II} with other Ni^{II}, has been disrupted by the presence of GeF_6^{2-} and low spin d^6 NiF_6^{2-}. Presumably the charge transfer is suppressed by the fact that many of the Ni^{II} would have Ge^{IV} neighbors and not Ni^{IV}. The gravimetry indicates that $x = 0.26$ and $y = 0.74$, thus the magnetic moment of the $NiGeF_6/Ni^{II}Ni^{IV}F_6$ solid solution is $\mu_{eeff} = 2.4$ β. This is somewhat greater than the moment observed for $Ni^{II}Ni^{IV}F_6$ (2.1 β), but is in rough agreement with the formulation.

Rose-tan colored Sample B is close in composition to $NiGeF_6$ since there was enough GeF_4 present to carry all of the NiF_3 to $NiGeF_6$ according to equation (2). The magnitude of the magnetic moment (μ_{eff} = 3.01 β) indicates one Ni^{II} per formula unit. In addition, the unit cell is larger than that of the solid solution (Sample A), as expected. There are several examples of mixed metal pseudo-trifluorides, which have been prepared in these labs, which contain Ni^{II} and M^{IV}, $NiFeF_6$, $NiCoF_6$, and $NiCuF_6$,[2] in addition to $NiMnF_6$ described by Hoppe *et. al.*[3] However, these materials all possess paramagnetic anions and are therefore more complex magnetically than the simple paramagnets of the $Ni^{II}_{x+y}Ge^{IV}_{x}Ni^{IV}_{y}F_6$ system.

The reaction between K_2NiF_6 and GeF_4 at -65 °C produced an exceptionally long-lived soluble Ni^{IV} species, as indicated by the absence of detectable F_2 evolution. The aHF and GeF_4 were removed before washing the tan solid free of K_2GeF_6. If the excess GeF_4 had remained in solution, it would have solvated the NiF_4 and carried it with the soluble byproducts to the other arm of the reactor during decantation and back-distillation. The tan solid deposited upon removal of aHF and GeF_4 (under which circumstances F_2 evolution as the system approached dryness would have been possible) gave a novel XRPP and had simple paramagnetic behavior. The identity of this solid has not yet been established, but it is possible to rule out some compositions. First, it is conceivable that the tan solid might be a mixture of NiF_4 with $NiGeF_6$, based on the similar magnetic behavior (with lower magnitude, if the only magnetic component present was $NiGeF_6$). However, the X-ray powder data (see Table 4.5.) do not reveal any

of the lines attributable to $NiGeF_6$ (see Table 4.3.).

A second possible composition is $KNiF_5$. Experience with other MF_6^{2-} salts in interaction with F^- acceptors had shown that aHF insoluble MF_5^- salts are sometimes the first product of such interactions.[4] That could be the situation here:

$$2\ NiF_6^{2-} + GeF_4 \longrightarrow 2\ NiF_5^- + GeF_6^{2-} \quad (3)$$

In this case however, the yield of K_2GeF_6 should be much less than observed (see Table 4.4.). This is because only half of the cation (K^+) concentration can appear in this salt, the remainder being required for $KNiF_5$. Whenever GeF_4 has been used in aHF to abstract F^- from AgF_4^- or AuF_4^-, the only germanium containing product formed has been the highly soluble K_2GeF_6 salt.[5] It is therefore probable that GeF_5^- is unstable in aHF with respect to dismutation to GeF_6^{2-} and GeF_4.

It is probable that the bulk of the tan solid is non-magnetic. This is consistent with the presence of a low spin d^6 Ni^{IV} species. All known NiF_6^{2-} salts are diamagnetic[6] and this could also be so for NiF_5^- or even NiF_4 itself. Based on the tendency of Ge^{IV} to form polymeric anions[7] and the comparable Lewis acidity of GeF_4 and NiF_4, it is possible that a material with the composition, $Ni^{II}Ni^{IV}Ge^{IV}F_{10}$ exists (*i.e.* $Ni^{2+}[NiGeF_{10}]^{2-}$). In this case, the Ni^{IV} would be present in a complex fluorine bridged anion with Ge^{IV}, $[Ni^{IV}Ge^{IV}F_{10}]^{2-}$ being analogous to a pentafluoride, many of which are tetrameric (M_4F_{20})[8] or polymeric.[9] The monoclinic structure of $BaZnFeF_7$ is made up of $[ZnFeF_{10}]^{5-}$ units, in which the metal octahedra share an edge.[10] Another possibility is that the cation is NiF^+ and the anion is $[Ni^{IV}Ge^{IV}F_9]^-$, this is perhaps more plausible, since Ni^{II} is known to have high Lewis

acidity, as it is able to abstract F^- from AsF_6^-, forming $NiFAsF_6$ from $Ni(AsF_6)_2$ (see Appendix A). Tetragonal structures of several compounds containing the $[M_2F_9]^-$ unit (face sharing octahedra) are known.[11]

The gravimetry of the reaction to produce Sample C is in accord with the formulation $Ni^{II}Ni^{IV}Ge^{IV}F_{10}$, with an expected mass of 0.3286g, 0.3250 g is observed. The observed and expected masses of K_2GeF_6 support this formulation as opposed to that for $KNiF_5$ formation.

The room temperature magnetic moment, when calculated on the basis of the formula weight of $Ni^{II}Ni^{IV}Ge^{IV}F_{10}$ gives $\mu_{eff} = 2.3\ \beta$. This is in harmony with the moment observed for $Ni^{II}Ni^{IV}F_6$ of *R*-NiF_3.

Since it appears that an acidic aHF solution may promote the formation of $NiGeF_6$, it is possible that avoidance of local acidity by very slow delivery of dilute GeF_4 (i.e., dry N_2 with GeF_4; 10 : 1) bubbled through a solution of K_2NiF_6 held at -65 °C could forestall the formation of $NiGeF_6$. Perhaps more importantly, the GeF_4 should be the limiting reagent. This might lead to the isolation of a pure sample of NiF_4 as the K_2GeF_6 byproduct is highly soluble at low temperatures. If the complete separation of K_2GeF_6 is effected, and the tan solid thoroughly dried, it is possible that NiF_4 would be stable.

4.4. Conclusion

The interaction of GeF_4 with dissolved K_2NiF_6 in aHF at ≤ -65 °C yields a tan solid. Gravimetric and magnetic data indicate the formulation $Ni^{II}Ni^{IV}Ge^{IV}F_{10}$, but this material has not been structurally characterized. The possibility of this material being $KNiF_5$ or a mixture of NiF_4 and $NiGeF_6$ has been ruled out.

In contrast with the behavior of other Lewis acids, the interaction of GeF_4 with dissolved K_2NiF_6 in aHF at 0 °C yields the novel relative of $Ni^{II}Ni^{IV}F_6$, $Ni^{II}Ge^{IV}F_6$. It has a rhombohedral structure akin to that of R-NiF_3 and is a simple paramagnet.

4.5. References

[1] Žemva, B.; Lutar, K.; Chacón, L.; Fele-Beuermann, M.; Allman, J.; Shen, C.; Bartlett, N. *J. Am. Chem. Soc.*, **1995**, *117*, 10025.
[2] Shen, C.; Elder, S. H.; Bartlett, N., unpublished results.
[3] Hoppe, R. Siebert, G. *Z. Anorg. Allg. Chem.* **1970**, *376*, 261.
[4] Casteel, Jr., W. J., Ph.D. Thesis (1992) U. C. Berkeley, Chapter 4.
[5] Lucier, G. M.; Whalen. J. M.; Bartlett, N. *J. Fluor. Chem.*, in press (1997).
[6] Hoppe, R. *Angew. Chem.*, **1950**, *62*, 339.
[7] Christe, K. O.; Wilson, R. D.; Goldberg, I. B. *Inorg. Chem.* **1976**, *15*, 1271.
[8] Morrell, B. K.; Zalkin, A.; Tressaud, A.; Bartlett N. *Inorg. Chem.* **1973**, *12*, 2640.
[9] in Landolt-Börnstein, New Series, Group III, vol. 7, **1973**, Part A, no. 243.
[10] Holler, H.; Babel, D. *Z. Anorg. Allg. Chem.*, **1982**, *491*, 137.
[11] Tressaud, A.; Babel, D. in Inorganic Solid Fluorides, P. Hagenmuller, Ed., Academic Press, NY, 1985, pp. 166.

Chapter 5. Cationic Ni^{IV}

5.1. Introduction

The general route to binary polymeric fluorides through the reaction of complex metal fluorides with Lewis acids in aHF solvent was established in 1989 in a collaboration of the Berkeley group with that of the Josef Stefan Institute in Ljubljana, Slovenia.[1] It was later noted that when an excess of Lewis acid (beyond the stoichiometric quantity required to abstract F^- to precipitate the binary fluoride) was added to binary fluorides in aHF, a colored solution resulted without immediate loss of F_2. This colored solution was believed to contain the metal in a cationic state, as the action of excess Lewis acid would tend to remove F^- from the binary fluoride. It is probable that the soluble cationic entity is a solvated fluoro-species such as $NiF_3(HF)_x^+$, but strong interaction of such a species with the particular Lewis acid anion could also occur. In this acidic medium, the highly oxidized metal is expected to be unstable with respect to loss of F_2, (because of the high electronegativity associated with the electron deficit), and consequently, a very powerful oxidizer.

Gantar, *et. al.* established that $Ag(SbF_6)_2$ and $AgFAsF_6$ crystals could be prepared from blue aHF solutions produced by the addition of AsF_5 or SbF_5 to AgF_2.[2,3] In the studies of the interaction of AgF_3 with AsF_5 and other acids in aHF carried out in these laboratories it was observed that this same blue Ag^{II} solution species was slowly formed.[4] Subsequently, G. M. Lucier in these laboratories established that the cationic Ag^{III} species derived from AgF_3 was capable of oxidizing PtF_6^- to PtF_6.[5] In the subsequent search for a cationic $Ag^{III}_{(solv)}$ species it was found[5,6] that even cationic $Ag^{II}_{(solv)}$ was capable of oxidizing Xe to Xe^+, O_2 to O_2^+, C_6F_6 to $C_6F_6^+$, and C_3F_6 to C_3F_8. This prompted the similar study of cationic $Ni^{IV}_{(solv)}$ described in this chapter.

Cationic Ni^{IV} ($Ni^{IV}_{(solv)}$) is prepared by the addition of a Lewis fluoroacid (GeF_4, PF_5, BF_3, AsF_5 or SbF_5) to a cooled solution (-65 °C) of K_2NiF_6. Upon addition of the Lewis fluoroacid to the K_2NiF_6 solution, a tan precipitate (NiF_4) is formed as the red color of NiF_6^{2-} disappears. Addition of an appropriate stoichiometric amount (e.g. 2 BF_3 or 1 GeF_4 for each NiF_6^{2-}) of Lewis fluoroacid gives a colorless solution over the tan solid, NiF_4. Addition of excess fluoroacid causes a yellow species to appear in solution. If a very large excess of acid is added, the color of the solution becomes deeper, eventually so intense that it appears dark brown.

The $Ag^{II}_{(solv)}$, $Ag^{III}_{(solv)}$ and $Ni^{IV}_{(solv)}$ may be ranked in order of oxidizing power by carrying out a series of reactions with third transition series hexafluorometallates. The hexafluorometallates(V) can be ordered by their ionization potential, (i.e. the electron affinity of the corresponding hexafluoride). The third transition series hexafluorides are

approximately of the same size[7,8] (as are their monoanions), [9] so the differences in their oxidizing power is essentially determined by the differences in their electron affinities. This energy term increases by ~1 eV for each unit increase in atomic number, z, of M, from W to Pt.[10] There is a similar trend in the second transition series but with a greater increase in electron affinity with increase in z, RuF_6 being comparable with PtF_6.[11] This is due to the steady lowering of the energy of the t_{2g} frontier orbitals as z increases.

R-NiF_3 and *H_O*-K_xNiF_3 also produce powerfully oxidizing yellow solutions when acidified with AsF_5 or BF_3 in aHF. Yellow solutions derived from either *R*-NiF_3 or *H_O*-K_xNiF_3 were able to oxidize RuF_6^- to RuF_6.

Attempts to characterize $Ni^{IV}_{(solv)}$ in solution by ^{19}F NMR, and in the solid state by isolation of the cationic species as a salt of SbF_6^-, are described.

5.2 Experimental

5.2.1. Preparation of Hexafluorometallate(V) Salts

$KPtF_6$ was prepared by the reaction of KF with O_2PtF_6.[12] $KRuF_6$ was prepared by the reaction of RuF_5 with a stoichiometric quantity of KF in aHF. The RuF_5 was prepared by the reaction of F_2 with powdered metal, reduced in a H_2 atmosphere at ~500 °C before use.

5.2.2. Oxidation of RuF_6^- to RuF_6

5.2.2.1. $Ni^{IV}_{(solv)}$

One arm of a T-reactor was loaded with K_2NiF_6 (0.294 g; 1.17 mmol) and $KRuF_6$ (0.0997 g; 0.392 mmol), and the aHF (~2 mL) was condensed onto the solids at -196 °C

and the mixture warmed to -65 °C. The active Ni^{IV} species was prepared *in situ* by adding BF_3 (4.74 mmol). Once the solution became dark brown in color (indicative of the presence of $Ni^{IV}_{(solv)}$), the reaction mixture was allowed to warm to -35 °C at which temperature it was agitated for 1.5 h to mix the reagents. During this time the brown color of the solution was replaced by the intense red color of RuF_6 in solution. The deep red gaseous RuF_6, along with aHF was then condensed to the other arm of the T-reactor at -196 °C. Once the transfer was complete, dry O_2 (3.63 mmol) was admitted to the reactor to combine with the RuF_6 producing a red crystalline solid under a yellow solution. The aHF was removed at temperatures below -20 °C to yield O_2RuF_6 (0.092 mmol, 23% yield, based on RuF_6^-). In a separate reaction, it was found that repeating the process of acidifying the solution with BF_3 (i.e., regenerating the oxidizing $Ni^{IV}_{(solv)}$ species), agitating and then condensing RuF_6 to the side-arm a second time, increased the yield of O_2RuF_6 twofold (49.8%). Presumably at the low temperatures necessary to maintain the $Ni^{IV}_{(solv)}$ the solubility of the $KRuF_6$ is low. An XRPP of O_2RuF_6 showed it to have the same unit cell (cubic, a = 10.004 Å) as reported previously.[13]

5.2.2.2. R-NiF_3

One arm of a T-reactor was loaded with *R*-NiF_3 (0.1138 g; 0.984 mmol), $KRuF_6$ (0.1264 g; 0.497 mmol), and aHF (~3.8 mL) was condensed onto the solids at -196 °C and the mixture warmed to -38 °C. BF_3 (6.23 mmol) was admitted to the reactor, with stirring. After 1 h, there was no sign of coloration of the aHF (although during a previous

attempt, there was a slight yellow tinting of the aHF). The BF_3 was evacuated from the reaction mixture at -35 °C. AsF_5 (9.48 mmol) was admitted to the reactor, forming a dark yellow-brown colored solution. After 1.5 h at -35 °C, the yellow-brown color of the solution had changed to red above a yellow solid. The red gaseous RuF_6 along with some aHF was condensed to the other arm of the reactor. Dry O_2 (2.33 mmol) was admitted to the reactor, and reacted with the RuF_6 at -30 °C, to form some orange and some gray-white crystalline material. As the O_2 and aHF were evacuated at -35 °C to dry the products, the crystalline solid became orange-yellow in color (0.1737 g; 141% if O_2RuF_6). The XRPP of this material showed a pattern like that of the O_2RuF_6 pattern, but with some additional lines. In addition, the unit cell was smaller than that of O_2RuF_6. The yellow nickel residue gave a pattern similar to that found for "$NiFAsF_6$", derived from $Ni(AsF_6)_2$ exposed to high vacuum (see Appendix A). Based on the gravimetry and the XRPP, it appeared that arsenic had been incorporated in the product.

5.2.2.3. H_O-K_xNiF_3

Acidified with BF_3. One arm of a T-reactor was loaded with H-NiF_3 (0.1037 g; 0.896 mmol), $KRuF_6$ (0.0884 g; 0.348 mmol), and aHF (~3.5 mL) was condensed onto the solids. At -36 °C, BF_3 (6.47 mmol) was admitted to the reactor, forming a yellow solution. The reagents were allowed to stir at -36 °C for 4 h, then the red gaseous RuF_6 and aHF were condensed to the other arm of the reactor and dry O_2 (0.896 mmol) was added. Orange-red crystals (O_2RuF_6 by XRPD) formed and were dried by evacuating the

aHF at -25 °C (0.0074 g; 9 % yield O_2RuF_6).

Acidified with AsF_5. One arm of a T-reactor was loaded with H-NiF_3 (0.1043 g; 0.9016 mmol), $KRuF_6$ (0.0883 g; 0.3474 mmol), and aHF (3.5 mL) was condensed on the solids at -196 °C and the mixture warmed to -36 °C. AsF_5 (3.58 mmol) was admitted to the reactor. After 25 minutes a red color was observed in solution, and the mixture was allowed to stir at -36 °C for 1 h, after which time the solution was red and the solid below was yellow. The red gaseous RuF_6 and aHF were transferred to the other arm of the reactor at -196 °C and dry O_2 (0.974 mmol) was admitted to the reactor, forming yellow and orange crystals, which were dried below -25 °C (yield 0.096 g; 112% if O_2RuF_6). An XRPP of the yellow-orange crystals was essentially that of O_2RuF_6 but again, with a smaller unit cell. This, the impossibly high yield of "O_2RuF_6", and the less intense orange color indicates that there was some arsenic incorporated in the product, as also observed in the product described in 5.2.2.2.

5.2.3. Oxidation of PtF_6^- to PtF_6

5.2.3.1. $Ni^{IV}_{(solv)}$

One arm of a T-reactor was loaded with K_2NiF_6 (0.152 g; 0.607 mmol) and $KPtF_6$ (0.104 g; 0.299 mmol), aHF (~2.5 mL) was condensed onto the solids at -196 °C and the mixture warmed to -61 °C. BF_3 (12.7 mmol) was added, producing a deeply colored brown solution. The reaction mixture was warmed to -35 °C and agitated for 1 h. During this time, the brown color of the $Ni^{IV}_{(solv)}$ was replaced by the intense red color of

PtF_6 in solution. The red gaseous PtF_6 was condensed, along with aHF, to the other arm of the reactor at -196 °C. Once the transfer was complete, dry O_2 (1.76 mmol) was admitted to the reactor, forming orange-red crystals below a yellow solution. After removal of the aHF at temperatures below -20 °C, this solid darkened to yield deep red crystalline O_2PtF_6 (0.0231 g; 0.0673 mmol; 22.5%). An XRPP of this material showed the same unit cell (cubic, a = 10.032 Å) as reported previously.[14]

5.2.4. Oxidation of O_2 to O_2^+

5.2.4.1. $Ni^{IV}_{(solv)}$

One arm of a T-reactor was loaded with K_2NiF_6 (0.2151 g; 0.857 mmol) and aHF (~1.5 mL) was condensed in at -196 °C and the solution warmed to -65 °C. AsF_5 (4.81 mmol) was admitted to the reactor, forming a deeply colored brown solution, over a tan solid. O_2 (1.53 mmol) was admitted to the reactor, forming a voluminous colorless precipitate. After the O_2 had been added there was a persistent yellow color to the solution. The soluble and insoluble products were separated by decantation and back-distillation of aHF (3 times), and dried under vacuum. The XRPP of the soluble yellow product indicated the mixture $Ni(AsF_6)_2$ and O_2AsF_6. The insoluble solid was off-white and had the XRPP of $KAsF_6$.

5.2.5. Attempted Oxidation of AuF_6^- to AuF_6 with $Ni^{IV}_{(solv)}$

One arm of a T-reactor was loaded with K_2NiF_6 (0.4580 g; 1.83 mmol) and XeF_5AuF_6 (0.2184 g; 0.407 mmol), and aHF (~5 mL) was condensed onto the solids at -196 °C, and the solution warmed to -65 °C. AsF_5 (~6 mmol) was admitted to the reactor,

forming a tan precipitate below a deep brown solution. No reaction was observed so the temperature was warmed to -35 °C for 1 h. To test for the presence of a colored gas, the opposite arm of the reactor was cooled to -196 °C, but no colored gas was seen moving through the reactor. The solution was warmed to -17 °C, then -10 °C and tested for colored gas at each temperature, with a negative result at each temperature. Cooling to -196 °C and opening the reactor to the line indicated the presence of non-condensable gas, (*i.e.* F_2) which was evacuated.

5.2.6. Characterization of NiF_6^{2-} and $Ni^{IV}_{(solv)}$ by ^{19}F NMR

Samples of NiF_6^{2-} and $Ni^{IV}_{(solv)}$ were prepared and sealed in FEP NMR tubes and analyzed by ^{19}F NMR. There were some experimental obstacles to overcome, first, the temperature of the $Ni^{IV}_{(solv)}$ had to be maintained below -65 °C, or risk decomposition of the $Ni^{IV}_{(solv)}$. Secondly, the K_2NiF_6 had to be 100% soluble. Any lower fluoride formed by reduction of K_2NiF_6, when acidified in aHF, could generate paramagnetic Ni^{II}, rendering the NMR experiment useless. BF_3 was first used to generate the $Ni^{IV}_{(solv)}$, but did not completely dissolve the NiF_4. AsF_5, used in the stoichiometry 16:1 (AsF_5 to K_2NiF_6) dissolved the NiF_4 completely. SbF_5, used in the stoichiometry 3:1 (AsF_5 to K_2NiF_6) also dissolved the NiF_4 completely. Each reaction was carried out in a reactor composed of an FEP NMR tube fused to a section of ¼" tubing, which connected to a valve. The NMR tube was used as the reactor so as to avoid transfer of the solution, which might destroy the species of interest if warming occurred. The use of an NMR tube as the reactor

limited the quantity of aHF used to ~0.3 mL in each case.

5.2.6.1. ^{19}F NMR of NiF_6^{2-}

K_2NiF_6 (0.0431 g; 0.172 mmol) was placed in an FEP NMR tube and aHF (~0.3 mL) was condensed onto it at -196 °C and the resulting solution warmed to -60 °C. The ^{19}F spectrum from -185 to -352 was recorded at -60 °C. It consisted of a resonance centered at -322 ppm, with a width at half height ($\Delta\nu_{1/2}$) of ~15 Hz.

5.2.6.2. K_2NiF_6 with AsF_5

K_2NiF_6 (0.0197 g; 0.170 mmol) was placed in an FEP NMR tube, and aHF (~0.3 mL) was condensed onto it at -196 °C and the solution warmed to -78 °C. AsF_5 (2.71 mmol) was admitted to the reactor, forming tan NiF_4. After two equivalents had been added, the solution became progressively darker yellow, until it was very intense and appeared dark brown. Immediately following the addition of 16 molar equivalents of AsF_5, there was still some tan solid present, along with colorless $KAsF_6$. The NMR tube was sealed and left at -78° C overnight. In the morning, no tan solid was visible, indicating that it had all been taken into solution by the AsF_5.

The ^{19}F NMR spectrum from +913 to -352 ppm was recorded at -76 °C. It consisted of a broad saddle-shaped resonance centered at -181 ppm, with $\Delta\nu_{1/2}$ = 16500 Hz. Peaks attributable to NiF_6^{2-} and AsF_6^- which typically occur around -310 ppm and -68 ppm, respectively, were not observed. The chemical shift of the observed resonance is close to that expected for HF solvent (-190 ppm), and the large

linewidth (typical non-exchanging ^{19}F linewidths are < 10 Hz) indicate rapid fluoride exchange between HF, AsF_5 and nickel fluorides in solution.

5.2.6.3. K_2NiF_6 with SbF_5

Using a glass pipette (vacuum dried at high temperature), SbF_5 (0.1766 g; 0.81 mmol; distilled, viscous) was pipetted into the FEP NMR tube, and allowed to settle to the bottom of the tube by standing the tube vertically in the drybox for 12 h. K_2NiF_6 (0.0573 g; 0.228 mmol) was loaded into a small container made to fit inside the NMR tube by drawing down ¼" FEP tubing, and the container placed in the bottom of the reactor. The vessel was taken out of the drybox and immediately cooled to -78 °C, to avoid reaction of SbF_5 vapor with K_2NiF_6. The connections were passivated and aHF (~0.3 mL) was condensed on the reagents and the temperature warmed to -60 °C. As some of the K_2NiF_6 and SbF_5 dissolved, a yellow solution was formed. About half of the K_2NiF_6 from the insert dissolved after inverting and agitating the tube, simultaneously ensuring that no warming above -60 °C occurred. A colorless precipitate was formed and the solution color intensified to dark brown (yellow in transmitted light). The solution was frozen to -196 °C, the reactor opened to vacuum and the NMR tube sealed with a flame. The tube was warmed to -76 °C for the NMR experiment. The sample upon warming contained a dark brown solution with some solid K_2NiF_6 (purple) in the bottom of the insert and some colorless $KSbF_6$ on the bottom of the tube.

The ^{19}F NMR spectrum from +176 to -388 ppm at -61 °C (see Figure 5.1)

consisted of several peaks due to SbF_6^- (singlet, -127.2 ppm) and SbF_5 and its oligomers with SbF_6^- in solution at low temperatures (singlets; -93.8, -120.6, -142.5 ppm).[15] The HF resonance, observed at -190 ppm indicates no exchange. A broad singlet ($\Delta\nu_{1/2}$ = 338 Hz) was observed at -235.2 ppm. No resonance due to NiF_6^{2-} was observed.

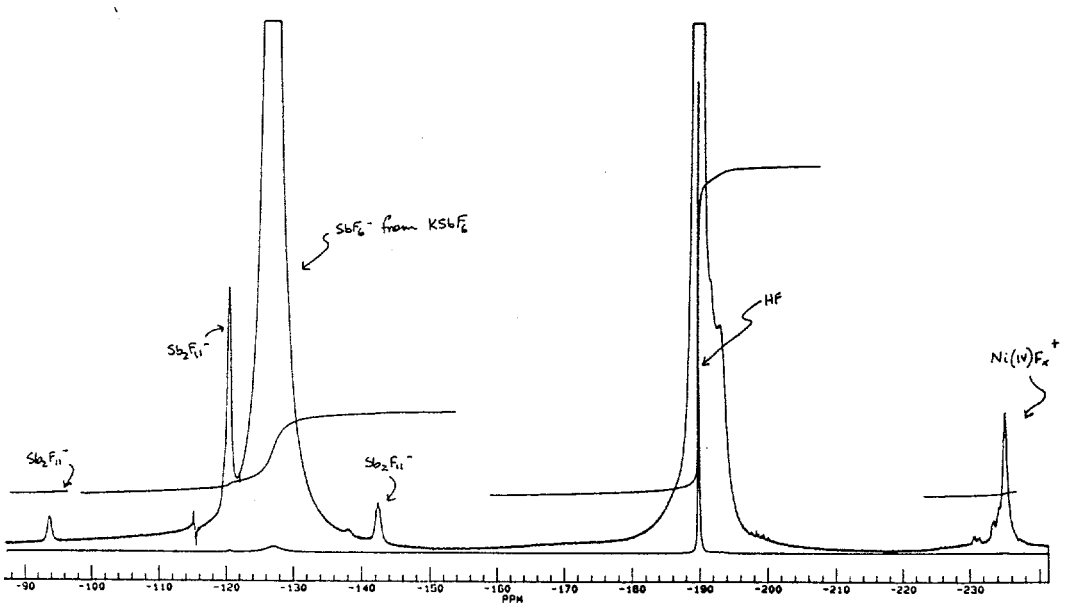

Figure 5.1. ^{19}F NMR Spectrum of Products of $\{K_2NiF_6 + 3SbF_5\}$ in aHF at -60°C

5.2.7. Attempted Isolation of $NiF_3^+SbF_6^-$

This reaction was carried out in a W-reactor, which consists of one continuous piece of FEP tubing bent into a W-shape. The two ends of the "W" are then connected via a Teflon T-union, using two openings that are at right angles to one another. This configuration allows for the decantation of a solution from one lobe of the "W" over the rise in the middle into the other lobe of the "W", while holding the entire apparatus at a low temperature (decanting through the Teflon T-union would warm the solution, decomposing some of the $Ni^{IV}_{(solv)}$).

K_2NiF_6 (0.101 g; 0.040 mmol) was loaded into one lobe of the "W" and SbF_5 (0.2706 g; 1.25 mmol) was pipetted into the other lobe of the "W". Two clamps were applied to the tube to prevent any premature reaction between any SbF_5 vapor and the solid, dry K_2NiF_6. The reactor was cooled to 0 °C to evacuate the argon (from the drybox atmosphere) without also evacuating the SbF_5 (m.p. 10 °C), then aHF (1.5 mL) was condensed onto both reagents and the W-reactor was cooled to -75 °C. The SbF_5 solution was poured onto the K_2NiF_6 solution, precipitating a tan solid at the interface of the two solutions. After a few minutes of agitation, a small amount of tan solid remained and a colorless solid had precipitated from the intensely colored yellow-brown solution. The solution was decanted to the lobe of the "W" that the SbF_5 had been in, and the reactor was opened to dynamic vacuum at -70 °C. Five days were required to remove the aHF at -70 °C, during which the color of the solution intensified as the volume of aHF decreased. Eventually, the last drop of solution was black and highly viscous. As the last of the aHF

was removed, a greenish-gold solid was deposited from the black liquid. The drastic color change was a good indicator for dryness, since the intense black color must have come from the solvated species. The solid remaining in the lobe of the reactor where the solutions were mixed was tan. An XRPP of the greenish-gold solid indicated $Ni(SbF_6)_2$, but in addition, a few lines of what is probably a second phase. The photo of the tan residue left over from the reaction mixture showed the pattern of $KSbF_6$ only.

5.3. Results and Discussion

Attempts to characterize a cationic Ni^{IV} species in the solid state were unsuccessful, but in solution, a ^{19}F NMR resonance was observed upon reaction of K_2NiF_6 with SbF_5 in aHF at -60 °C. This establishes that the species in solution is not paramagnetic, which is in harmony with the low spin d^6 configuration of Ni^{IV}. The resonance which has been assigned to cationic Ni^{IV} (-235 ppm) is significantly deshielded with respect to NiF_6^{2-} in aHF at the same temperature (-322 ppm). This is in accordance with the removal of electron density from Ni^{IV} upon transition from NiF_6^{2-} to a cationic Ni^{IV} species. It is notable that in the reaction of K_2NiF_6 with AsF_5, fluoride exchange processes prevented the observation of distinct peaks. It was demonstrated that AsF_5 is not a sufficiently strong Lewis acid to arrest fluoride exchange with the solvated cationic Ni^{IV} species in aHF. The observation of resonances due to distinct species in the case of K_2NiF_6 with SbF_5 is consistent with the fact that SbF_5 is a stronger Lewis acid than AsF_5, and thus able to arrest the fluoride exchange process.

In the case of cationic Ni^{IV} prepared by the addition of GeF_4, there is the

possibility that at temperatures above -65 °C, the colored solution derived from the addition of excess GeF_4 may not be a Ni^{IV} species. This remark is prompted by the findings of Chapter 4, in which Ni^{II} is always observed in the products. It is possible that formation of the doubly charged GeF_6^{2-} drives the loss of F, to rapidly form Ni^{2+} in solution. In any case, the oxidizing power of solutions prepared from GeF_4 has not been studied.

The oxidizing power of $Ni^{IV}_{(solv)}$ was characterized by reactions with O_2, RuF_6^- and PtF_6^-. These experiments indicated that $Ni^{IV}_{(solv)}$ has an oxidizing potential greater than that of PtF_6^-, the electron affinity of which is 184 kcal/mol.[16] $Ni^{IV}_{(solv)}$ and $Ag^{III}_{(solv)}$ are each capable of oxidizing Pt(V) to Pt(VI), but neither one is capable of oxidizing Au(V) to Au(VI).

It is believed that the oxidizing ability of *R*-NiF_3 and *Ho*-K_xNiF_3 derives from $Ni^{IV}_{(solv)}$, rather than a cationic Ni^{III} species. The mixed oxidation state nature of *R*-NiF_3 is in harmony with this (see Chapter 2). The color of the oxidizing solution is the same for solutions derived from NiF_4 or NiF_3. When AsF_5 is used to produce the $Ni^{IV}_{(solv)}$, the product of the RuF_6^- oxidation appears to incorporate arsenic in the solid state. These microcrystalline yellow solids have powder patterns similar to that of O_2RuF_6, but with smaller unit cells, as expected for a solid solution of O_2RuF_6 with O_2AsF_6. The gravimetry of these reactions is in accord with this conclusion, as the mass of the products is greater than is possible for 100% conversion of RuF_6^- to RuF_6.

The anion SbF_6^- is one of the most stabilizing anions, and the most likely to have

the capability to stabilize NiF_3^+. Thus highly polarizing cations such as Ag^{2+} (ref. 17) and Au^{2+} (ref. 18) and KrF^+ (ref. 11) have been isolated in combination with SbF_6^-. It is unlikely that removal of aHF can be realized at temperatures much lower than the -70 °C in these studies, as the freezing point is -82 °C. The production of RuF_6 and PtF_6 by $Ni^{IV}_{(solv)}$ and $Ag^{III}_{(solv)}$ indicates that they are perhaps the most powerful oxidizers known to date. Previously, KrF^+ had been identified[19] as the most powerful oxidizing species, but has been reported to decompose in solution with formation of PtF_5.[20] This indicates that KrF^+ does not capture the electron from PtF_6^-, but rather the F^- ion. Bartlett has estimated[21] from a Hess' law cycle that the electron affinity of KrF^+ must be at least 12 eV, which is in accord with the observation of Gillespie and Schrobilgen[11] that KrF^+ salts oxidize oxygen to O_2^+. Stein showed many years ago that O_2^+ salts oxidize Xe to give XeF^+ salts.[22] The hierarchy of oxidizing power of these species therefore appears to be:

$$XeF^+ < O_2^+ \cong Ag^{II}_{(solv)} < KrF^+ < RuF_6 \cong PtF_6 < Ag^{III}_{(solv)} \cong Ni^{IV}_{(solv)}$$

5.4. Conclusion

It appears that isolating a stable salt of NiF_3^+ may not be possible with anions of the Lewis fluoroacids. However, a broad NMR signal at -235 ppm has been obtained for what may be a cationic species of Ni^{IV} in solution.

The hierarchy of oxidizing power of the species studied appears to be:

$$XeF^+ < O_2^+ \cong Ag^{II}_{(solv)} < KrF^+ < RuF_6 \cong PtF_6 < Ag^{III}_{(solv)} \cong Ni^{IV}_{(solv)}$$

5.5. References

[1] Žemva, B.; Lutar, K.; Jesih, A.; Casteel, W. J., Jr.; Bartlett, N. *J. Chem. Soc., Chem Commun.* **1989**, *6*, 346.
[2] Gantar, D.; Leban, I.; Frlec, B.; Holloway, J. H. *J. Chem. Soc. Dalton Trans.* **1989**, 2379.
[3] Gantar, D..; Frlec, B.; Russell, D.R.; Holloway, J. *Acta Cryst. Sec. C Cryst. Struct. Commun.* **1987**, *42*, 618.
[4] Casteel, W. J., Jr.; Ph. D. Thesis **1992**, Chapter 7, UC Berkeley.
[5] Lucier, G.; Shen, C.; Casteel, W. J., Jr.; Chacón, L.; Bartlett, N. *J. Fluorine Chem.* **1995**, *72*, 157.
[6] Žemva, B.; Hagiwara, R.; Casteel, W. J., Jr.; Lutar, K.; Jesih, A.; Bartlett, N. *J. Amer. Chem. Soc.*, **1989**, *112*, 4846.
[7] Siegel, S.; Northrop, D. A. *Inorg. Chem.*, **1966**, *5*, 2187.
[8] Kimura, M.; Shomaker, V.; Smith, D. W.; Weinstock, B. *J. Chem. Phys.*, **1968**, *48*, 4001.
[9] Casteel, W. J., Jr.; Horowitz, T. *Eur. J. Solid State Inorg. Chem.* **1992**, *29*, 649.
[10] Bartlett, N. *Angew. Chem., Int. Ed. Engl.*, **1968**, *7*, 433.
[11] Nikitin, M. I.; Sodorov, L. N.; Korobov, M. V. *Int. J. Mass Spec. Ion Phys.*, **1981**, *37*, 13.
[12] Lucier, G. *Ph.D. Thesis*, **1995**, 24.
[13] Edwards, A. J.; Falconer, W. E.; Griffiths, J. E.; Sunder, W. A.; Vasile, M. J. *J. Chem. Soc. Dalton Trans.*, **1974**, 1129.
[14] Bartlett, N.; Lohmann, D. H. *J. Chem. Soc.* **1962**, 5253.
[15] Bacon, J.; Dean, P. A. W.; Gillespie, R. J. *Can. J. Chem.* **1970**, *48*, 3413.
[16] Nikitin, M. I.; Sodorov, L N.; Korobov, M. V. *Int. J. Mass Spec. Ion Phys.*, **1981**, *37*, 13.
[17] Gantar, D.; Leban, I.; Frelc, B.; Holloway, J. *J. Chem. Soc., Dlaton Trans.*, **1987**, 2379.
[18] Elder, S. H.; Lucier, G. M.; Hollander, F. J.; Bartlett, N. *J. Am. Chem. Soc.*, **1997**, *119*, 1020.
[19] Christie, K.O.; Dixon, D. A. *J. Am. Chem. Soc.*, **1992**, *114*, 2978.
[20] Gillespie, R. J.; Schrobilgen, G. J. *J. Chem. Soc., Chem. Commun.*, **1974**, 90 and *Inorg. Chem.* **1976**, *15*, 22.
[21] Bartlett, N. *Endeavour*, **1972**, *XXXI*, 107.
[22] Stein, L. *Nature*, **1973**, *243*, 30.

Chapter 6. Fluorination of Organic Compounds with Nickel Fluorides

6.1. Introduction

In 1949, an electrochemical method for fluorination of organic compounds was discovered by J. H. Simons.[1,2] The fluorinations were achieved using an electrochemical cell which containing hydrogen fluoride solvent, and nickel electrodes, which were found to be most effective in the fluorination process. This provided for the facile substitution of fluorine for hydrogen to give the perfluorinated relatives of organic molecules. This was particularly important in the early days of organofluorine chemistry, and a modern version of this method remains an important industrial synthetic method for organofluorine chemicals today.[3]

It has been frequently speculated that a higher nickel fluoride (NiF_x, $2 < x < 3$) played a role in the Simons Electrochemical Fluorination (ECF) Process fluorination reactions.[4,5] Until 1989, however, the only established binary fluoride of nickel was NiF_2, a yellow solid.

Stein *et. al.* showed that operation of a Simons-like cell containing cell electrolytes KF or

NH_4F (0.2-0.5 M) produced "brown-black" deposits on the nickel anode.[6] In addition, a red-brown solid was isolated from the electrochemical cell. The brown-black and red-brown deposits were highly reactive, liberating I_2 from I^- and becoming yellow upon exposure to air. Stein *et. al.* also observed a red coloration of the aHF solution near the electrodes when voltages of ~10 V were employed in the presence of higher concentrations of KF or NH_4F (0.5 - 1.5 M). Both NiF_6^{2-} and NiF_6^{3-} were identified by infrared analysis of solids obtained by evaporation of the red solutions. These authors also reported a reaction between K_2NiF_6 and aHF producing small amounts of a red-brown solid. Such a solid was also observed by Court and Dove, who found the oxidation state of nickel to be 2.45 - 2.51.[7]

Partial disproportion of K_3NiF_6 was also observed by Stein *et. al.*, who gave the equation:

$$2\ K_3NiF_6 \longrightarrow 6\ K^+ + NiF_6^{2-} + NiF_2 + 4\ F^- \qquad (2)$$

to account for the disproportionation of K_3NiF_6 even though the precipitate was described as red-brown and must have contained nickel in an oxidation state greater than +2, as it liberated I_2 from I^- and was reduced to yellow NiF_2 when exposed to air. Court and Dove later found this red-brown solid to contain nickel in an oxidation state between 2.25 and 2.35. The latter authors also report XRPPs containing diffuse lines which were similar in position and intensity to those of NiF_2.

Recent evidence, reported by Sartori, *et. al.*,[8] supports the hypothesis that a higher nickel fluoride, NiF_x ($2 < x < 3$) is active as a fluorinating agent in the ECF Process. In

these experiments, an ECF cell with a pack of Ni electrodes in aHF was polarized by a voltage of 5.0-5.3 V for 48 h, and then the current supply turned off. The substrate $CF_3SO_2N(CH_3)_2$ was admitted to the unpowered cell, and after 18 h, the following fluorinated products were observed: $CF_3SO_2N(CH_2F)CHF_2$, $CF_3SO_2N(CHF_2)_2$, $CF_3SO_2N(CF_3)CHF_2$, $CF_3SO_2N(CF_3)_2$. The absence of current implies chemical reaction of NiF_x coated on the anode with $CF_3SO_2N(CH_3)_2$.

This "no current" argument for fluorination by NiF_x has been disputed by Rüdiger, *et. al.*,[9] who note that the anode potential decays over a prolonged period of time after the power supply has been disconnected. This would allow for electrochemical fluorination of $CF_3SO_2N(CH_3)_2$ at the charged anode.

Another major method of synthesis of organofluorine compounds has been via the fluorination by high valent and complex metal fluorides. Fluorination with CoF_3 was first suggested in 1929 by Ruff and Ascher[10] and the fluorination of CCl_4 was accomplished in 1931.[11] In the 1940's, renewed interest led Fowler to discover that at elevated temperatures (up to 400 °C) CoF_3 readily fluorinated organic vapor passed over the solid fluoride, replacing hydrogen, and producing CoF_2 and HF.[12] The CoF_2 was regenerated to CoF_3 by passing a stream of fluorine through the reactor above 150 °C. This in turn led to a body of work investigating the use of other metal fluorides, such as AgF_2, MnF_3 and CeF_4 as fluorinating agents for a vast array of organic substrates.[3] Complex cobalt fluorides, $ACoF_4$ (A = Li, K, Rb, Cs),[13,14] and K_3CoF_6[15] in reaction with organic vapors have also been studied. It is important to note that all of the aforementioned studies were

carried out between the dry, solid metal fluoride and vapor phase organic substrate. Fluorination by such high valent fluorides using aHF as the substrate solvent has been neglected, probably because of container problems posed by this solvent.

In the studies reported in this chapter the novel nickel fluorides prepared and characterized in these laboratories have been applied to the fluorination of organic compounds with the intent of comparing the fluorinating action to that of the Simons ECF process. Cleaner, easier and more efficient fluorinations were also hoped for. Direct comparison of the new nickel fluorides with CoF_3 and other higher valent nickel fluorides was also made.

Nickel fluorides to be used as oxidative fluorinators were selected on the basis of the likelihood that they might be present in an active Simons cell. *R*-NiF_3 was of primary interest, as it has been observed that the nickel anode develops a black coating during prolonged operation of the cell.[16] The observations of Stein *et. al.* and of Court and Dove of the red-brown higher fluoride (~$NiF_{2.5}$) suggested that it should also be investigated as a fluorinator.

Dove and his coworkers had also observed that solutions of K_2NiF_6 in aHF were able to oxidize xenon.[17] This and the reports that K_2NiF_6 was able to perfluorinate benzene, [18] although this had been with gaseous benzene passed over dry K_2NiF_6 at temperatures of 120 - 350°C, suggested that K_2NiF_6 solutions in aHF should be examined for their effectiveness in fluorination of organic substrates.

6.2. Experimental

Preliminary experiments with dry *R*-NiF_3 and CH_3CN vapor in the absence of aHF solvent resulted in combustion at room temperature. This led to the use of aHF as a moderator in all reactions, even though *R*-NiF_3 and NiF_x are not soluble in aHF, the high heat capacity of aHF and the lower temperatures that can be used with this solvent (down to -82 °C) aid in the control of the vigorously exothermic reactions.

The organic substrates were selected on the basis of simplicity of structure to aid in the characterization by NMR spectroscopy. A range of functional groups was examined to assess the ability of these fluorinators with a variety of organic functional groups. Of the substrates investigated, CH_3CN, CH_3COF, $(CH_3)_2CO$ and $(CH_3)_4N^+$ were the most thoroughly characterized. $CH_3C(O)NH_3^+$ was found to undergo significant cleavage reactions and was not studied further. N_2O was unreactive with *R*-NiF_3, K_2NiF_6, and cationic Ni^{IV}.

Finally, the determination of the appropriate reaction conditions was critical. Reactions involving the binary fluorides NiF_3 and NiF_4 were seen to be highly energetic, and if not properly moderated led to substrate fragmentation. This was controlled to some extent by initiating reactions at low temperatures and holding the reaction mixture at a low temperature for a period of hours before warming to room temperature. An example is CH_3CN, for which initial temperatures were found to be critical in the prevention of fragmentation reactions. It was discovered that when the CH_3CN was added to *R*-NiF_3 in aHF above -20 °C, extensive cleavage of the C≡N bond occurred, giving rise to CF_3CF_3

and NF_3 as the major products. When the addition was initiated at -25 °C and held below -20 °C for several hours, minimal cleavage was observed and CF_3CN was the major product, even though the temperature was eventually raised to the same end point, room temperature.

Reactions were carried out in ¼" FEP T-reactors, one arm consisting of a section of NMR sample tubing fused to the ¼" tubing, shown in Figure 6.1. The scale of the reactions was tailored to satisfy the concentration (0.1 - 0.5 M) required for NMR analysis. Reactions were carried out in the lower limb of the reactor, and the temperature was controlled by placing this arm in a dewar containing a dry ice/acetone bath. The solution was decanted after completion of the reaction and volatile products and the remaining aHF were transferred to the NMR tube by cooling to -196 °C. While the products were frozen at -196 °C, the reactor was opened to vacuum and the NMR tube immediately sealed near the top by heating with a flame. The FEP NMR sample tube was then warmed to room temperature and inserted into a glass NMR tube for analysis in the spectrometer. The solid products were analyzed by XRPD.

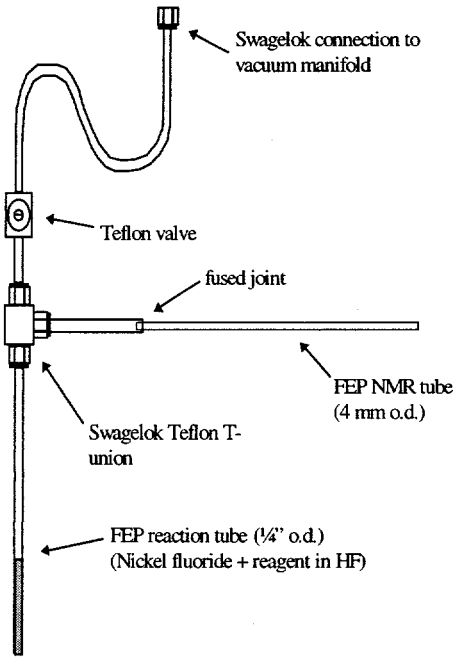

Figure 6.1. Typical Reactor for Fluorination of Organic Substrates

Completion of the reaction was determined by the color of the nickel residue. The *R*-NiF_3 began as a black solid, becoming successively brown, red-brown, tan and finally yellow, as it was reduced to NiF_2. Upon reaction with organic substrates, red K_2NiF_6 solutions precipitated red-brown solids which became tan and then yellow upon reduction to NiF_2. Red-brown NiF_x ($2 < x < 3$) became pale tan and then yellow upon reduction to NiF_2. Thus, the rate of the color change to tan or yellow indicated the rate of the reaction, and was carefully noted as the reaction progressed.

The stoichiometry of the oxidizer to the substrate was calculated on the basis of two oxidizing equivalents required to perform one C–H bond replacement. The necessary steps are: cleavage of a C–H bond (most likely with subsequent formation of HF), and formation of a C–F bond. Each *R*-NiF_3 has only one oxidizing equivalent, therefore two molar equivalents are needed per mole of C–H bond substitution. K_2NiF_6 has two oxidizing equivalents, therefore one molar equivalent was needed per C–H bond substitution. NiF_x (if it is $NiF_{2.3}$) has only 0.3 oxidizing equivalent, therefore 6.7 molar equivalents were needed per C–H bond substitution.

To determine that HF substitution reactions did not lead to fluorination of the organic substrates under the conditions employed, control reactions were carried out under identical conditions without oxidizer. In no instance was any fluorination of organic substrates by aHF observed under the given reaction conditions. Each of the control samples gave a clean NMR spectrum of the organic substrate in aHF, which was

used as a standard spectrum.

6.2.1. CH_3CN

6.2.1.1. R-NiF_3 with CH_3CN (molar ratio 10:1)

R-NiF_3 (0.1711 g; 1.48 mmol) was loaded into the ¼" tube of the reactor and aHF (0.4 mL) was condensed onto it before adding CH_3CN (0.15 mmol), and the mixture warmed to -25 °C. The temperature was held between -25 and -20 °C for 3 h. After 30 min., the black solid had become darker brown, and after 3 h, was red-brown. The temperature of the cooling bath was allowed to warm slowly to room temperature over 9 h, at which point the solid was yellow. All volatiles were condensed into the NMR tube at -196 °C and the tube sealed under dynamic vacuum. The X-ray powder photograph of the brown solid showed NiF_2 and the first three lines of the Ni_2F_5 pattern obtained from the reaction of R-NiF_3 with Xe (see Table 2.3). The corrected normalized integrations of the products determined by NMR analysis are shown in Table 6.1.

6.2.1.2. K_2NiF_6 with CH_3CN (molar ratio 5:1)

K_2NiF_6 (0.2052 g; 0.818 mmol) was loaded into the ¼" arm of the reactor, aHF (0.6 mL) was condensed in and the solution warmed to -55 °C. CH_3CN (0.15 mmol) was added to the solution, where it began reacting at the surface of the solution, precipitating a dark-brown solid. The temperature was raised to -45 °C over 25 minutes, at which point the solution was still red (NiF_6^{2-}). Over 13.5 hours, the temperature warmed to -30 °C, to give a brown solid with a faint red color in solution. Warming to room temperature

resulted in some gas evolution and color change of the solid to a lighter shade of brown. After 4 hours at room temperature, the volatiles were condensed to the NMR sample tube at -196 °C and the tube sealed under dynamic vacuum. The X-ray powder photograph of the brown solid showed KHF_2 and a diffuse pattern of NiF_2. The corrected normalized integrations of the products determined by NMR analysis are shown in Table 6.1.

6.2.1.3. K_3NiF_6 with CH_3CN (molar ratio 10:1)

K_3NiF_6 (0.4792 g; 1.65 mmol) was loaded into the ¼" arm of the reactor, aHF (0.6 mL) was condensed in and the solution warmed to -55 °C. When the aHF was added, a voluminous red-brown precipitate formed immediately and filled the entire volume of the aHF solution so there was no free liquid. CH_3CN (0.15 mmol) was added to the mixture. The temperature was held between -55 °C and -30 °C for 14 h, with only a color change to a lighter red-brown observed. Warming to room temperature resulted in a slow color change of the solid to a slightly lighter shade of red-brown. After 4 hours at room temperature, the volatiles were condensed to the NMR sample tube at -196 °C and the tube sealed under dynamic vacuum. The X-ray powder photograph of the brown solid showed a broad-lined NiF_2 pattern. The corrected normalized integrations of the products determined by NMR analysis are shown in Table 6.1.

Table 6.1. Corrected normalized integrations of products of CH_3CN fluorinations and comparison with the ECF Method

R-NiF_3		K_2NiF_6		K_3NiF_6		ECF[19]	
CF_3CN	**100**	CF_3CN	8	**CF_3CN**	**100**	**CF_3CN**	**100**
$CF_3CF_2NF_2$	5	**$CF_3CF_2NF_2$**	**100**	$CF_3CF_2NF_2$	8	$CF_3CF_2NF_2$	20
CF_3CF_3	12	CF_3CF_3	25	CF_3CF_3	< 1		
CF_4, NF_3	< 4	CF_4, NF_3	< 3	NF_3	< 1		

6.2.2. CH_3COF

6.2.2.1. R-*NiF_3 with CH_3COF (molar ratio 6:1)*

Two reactions were carried out with this stoichiometry, the first reaction was initially held between -15 and -10 °C for 3 h, then warmed to room temperature and held there for 8 h. This reaction resulted in cleavage of CH_3COF, to form COF_2 and CHF_3. Initiating the second reaction at -30 °C did not appear to significantly inhibit this cleavage, nor was CF_3COF observed.

R-NiF_3 (0.1054 g; 0.911 mmol) was loaded into the ¼" arm of the reactor, and aHF (0.6 mL) was condensed onto it and the temperature warmed to -30 °C. CH_3COF (0.15 mmol) was condensed into the reactor, resulting in an immediate vigorous reaction, which bumped some of the solid on the wall of the tube above the level of the cooling bath. The color of this uncooled solid changed from black to red-brown over 10 seconds. After 10 minutes, the bulk of the cooled solid in the reactor was brown. After 3 h, the bath temperature was allowed to slowly warm to 0 °C over 14 h, at which point the solid had become golden tan, and then to room temperature over 1.5 h, to give a yellow solid.

All volatiles were condensed to the NMR sample arm of the reactor at -196 °C and the tube sealed under dynamic vacuum. The XRPP of the yellow solid was similar to that obtained by the reduction of *R*-NiF_3 with Xe (pattern shown in Table 2.3). The corrected normalized integrations of the products determined by NMR analysis are shown in Table 6.2.

6.2.2.2. K_2NiF_6 with CH_3COF (molar ratio 3:1)

K_2NiF_6 (0.1134 g; 0.452 mmol) was loaded into the ¼" arm of the reactor, and aHF (0.6 mL) was condensed onto it, forming a red solution with no solid observed. The solution was warmed to -30 °C and CH_3COF (0.15 mmol) was condensed into the reactor. After 5 minutes, a yellow-tan solid was observed forming at the liquid-gas interface. After 10 minutes, there was no red color remaining in solution and the bulk of the aHF was occupied by the yellow-tan solid. The temperature was held below -30 °C for 3 h, then warmed to 0 °C over 14 h and finally warmed to room temperature over 1.5 h. The color of the solid became slightly more yellow over this period, but indicated nearly complete reduction to NiF_2 after only 10 minutes of contact with CH_3COF. All volatiles were condensed to the NMR sample arm of the reactor at -196 °C and the tube sealed under dynamic vacuum. The XRPP of the yellow indicated NiF_2 of small particle size (broad-lined pattern) and KHF_2. The corrected normalized integrations of the products determined by NMR analysis are shown in Table 6.2.

This reaction was repeated with an initial temperature of -60 °C. The reaction

progressed more slowly, but produced much less CF_3COF than did the faster reaction.

6.2.2.3. NiF_x with CH_3COF (molar ratio 6:1)

NiF_x (0.1928 g; 1.88 mmol if $NiF_{2.3}$) was loaded into the ¼" arm of the reactor and aHF (0.6 mL) was condensed onto it and the temperature warmed to - 60 °C. CH_3COF (~0.3 mmol) was condensed into the reactor at -60 °C. There was no observed reaction upon addition of CH_3COF. The temperature was warmed to -35 °C over 16.5 h, at which point there was a colorless solution above the column of settled solid, of which the top 1/3 of the column was yellow in color, and the lower 2/3 was red-brown in color. The reactor was agitated to mix the solids and held below -30 °C for 22h, at which point the solid was still pale tan. The temperature was warmed to room temperature, which resulted in some bubbling and a color change to yellow tan. All volatiles were condensed to the NMR sample arm of the reactor at -196 °C and the tube sealed under dynamic vacuum. The XRPP of the yellow solid indicated NiF_2 of small particle size (broad-lined pattern). The corrected normalized integrations of the products determined by NMR analysis are shown in Table 6.2.

Table 6.2. Corrected normalized integrations of products of CH_3COF fluorinations and comparison with ECF

R-NiF_3		K_2NiF_6		NiF_x		ECF[20]	
$CH_3C(O)F$	43	**$CH_3C(O)F$**	**100**	**$CH_3C(O)F$**	**100**		
$CF_3C(O)F$	n.o.	$CF_3C(O)F$	44	$CF_3C(O)F$	n.o.	**$CF_3C(O)F$**	**85**
$C(O)F_2$	**100**	$C(O)F_2$	91	$C(O)F_2$	23		
CHF_3	97	CHF_3	54	CHF_3	23		
CF_4	9	CF_4	13	CF_4	3		

6.2.3. $(CH_3)_2CO$

6.2.3.1. R-NiF_3 with $(CH_3)_2CO$ (molar ratio 14:1)

R-NiF_3 (0.2491 g; 2.15 mmol) was placed in the ¼" arm of a reactor, and aHF (~0.6 mL) was condensed onto it. $(CH_3)_2CO$ (0.15 mmol) was condensed in, and the reactor was allowed to warm to -65 °C. The temperature was maintained between -60 and -65 °C for 1 h, then allowed to warm slowly to room temperature. After 0.5 h at -65 °C the solid had become dark brown in what appeared to be a very slow reaction. After another 2 h, it was slightly lighter in color, and the temperature was -57 °C. After 46 h, the color had lightened to tan-yellow and the temperature was 1 °C. The bath was then warmed to room temperature, resulting in bubbling and the color changing to bright yellow. All volatiles were condensed to the NMR sample arm of the reactor at -196 °C and the tube sealed under dynamic vacuum. The XRPP of the yellow solid contained four very broad lines, the first line similar in position to the first line of the NiF_2 pattern and the last three similar to those of the product of the reaction of xenon with *R*-NiF_3 (Table 2.3.) The corrected normalized integrations of the products determined by NMR analysis are shown in Table 6.3.

6.2.3.2. K_2NiF_6 with $(CH_3)_2CO$ (molar ratio 6:1)

K_2NiF_6 (0.2346 g; 0.935 mmol) was placed in the ¼" arm of a reactor, and aHF (~0.3 mL) was condensed onto it. $(CH_3)_2CO$ (0.15 mmol) was condensed in and the reactor was allowed to warm to -27 °C. Upon warming, a tan solid was precipitated, with

copious bubbling. The color of the solid became even lighter over the next three hours, as the bubbling slowed. The reactor was then allowed to warm to room temperature, resulting in further gas evolution, and the color of the solid becoming lighter. The reactor was allowed to sit at room temperature for 16.5 hours, yielding a yellow solid. The volatiles were condensed to the NMR arm of the reactor at -196 °C and the tube sealed under dynamic vacuum. The XRPP of the yellow solid (0.2683 g) showed a faint, broad-lined NiF_2 pattern and KHF_2. The corrected normalized integrations of the products determined by NMR analysis are shown in Table 6.3.

6.2.3.3. NiF_x with $(CH_3)_2CO$ (molar ratio 29:1)

NiF_x (0.4459 g; 4.35 mmol if $NiF_{2.5}$) was placed in the ¼" arm of a reactor, and aHF (~1 mL) was condensed onto it. $(CH_3)_2CO$ (0.15 mmol) was condensed in, and the reactor was allowed to warm to -65 °C. The temperature was maintained between -60 and -65 °C for 1 h, then allowed to warm slowly to room temperature. After 0.5 h at -65 °C the solid had become a lighter red-brown. Over the next 48 h the color slowly lightened to tan-yellow and the temperature was 1 °C. The bath was then warmed to room temperature, resulting in bubbling and the color changing to bright yellow. All volatiles were condensed to the NMR sample arm of the reactor at -196 °C and the tube sealed under dynamic vacuum. The XRPP of the yellow solid was very a broad-lined NiF_2 pattern. The corrected normalized integrations of the products determined by NMR analysis are shown in Table 6.3.

Table 6.3. Corrected normalized integrations of products of $(CH_3)_2CO$ fluorinations and comparison with ECF

R-NiF_3		K_2NiF_6		NiF_x		ECF[21]
$(CF_3)_2CO$	4	$(CF_3)_2CO$	39	$(CF_3)_2CO$	1	reported to
$C(O)F_2$	**100**	$C(O)F_2$	52	$C(O)F_2$	52	produce only
CH_3CF_3	73	CH_3CF_3	10	**CH_3CF_3**	**100**	fluorocarbons
CHF_3	**99**	**CHF_3**	**100**	CHF_3	75	
CF_4	86	CF_4	16	CF_4	24	

6.2.4. 2,5-bis(2H-hexafluoropropyl)tetrahydrofuran

Samples of 2,5-bis(2H-hexafluoropropyl)tetrahydrofuran were supplied by the R. D. Chambers group of the University of Durham, UK. The perfluorination of this material was investigated along with that of other model compounds.[22] This compound is efficiently fluorinated by the Simons process ECF and also by CoF_3.[23,24] Due to the limited solubility of the organic liquid in aHF, a reactor was designed (Figure 6.2.) that would allow for quantitative addition of the organic to the *R*-NiF_3-aHF mixture. A small bucket was fashioned from FEP tubing, with a magnet sealed into the upper part of the tubing to aid in manipulation of the bucket during the

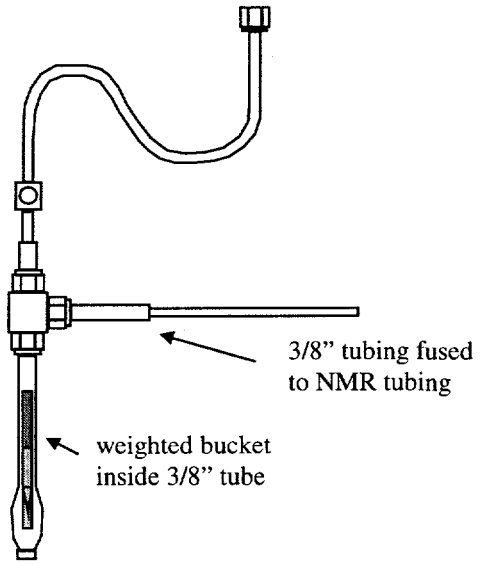

Figure 6.2. Reactor with Weighted Bucket for Quantitative Delivery of Organic Substrate to Oxidizer

reaction, and also to hold the opening of the bucket below the level of the *R*-NiF_3-aHF mixture.

2,5-bis(2H-hexafluoropropyl) tetrahydrofuran (0.0571 g; 0.15 mmol) was loaded into the weighted bucket which was suspended above the *R*-NiF_3 loaded in the bottom of the ⅜" tube (0.4399 g; 3.8 mmol) by taping a magnet to the outside of the reactor. A -28 °C bath was used to slowly condense aHF (1.5 mL) onto the *R*-NiF_3. The bucket was lowered into the aHF and the temperature maintained between -28 and -20 °C for 2.5 h. There was no sign of reaction until after 2 h, the color had changed from black to dark brown. The temperature was held between -30 and -10 °C for 12 h, at which point the color of the solid was a lighter shade of brown. The bath was allowed to come to room temperature over 28 h, at which point the solid was red-brown. The solution was decanted to the NMR sample tube arm of the reactor, which was then cooled to -196 °C and sealed under dynamic vacuum. The XRPP of the red-brown material indicated small particle size (broad-lined pattern) NiF_2. The ^{19}F NMR spectrum indicated perfluorination to 2,5-bis-(perfluoropropyl)tetrafluorofuran, with no starting material present in the sample.

6.2.5. K_2NiF_6 with $(CH_3)_4N^+$

The desire to synthesize the yet unknown perfluorinated relative of $(CH_3)_4N^+$, namely $(CF_3)_4N^+$, led to the discovery of the novel fluorinated cation, $N(CHF_2)_3CH_3^+$. This was the first reported example of a partially fluorinated tetramethylammonium (TMA) cation. Other products included $N(CF_3)_3$, NF_3, CHF_3 and CF_4. The fluorination of

tertiary amines (NR_3, R = Et, Pr, Bu) and tetraalkylammonium cations (NR_4^+, R = Et) via ECF is well documented.[25] However, the ECF of NR_4^+ cations results in the formation of perfluorinated tertiary amines rather than corresponding perfluorinated ammonium cations (i.e., cleavage of one C–N bond always occurs).[26] Indeed, it has been argued[27] for the tetraethylammonium (TEA) cation that it was not possible to fluorinate at the α-position via ECF, on the grounds that the electron-withdrawing effect of the quaternary nitrogen in the protonated TEA should prevent the α-hydrogen atoms from leaving with their electrons to form HF in a free-radical fluorination process. Clearly, the use of K_2NiF_6 allows for fluorination on the carbon atoms adjacent to the quaternary nitrogen.

The low-temperature reaction was carried out in a Teflon/FEP reactor, which was designed for the dropwise addition of a K_2NiF_6 solution to a -70 °C solution of $N(CH_3)_4^+BF_4^-$, shown in Figure 6.4. Mixing was achieved by means of a magnetic stirrer in the lower limb of the reactor. K_2NiF_6 (0.7209 g; 2.87 mmol) was loaded into the reservoir section of the addition reactor and $N(CH_3)_4^+AsF_6^-$ (0.0653 g; 0.248 mmol) was loaded into the lower limb, and aHF was

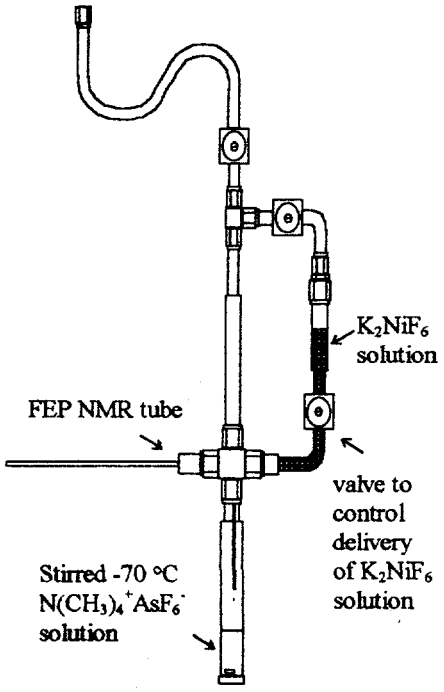

Figure 6.4. Low-temperature reactor for the addition of K_2NiF_6 solution to a cooled solution of $N(CH_3)_4^+AsF_6^-$

condensed onto each reagent (~1 mL to K_2NiF_6 and 0.5 mL to the $N(CH_3)_4^+AsF_6^-$). The reactor was pressurized to 1300 torr with dry N_2 to prevent the aHF in the upper reservoir from condensing to the lower limb (held at -70 °C). Once the lower limb was cooled to -70 °C the K_2NiF_6 solution was admitted dropwise to the $N(CH_3)_4^+AsF_6^-$ solution, precipitating a brown solid. A plug in the addition funnel developed and gave way rapidly at one point, delivering the remainder of the K_2NiF_6 solution all at once. The temperature of the reaction mixture was warmed to 10 °C over 3 days, then the colorless solution was decanted directly into the NMR sample tube, cooled to -196 °C, and sealed under dynamic vacuum. The nickel residue was not separated from the soluble products.

The ^{19}F NMR spectrum of the solution showed a doublet centered at -108.8 ppm, indicating the presence of $-CHF_2$ groups. In the ^1H NMR spectrum, there was a $-CH_3$ resonance equal in intensity to the $-CHF_2$ resonance. A ^{19}F-^1H NOESY NMR experiment established the $-CH_3$ and $-CHF_2$ groups to be in the same ion. Proton decoupled ^{14}N NMR showed a binomial septet for the nearly tetrahedral nitrogen atom directly bonded to three chemically equivalent $-CHF_2$ groups. The cation was therefore unambiguously determined to be $N(CHF_2)_3CH_3^+$. The spectra and coupling constants are shown in Figure 6.5. and Table 6.4., respectively. The $N(CHF_2)_3CH_3^+AsF_6^-$ is stable at room temperature indefinitely, however the BF_4^- salt decomposes within one week at room temperature. Decomposition of $N(CHF_2)_3CH_3^+BF_4^-$ at 65 °C yielded $N(CHF_2)_2CH_3$, BF_3 and CHF_3. The analogous decomposition of $N(CH_3)_4^+BF_4^-$ occurs at 362 °C.[28]

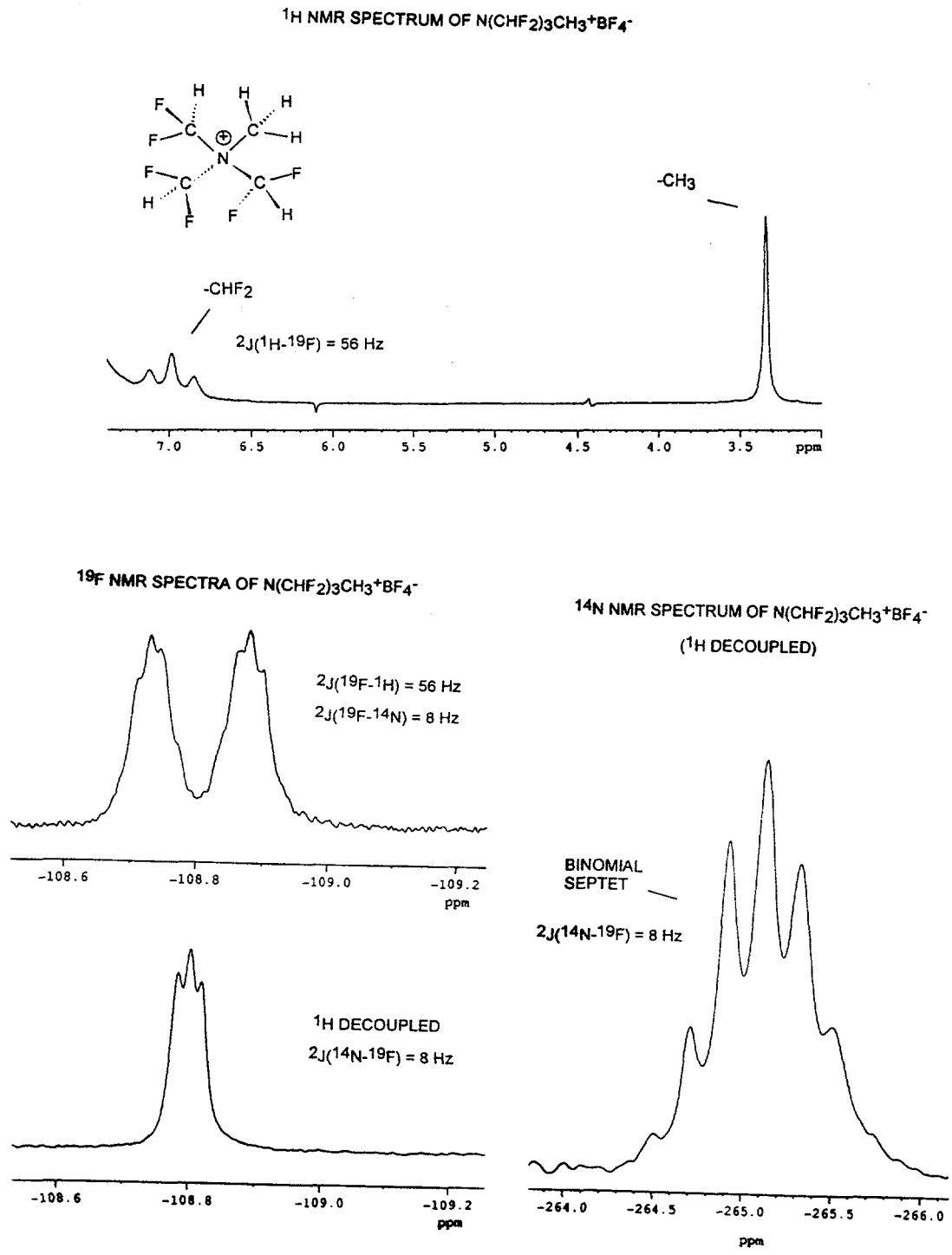

Figure 6.5. ^{1}H, ^{19}F, and ^{14}N NMR spectra of $N(CHF_2)_3CH_3^+$

Table 6.4. NMR (^{1}H, ^{13}C, ^{19}F and ^{14}N) Parameters for the $N(CHF_2)_3CH_3^+BF_4^-$ and Related Species

Species	$\delta(^{1}H)$ (ppm)	$\delta(^{19}F)$ (ppm)	$\delta(^{13}C)$ (ppm)	$\delta(^{14}N)$ (ppm)	J (Hz)
$N(CHF_2)_3CH_3^+$[a]	7.17 (CHF_2)[b]	-108.8 (CHF_2)[c]	114.3 (CHF_2)[d]	-265.7[e]	$^{1}J(^{19}F\text{-}^{13}C)$ 288
	3.54 (CH_3)	-153.6 (BF_4^-)	34.2 (CH_3)		$^{2}J(^{19}F\text{-}^{1}H)$ 56
					$^{2}J(^{19}F\text{-}^{14}N)$ 8
					$^{1}J(^{13}C\text{-}^{1}H)$ 152
$CHF_2NH_3^+$[f]	5.75 (CH)	-105.2	108.1	-325.7	$^{1}J(^{19}F\text{-}^{13}C)$ 263
	6.52 (NH)				$^{2}J(^{19}F\text{-}^{1}H)$ 58
					$^{2}J(^{19}F\text{-}^{14}N)$ 8
$N(CHF_2)_3$[g]	6.96	-96.4	108.5		$^{1}J(^{19}F\text{-}^{13}C)$ 247
					$^{2}J(^{19}F\text{-}^{1}H)$ 59
					$^{2}J(^{19}F\text{-}^{14}N)$ n.o.[h]

[a] This work. [b]Binomial triplet arising from $^{2}J(^{1}H\text{-}^{19}F)$. [c]Doublet splitting, arising from $^{2}J(^{19}F\text{-}^{1}H)$; further split into 1:1:1 triplets from $^{2}J(^{19}F\text{-}^{14}N)$. [d]Binomial triplet arising from $^{1}J(^{13}C\text{-}^{19}F)$. ^{13}C NMR data obtained from a standard $^{13}C\text{-}^{1}H$ DEPT 90 pulse sequence, using a delay, $1/[2J(^{13}C\text{-}^{1}H)]$, of 0.0025 s. [e]Singlet, $\Delta\nu_{1/2}$ = 26 Hz. [f]Data obtained in HF solvent at -15 °C. Chemical shifts referenced as in (a) above. Ph.D. thesis, Adel A.A. Emara, McMaster University, 1991. [g]J. Fluorine Chem., 15 (1980) 231-237. Chemical shifts referenced with respect to $CFCl_3$ (^{19}F) and $Si(CH_3)_4$ (^{13}C, ^{1}H). [h] $^{2}J(^{19}F\text{-}^{14}N)$ not observed; attributable to rapid quadrupolar relaxation of ^{14}N in a low symmetry environment (pyramidal geometry).

6.3. Results and Discussion

Nickel fluorides were found to be highly effective in the fluorination of organic compounds in aHF. The *R*-NiF_3 and NiF_x fluorination reactions gave similar products for a given organic substrate. The K_2NiF_6 reactions, however, gave significantly different products. For instance, the major product of CH_3CN fluorination with *R*-NiF_3 or NiF_x was CF_3CN, whereas with K_2NiF_6 it was $CF_3CF_2NF_2$. The Simons ECF Process gives a predominance of CF_3CN over $CF_3CF_2NF_2$, and thus is more akin to the *R*-NiF_3 and NiF_x oxidations. CH_3COF was much more prone to fragmentation reactions and COF_2 was produced in large quantities regardless of the oxidizer. The milder oxidizer, K_2NiF_6, gave CF_3COF, whereas it was not produced by *R*-NiF_3 and NiF_x, cleavage products such as COF_2 being dominant with these more potent oxidizers. The Simons ECF Process reportedly gives high yields of CF_3COF. This may be because the CF_3COF made in that process is quickly swept from the anode whereas in the reactions reported here, any CF_3COF formed had ample opportunity to react further with the oxidizer. $(CH_3)_2CO$ was, like CH_3COF, prone to further oxidation. K_2NiF_6 produced more $(CF_3)_2CO$ than did either *R*-NiF_3 or $NiF_{2.3}$, which only gave minute quantities of $(CF_3)_2CO$ with large amounts of CH_3CF_3 and COF_2. The Simons ECF Process reportedly produces only fluorocarbons.[21]

The perfluorination of 2,5-bis(2H-hexafluoropropyl)tetrahydrofuran with *R*-NiF_3 was a demonstration of the similarity of this oxidizer to the Simons ECF method. Overall, the *R*-NiF_3 and NiF_x gave results comparable with ECF, whereas K_2NiF_6 was

significantly less potent. The exception is CH_3COF as already remarked upon. The oxygen-containing substrates seemed overall to be much more prone to further fluorination than the nitrogen-containing substrates.

The effectiveness of *R*-NiF_3 as a fluorinator was also compared with that of CoF_3.[22] The substrate was an adamantane derivative containing partially fluorinated propyl groups. With *R*-NiF_3, the perfluoro relative was formed at 20 °C, but with CoF_3 at 360 °C, the products were entirely those of the fragmented molecule; no formation of the perfluoro compound was detected.

The formation of the novel $N(CHF_2)_3CH_3^+$ with K_2NiF_6 is a breakthrough in the synthesis of fluorinated tetraalkylammonium compounds. This ability to fluorinate cationic substrates is probably enhanced by the negative charge carried by the NiF_6^{2-} oxidizer in solution. *R*-NiF_3 when reacted with the same substrate produces only $N(CF_3)_3$ and CF_4, with no evidence of partially fluorinated products. The Simons ECF Process also produces fluorinated tertiary amines and fluorocarbons from tetraalkylammonium compounds.

Several further experiments between K_2NiF_6 and $(CH_3)_4N^+$ salts led to the observations that when the stoichiometry of the reaction is less than the amount required to perfluorinate the $(CH_3)_4N^+$, lower fluorinated products are observed.[29] These have not been identified unambiguously, but must be variants of the type, $N(CH_3)_x(CHF_2)_y(CH_2F)_z^+$, where $x + y + z = 4$. Fluorinated neutral products containing some -H have also been observed in cases of excess substrate. When the molar ratio of

the K_2NiF_6 is in excess of the amount required to perfluorinate the $(CH_3)_4N^+$, the only cationic product observed is $N(CHF_2)_3CH_3^+$, the other products being $N(CF_3)_3$, CF_4 and NF_3. This indicates that fluorination beyond $N(CHF_2)_3CH_3^+$ results in fragmentation of the substrate. The electron withdrawing effect of additional -F ligands destabilizes the cationic nitrogen center, and leads to the formation of a more stable neutral species.

It was found that $N(CHF_2)_3CH_3^+BF_4^-$ was unstable with respect to decomposition to $N(CHF_2)_2CH_3$, BF_3 and CHF_3 at room temperature. Decomposition of $N(CHF_2)_3CH_3^+BF_4^-$ requires F^- abstraction from BF_4^-, but with the stronger anion AsF_6^-, this does not occur, thus salts of AsF_6^- are stable indefinitely at room temperature.

Interestingly, there are no published reports of high valent metal fluoride organic fluorination reactions carried out in aHF as a solvent. It would be interesting to investigate the fluorinating ability of other aHF soluble complex fluorides such as $KAgF_4$ and K_3CoF_6. It is possible that they may ultimately be of greater use than K_2NiF_6 as a fluorinating agent, as K_2NiF_6 is in many cases, too aggressive a reagent, causing cleavage reactions of most organic substrates investigated. Transition metal anions with lower electronegativities would be milder fluorinating agents, and perhaps less likely to destroy the skeleton of the organic substrate.

6.4. Conclusion

The fluorination of organic substrates by *R*-NiF_3 and NiF_x was found to give products similar to those produced by the Simons ECF Process. This adds support to the claim that a higher nickel fluoride may be active as a fluorinator in the Simons ECF process. K_2NiF_6 was found to give different fluorinated products than *R*-NiF_3, NiF_x and ECF. The fluorination of $(CH_3)_4N^+$ with K_2NiF_6 gave the first reported example of a partially fluorinated $(CH_3)_4N^+$ cation.

The use of these nickel fluorides as fluorinators of organic compounds should be investigated further as they have demonstrated great promise in this field. In addition, the end product of reduction, NiF_2 can be recycled to the starting material K_2NiF_6 via a UV-irradiation reaction described in Chapter 7.

6.5. References

[1] Simons, J. H. *J. Electrochem. Soc.* **1949**, *95*, 47.
[2] Simons, J. H., (ed.), in *Fluorine Chemistry*, Vol. 1, p. 414; Academic, New York, **1950**
[3] Alsmeyer, Y. W.; Childs, W. V.; Flynn, R. M.; Moore, G. G. I.; Smeltzer, J. C. in "Organofluorine Chemistry: Princip;les and Commercial Applications", Ed. Banks, R. E. *et. al.*, Plenum Press, NY, **1994**, pp. 121-143.
[4] Burdon, J.; Tatlow, J. C. in *Adv. in Fluorine Chem.*, Vol. 1, p. 129-165; Butterworths Sci. Pubs., London, **1960**.
[5] Nagase, S. *Fluor. Chem. Rev.* **1967**, *1*, 1967.
[6] Stein, L.; Neil, J. M.; Alms, G. R. *Inorg. Chem.*, **1969**, *8*, 2473.
[7] Court, T. L.; Dove, M. F. A. *J. Chem. Soc., Dalton Trans.* **1973**, 1995.
[8] Sartori, P.; Ignat'ev, N.; Datsenko, S. *J. Fluor. Chem.* **1995**, *75*, 157-161.
[9] S. Rüdiger, A. Dimitrov and K. Hottmann, *J. Fluor. Chem.*, 76 (1996) 155-160.
[10] Ruff, O.; Ascher, E. *Z. Anorg. Chem.* **1929**, *183*, 193.
[11] Ruff, O.; Keim, R. *Z. Anorg. Chem.* **1931**, *201*, 245.
[12] Fowler, R. D.; Burford, W. B.; Hamilton, J. M.; Sweet, R. G.; Weber, C. E.; Kasper, J. S. and Litant, I. *Ind. Eng. Chem.* **1947**, *39*, 292; and *Preparation Porperties and Technology of Fluorine and Organic Fluoro-compounds*, Slesser and Schram, eds., p. 349, New York, McGraw-Hill, **1951.**
[13] Coe, P. L., Plevery, R. G.; Tatlow, J. C. *J. Chem. Soc. (C)* **1969**, 1060 and Burdon, J.; Chivers, G. E.; Tatlow, J. C. *ibid.* **1969**, 2585.
[14] Edwards, A. J.; Plevey, R. G.; Sallomi, I. J.; Tatlow, J. C. *J. Chem. Soc, Chem. Commun.*, **1972**, 1028.
[15] Plevey, R. G.; Steward, M. P. Tatlow, J. C.; *6th Int. Symp. Fluorine Chem., Durham, U.K.* **1971.**
[16] Childs, W. V., personal communication.
[17] Court, T. L.; Dove, M. F. A. *J. Fluor. Chem.* **1975**, *6*, 491.
[18] Plevey, R. G.; Rendell, R. W.; Steward, M. P. *J. Fluor. Chem.* **1973/74**, *3*, 267.
[19] Watanabe, N.; Haruta, M. *Kenkyu Hokoku Asahi Garasu Kogyo Gijutsu Shoreikai*, 1975/76, **27**, 1/10, and 1974, **25**, 11/20.
[20] Scholberg, H. M.; Brice, H. G. *U. S. P. 2,717,871* (Sept. 13, 1955)
[21] Burdon, J.; Tatlow, J. C. *Adv. Fluor. Chem.*, **1960**, *1*, 157.
[22] Bartlett, N.; Chambers, R. D.; Roche, A. J.; Spink, R. C. H.; Chacón, L. C.; Whalen, J. M. *Chem. Commun.* **1996**, 1049.
[23] Chambers, R. D.; Grievson, B.; Drakesmith, F. G.; Powell, R. L. *J. Fluor. Chem.*, **1985**, *29*, 323.
[24] Chambers, R. D.; Fuss, R. W.; Jones, M. *J. Fluor. Chem.* **1990**, *49*, 409.
[25] S. Rüdiger, A. Dimitrov, K. Hottmann *J. Fluor. Chem.* **1996**, *76*, 155, and references therein.

---

[26] A. Dimitrov, W. Radeck, St. Rüdiger, O. Bechstein *J. Fluor.Chem.* **1993**, *60*, 57.
[27] Dimitrov, A.; Rüdiger, St.; Seppelt, K.; Peplinski, T. *J. Fluor. Chem.* **1994**, *68*, 15-19.
[28] G. Zabinska et. al. *Thermochimica Acta,* **1987**, *122*, 87.
[29] Whalen, J. M.; Chacón, L. C.; Bartlett, N. *J. Electrochem. Soc.* in press.

Chapter 7. Generation of NiF_6^{2-} Salts from NiF_2

7.1. Introduction

Subsequent to the discovery that nickel fluorides were potent fluorinators of organic compounds, an interest arose in the preparation of NiF_6^{2-} salts from NiF_2 residues. In order to encourage the study and use of nickel fluorides such as *R*-NiF_3 and K_2NiF_6 as fluorinating agents, it was important to address the issue of disposal of large quantities of NiF_2 waste. It was found that a direct fluorination of NiF_2 mixed with KF at high temperatures and high pressures of F_2 did not lead to effective synthesis of K_2NiF_6. In general, the synthesis of complex fluorides A_2NiF_6 and A_3NiF_6 depend on a Ni^{II} starting material that is more easily oxidized, such as $NiCl_2$,[1,2] $[Ni(NH_3)_6]Cl_2$,[3] or Na_2NiO_3.[4]

Concurrently in this laboratory, experiments were underway in the synthesis of complex metal fluorides by a room temperature reaction of a noble metal, alkali fluoride and F_2 in aHF. This approach was found[5] to be successful in the synthesis of alkali salts of AuF_4^-, RuF_6^-, RuF_6^{2-}, OsF_6^-, IrF_6^-, PtF_6^-, and PdF_6^{2-}. In these reactions, a large excess

of alkali fluoride was found to be beneficial in the formation of the anion from the metal. Silver metal did not react with F_2 in basic aHF, likely due to its high effective nuclear charge.[6] However, it was found by G. M. Lucier of this group that both AgF_2 and NiF_2 were reactive when the reaction mixture (MF_2 with alkali fluoride and F_2 in aHF) was irradiated with U.V. light (to produce F atoms), resulting in colored solutions (yellow for Ag, red for Ni). In the case of NiF_6^{2-} synthesis a quantitative assessment of this method was not carried out by Dr. Lucier.

The optimum conditions for the synthesis of NiF_6^{2-} salts of K^+, Li^+, Na^+ and Cs^+ were then studied, with attention to concentration of alkali fluoride in solution and length of irradiation.[7] This novel approach to the synthesis of complex metal fluorides led to the synthesis of the new salt Li_2NiF_6, which was characterized by XRPD. Previously, the highest known oxidation state lithium hexafluoronickelate was Li_3NiF_6, containing Ni(III), prepared (500 °C; 70 atm. F_2) by Grannec, *et. al.*[8]

7.2. Experimental

Reactions to form K_2NiF_6 and Li_2NiF_6 were carried out side by side under nearly identical conditions in order to determine which reaction was more efficient for the production of NiF_6^{2-} salts. Several variables were nearly identical for the two reactions: mass of NiF_2, quantity of aHF, molar concentration of alkali fluoride, and distance from the light source. Reactions to produce Li_2NiF_6 were also carried out to determine the effect of a saturated alkali fluoride solution on the yield. Some reactions were carried out under sunlight rather than a UV lamp. In addition, the reaction between K_2NiF_6 and NiF_2

was investigated.

Preparations were carried out in ½" FEP T-reactors, unless otherwise noted. Ultraviolet irradiation of reaction mixtures was provided by a 450 watt immersion type Hanovia UV lamp (Ace Glass, Inc.) in a water-cooled jacket or strong sunlight with curved reflectors surrounding and parallel to the limb of the reactor containing the reaction mixture. Each reactor was then pressurized with F_2 (from ~1000 to 1500 torr partial pressure), which was replenished periodically throughout the reaction as it was consumed. The limbs of the reactors containing the reaction mixture were clamped in a horizontal position (to maximize the gas-liquid interface) and were placed approximately 3 in. from the UV source. The reaction mixtures were agitated by means of a rotating arm which shook the tubes vigorously each time it passed.

7.2.1. Room Temperature Synthesis of NiF_6^{2-} Salts

7.2.1.1. Comparative Study of K_2NiF_6 vs. Li_2NiF_6 Efficiency

In one FEP T-reactor, NiF_2 (0.0377 g; 0.390 mmol) and KF (0.0582 g; 1.00 mmol) were loaded in opposite arms. In a second FEP reactor, NiF_2 (0.0377 g; 0.390 mmol) and LiF (0.0258 g; 1.00 mmol) were loaded in opposite arms. To each reactor, aHF (3 mL) was added to the alkali fluoride. The resulting solution was poured onto the NiF_2 and the alkali fluoride arm was washed several times to ensure a quantitative addition. The F_2 pressure in each reactor was ~1000 torr.

The NiF_2 in the K_2NiF_6 reaction became darkened uniformly from yellow to a pale red-brown over 16 h of irradiation, while the NiF_2 in the Li_2NiF_6 reaction was still

yellow at that point. Both solutions remained colorless. After 37 h of irradiation, the solution in the K_2NiF_6 reactor was pale red and the solid red-brown, while there was still a colorless solution and yellow solid in the Li_2NiF_6 reactor. The solution in the Li_2NiF_6 reactor had developed a red tint after 54 h, and after 81 h, had become much darker red. The K_2NiF_6 solution became darker red and the solid darker red-brown over the same period.

The soluble and insoluble products of each reaction were separated by decantation followed by back-distillation of aHF (two repetitions), and the products dried under vacuum. The products of the K_2NiF_6 reaction were a tan solid (0.0296 g) and an inhomogeneous pink/white solid (0.0819 g) isolated from the decanted red solution. Products of Li_2NiF_6 reaction were a red-brown solid (0.0321 g) and an inhomogeneous pink/white solid (0.0321 g) isolated from the decanted red solution. XRPD showed that each insoluble residue had the pattern of NiF_2 and the soluble mixed pink/white solids had the patterns of the respective hexafluoronickelate salt mixed with alkali bifluoride. Based on the mass of NiF_2 consumed in each reaction, K_2NiF_6 was produced in 21% yield and Li_2NiF_6 was produced in 8% yield.

7.2.1.2. The effect of saturated LiF solution on Li_2NiF_6 yield

The amount of aHF was limited in this reaction so that there would be a saturated solution of LiF (0.103 g/mL) at all times up to the endpoint of the reaction (complete conversion of NiF_2 to Li_2NiF_6).

NiF_2 (0.170 g; 1.76 mmol) and LiF (0.1375 g; 5.3 mmol) were placed in one arm

of a T-reactor, and aHF (0.5 mL) was condensed onto the solids and the mixture stirred by a magnetic stir bar. The reactor was pressurized to 1500 torr with F_2 and the reaction mixture irradiated for 34 h. The nickel residue was washed until there was no further coloration of the aHF by the NiF_6^{2-} ion to yield 0.088 g of insoluble red-brown solid (NiF_2 by XRPD) and 0.3135 g of a soluble mixed pink/white solid (Li_2NiF_6 and $LiHF_2$ by XRPD). Based on the amount of NiF_2 consumed, the yield of Li_2NiF_6 was 48%.

7.2.1.3. Synthesis of Li_2NiF_6 in Sunlight

NiF_2 (0.2626 g; 2.71 mmol) and LiF (0.3768 g; 14.5 mmol) were loaded into a 1" (o.d.) FEP tube, and aHF (2.3 mL) was condensed onto the reagents. The reactor was pressurized to 1500 torr with F_2 and the reactor placed in full sunlight for a total of 37 h, with agitation provided by a rotating arm. The solid residue was washed with aHF until the solution was colorless, and the solids dried to give an insoluble red-brown solid (0.1801 g; NiF_2 by XRPD) and a soluble mixed pink/white solid (0.7279 g; Li_2NiF_6, $LiHF_2$ and LiF by XRPD). Based on the amount of NiF_2 consumed, the yield of Li_2NiF_6 was 31%.

7.2.1.4. Reaction between NiF_6^{2-} and NiF_2

7.2.1.4.1. Approximation of UV-Irradiation Reaction Conditions

To study the observed reaction between K_2NiF_6 and NiF_2, the UV-irradiation reaction conditions were approximated by the molar ratio 3.5 NiF_2: 10 KF : 1 K_2NiF_6. NiF_2 (0.0901 g; 0.932 mmol) was loaded into one arm of an FEP T-reactor and KF (0.1422 g; 2.45 mmol) and K_2NiF_6 (0.0705 g; 0.28 mmol) were loaded into the opposite

arm, and aHF (1.5 mL per reagent) was condensed onto the solids. The resulting red solution of KF/K_2NiF_6 was poured into the suspension of NiF_2 dropwise. With the first aliquot, an immediate reaction occurred, with effervescence, consuming the red color of the K_2NiF_6 and forming a pale off-white solid. Further dropwise addition of K_2NiF_6 did not produce effervescence, but did cause the color of the off-white solid to darken to tan. The next aliquot caused further darkening of the solid. Further addition of K_2NiF_6 caused progressive darkening, and eventually, the solution remained red. The solid was inhomogeneous, tan with some black and yellow agglomerates. The reaction mixture was cooled to 0 °C to prevent decomposition and the solid residue washed by decantation and back-distillation of aHF until the solution was colorless. The solids were dried and analyzed by XRPD, the insoluble tan solid (0.1064 g) gave the XRPP of NiF_2 and the soluble pink/white solid (0.2689 g) gave the XRPP's of K_2NiF_6 and KHF_2.

7.2.1.4.2. Synthesis of Chemically Pure NiF_2

To ensure that the reaction described in section 8.2.1.4.1was not due to adsorbed water or NiO (sometimes gray or black) present in the NiF_2, a fresh supply of NiF_2 was prepared by the reaction of $Ni(AsF_6)_2$ with KF, rather than by fluorination of commercially available NiF_2.

$Ni(AsF_6)_2$ (0.6721 g; 1.54 mmol) was loaded into one arm of an FEP T-reactor and KF (0.2305 g; 3.97 mmol; previously dried under high vacuum at room temperature for two days) was loaded into the other arm, and aHF (4 mL to $Ni(AsF_6)_2$ and 0.5 mL to KF) was condensed onto the reagents. The KF dissolved completely but the $Ni(AsF_6)_2$

was slightly turbid. The KF solution was poured into the $Ni(AsF_6)_2$ solution, precipitating a yellow solid, which was allowed to settle before decantation and back distillation to wash the residue (8 times). This yielded a yellow solid (0.1427 g), the XRPP of which indicated NiF_2 (94% yield) and a colorless solid (0.7519 g) which gave the XRPP of $KAsF_6$.

7.2.1.4.3. K_2NiF_6 with NiF_2 (molar ratio 1:1)

K_2NiF_6 (0.2532 g; 1.01 mmol) and NiF_2 (0.0955 g; 0.988 mmol) were loaded into opposite arms of an FEP T-reactor and aHF (1.5 mL per reagent) was condensed into the reactor. Approximately ¼ of the resulting red solution of NiF_6^{2-} was poured into the suspension of NiF_2 in aHF resulting in an immediate reaction to form a red-brown solid below a colorless solution. Addition of the remaining K_2NiF_6 solution had no visible affect, but the reaction mixture was stirred at 0 °C overnight. The soluble and insoluble products were separated by decantation and back-distillation of aHF (5 times) and the solids dried. The XRPP of the red-brown solid showed NiF_2 and the XRPP of the pink/white mixture showed K_2NiF_6 and KHF_2.

7.3. Results and Discussion

The F–F bond is known to be readily dissociated by the absorption of relatively high-energy photons. The absorption maximum is near 3000 Å, and has a broad tail into the visible region. The absence of band structure in the absorption spectrum of F_2 indicates that the absorption is due to promotion of electrons from the bonding levels to the σ^* orbital, causing dissociation.[9,10] In a fluorobasic aHF solution, photodissociation

of F_2 to F·, may be stabilized by the formation of short-lived species such as $F\cdot_2^-$, which would be further stabilized by HF solvation. In a fluorobasic aHF solution, the solubility of F· radicals may be enhanced relative to the solubility of F· in neutral aHF.

The side-by-side reactions to form K_2NiF_6 and Li_2NiF_6 showed that the K_2NiF_6 is the more efficiently produced. This was interesting, in that it was contrary to the expectation that the low solubility of the Li_2NiF_6 (and its eventual crystallization from the reaction mixture) would drive that reaction farther. These were some of the preliminary reactions, carried out before the effect of alkali fluoride concentration was studied. It was found that a saturated basic solution considerably increased the yield of NiF_6^{2-}, in the case of Li_2NiF_6, from 8% to 48%. However, even when the two reactions are carried out in saturated fluorobasic solutions, K_2NiF_6 was still more efficiently produced, giving 100% conversion of NiF_2 to NiF_6^{2-}, under certain conditions.[7] The oxidation of NiF_2 appears to begin with a uniform darkening of the solid from yellow to tan to red-brown, before the appearance of a red-tinted solution.

During this study, it was observed on several occasions that when agitation of the reaction mixture was not sufficient to ensure adequate mixing, an irreversible reaction between the red tinted solution and the yellow NiF_2 residue was observed, forming a brown solid. This brown solid was not reactive with low concentrations of alkali fluoride and F_2 and did not form NiF_6^{2-} even after lengthy periods of irradiation. When the NiF_2 was settled out below the solution with no mixing, only the top layer was in contact with the solvent carrying the fluorine atom source. The top layer could react to form NiF_6^{2-} but

when the pure NiF_2 from below was disturbed, it reacted with the NiF_6^{2-} in solution. Court and Dove reported a reaction between NiF_2 and K_2NiF_6 which led to an insoluble brown solid of composition $NiF_{2.05}$, with a magnetic moment, $\mu_{eff} = 2.83$ B.M.. Since the magnetic moment was not different from that of NiF_2, they concluded that the reaction between NiF_2 and K_2NiF_6 was only a surface reaction.[11] This phenomenon was only observed at low concentrations of alkali fluoride. At high concentrations, the yields of NiF_6^{2-} were high. This $NiF_{2+\delta}$ is eventually fluorinated to a composition which does interact with $F^-_{(solv)}$, giving NiF_6^{2-}. The color of the solid before a red tint is observed is always red-brown, however on some occasions, small black particles have been observed. It is possible that NiF_3 is formed, which might then react with F^-, undergoing the disproportionation described in Chapter 2:

$$2\ NiF_3 \quad + \quad 2\ KF \longrightarrow K_2NiF_6 \quad + \quad NiF_2 \qquad (1)$$

In practice, this problem of K_2NiF_6 reacting with NiF_2 was remedied through the use of concentrated basic solutions.

The development of this synthetic method in conjunction with the use of high oxidation state nickel fluorides as fluorinating agents of organic compounds described in Chapter 6 enables the process to be a cyclic one. K_2NiF_6 is commercially available, as are BF_3 and aHF. These are required for the synthesis of *R*-NiF_3, which is straightforward at 0 °C. The *R*-NiF_3 can be separated from KBF_4 and used to fluorinate organic substrates, leading to NiF_2 and NiF_x residues. From these residues, K_2NiF_6 can be regenerated as

described in this chapter. Also, the KBF_4 can be reverted to KF and BF_3 by thermolysis at 550 °C (if Li_2NiF_6 is used, $LiBF_4$ is thermolyzed at 350 °C). The BF_3 could be easily trapped and reused in the synthesis of *R*-NiF_3.

In the case of fluorinations by NiF_6^{2-}, the reduced product mixture contains NiF_2 and AHF_2 ($A = K^+, Li^+$) and can be converted to A_2NiF_6 in a concentrated fluorobasic solution of the appropriate alkali fluoride and F_2. In the case of Li_2NiF_6 as the fluorinating agent, its lower solubility (0.5 g/100g aHF at 0 °C) would afford a mechanism for slow delivery of the fluorinating agent to the substrate in solution. In addition, Li_2NiF_6 is more readily separated from the LiF used in regeneration, due to its low solubility and its tendency to be precipitated by the common ion effect. In the case of K_2NiF_6 as a fluorinating agent in aHF, the excess KF used in regeneration is not easily separable from it due to the high solubility of both K_2NiF_6 and KF. However, in most cases, the presence of excess F^- might only serve to enhance the fluorinating ability of NiF_6^{2-}, as F^- is likely active as a nucleophile in the fluorination of organic substrates.

7.4. Conclusion

Salts of NiF_6^{2-} have been synthesized by the UV-irradiation of NiF_2 residues in the presence of alkali fluoride and F_2 in aHF solvent. This method led to the isolation of the novel NiF_6^{2-} salt, Li_2NiF_6. The reaction between NiF_6^{2-} and NiF_2 is of concern as it diminishes the NiF_6^{2-} yield, but maintaining a saturated fluorobasic solution avoids this problem.

This novel synthetic route to NiF_6^{2-} salts, in conjunction with the finding that high oxidation state nickel fluorides are excellent fluorinators of organic substrates, may encourage the study and use of nickel fluorides in organic fluorination reactions on a larger scale.

7.5. References

[1] Klemm, W.; Huss, E. *Z. Anorg. Chem.* **1949**, *258*, 221.
[2] Bode, H.; Voss, E. *Z. Anorg, Allg. Chem.* **1956**, *286*, 136.
[3] Alter, E.; Hoppe, R. *Z. Anorg. Allg. Chem.* **1974**, *405*, 167.
[4] Henkel, H.; Hoppe, R. *J. Inorg. Nucl. Chem.* **1969**, *31*, 3855.
[5] Lucier, G.; Elder, S. H.; Chacón, L.; and Bartlett, N. *Eur. J. of Solid State and Inorg. Chem.* **1996**, *33*, 809.
[6] Žemva, B.; Lutar, K.; Jesih, A. Casteel, Jr., W. J.; Wilkinson, A. P.; Cox, D. E.; Von Dreele, R. B.; Borrmann, H.; Bartlett, N. *J. Amer. Chem. Soc.*, **1991**, *113*, 4192.
[7] Whalen, J. M; Lucier, G. M.; Chacón, L. *J. Fluor. Chem.* **1997**, in press.
[8] Grannec, J; Lozano, L; Sorbe, P.; Portier, J.; Hagenmüller, P *J. Fluor. Chem.* **1975**, *6*, 267.
[9] Herzberg, G. "Spectra of Diatomic Molecules", D.Van Nostrand Co., Inc., New York, **1964**, pp. 389-390.
[10] Rees, A. L. G. *J. Chem. Phys.* **195***726*, 1567.
[11] Court, T. L.; Dove, M F A. *J. Chem. Soc., Dalton Trans.* **1973**, 1995.

Appendix A: XRPP of $Ni(AsF_6)_2$

The X-ray powder pattern of $Ni(AsF_6)_2$ differs significantly from that published by Frlec, *et. al.*[1] However, it appears to be isostructural with that published by Christie *et. al.* for $Ni(SbF_6)_2$.[2] All first transition series metal (M) salts, $M(M'F_6)_2$ (M' = As, Sb, Bi) except $Mn(AsF_6)_2$ have the hexagonal symmetry seen here.[3]

The hexagonal unit cell parameters obtained are: $a_o = 4.98(5)$ Å, $c_o = 26.59(1)$ Å, V = 571 Å^3. Since the formula unit volume of AsF_6^- is ~95 Å^3 (e.g. formula unit volume for $LiAsF_6$ is 95.3 Å^3)[4] and the formula unit has two such anions, the unit cell must contain three formula units, of 190 Å^3 each.

---

[1] Frlec, B.; Gantar, D.; holloway, J. H. *J. Fluor. Chem.* **1982**, *19*, 485.
[2] Christe, K. O.; Wilson, W. W.; Bougon, R. A.; Charpin, P. *J. Fluor. Chem.* **1987**, *34*, 287.
[3] Shen, C.; Lucier, G. M., unpublished observations in these laboratories.
[4] Kemmitt, R. D.; Russell, D. R.; Sharp, D. W. A. *J. Chem. Soc.*, **1963**, 4408.

	$1/d^2_{hkl}$ x 10^4				
I_{obs}	Observed	Calculated	*h*	*k*	*l*
vw	205	---	---	---	---
m	509	509	0	0	6
vw	542	538	1	0	0
s	593	595	1	0	2
vs	763	764	1	0	4
vvw	824	---	---	---	---
vvw	966	---	---	---	---
vvw	1036	1047	1	0	6
m	1446	1443	1	0	8
w	1614	1614	1	1	0
vvw	1869	1840	1	1	4
vvw	1955	1952	1	0	10
---	---	2037	0	0	12
s	2123	2123	1	1	6
---	---	2152	2	0	0
vvw	2210	2209	2	0	2
w	2382	2378	2	0	4
m	3063	3057	2	0	8
vvvw	3311	3310	1	0	14
vvvw	3576	3566	2	0	10
s	3662	3651	1	1	12
w	3818	3823	2	1	2
m	3996	3992	2	1	4
w	4172	4189	2	0	12
m	4688	4671	2	0	8
m	4846	4842	3	0	0
vw	4936	4924	2	0	14
w	5194	5180	2	1	10
vw	5357	5351	3	0	6
mw	5788	5803	2	0	12
mw	6214	6256	3	0	10

Appendix B: Nomenclature of HTB Structural Variants

I. HTB-type nomenclature

H- undistorted HTB structure

H_O- orthorhombic distortion of HTB structure

$(A)_x$ indicates guest cation/neutral molecule composition, absence indicates empty channels

Examples:

H-FeF_3	HTB structure, empty channels
H_O-$(H_2O)_{0.22}FeF_3$	orthorhombic distortion of HTB structure, H_2O in channels
H-$(NH_4^+)_{0.25}VF_3$	HTB structure, NH_4^+ in channels
H_O-VF_3	orthorhombic distortion of HTB structure, empty channels
H_O-$K_{0.22}NiF_3$	orthorhombic distortion of HTB structure, K^+ in channels